CERN / ALICE-INT-047 v.1
ALICE Internal Note
Date: 18 November 2005

Event by event physics in ALICE

M.M. Aggarwal[1)], A.G. Asryan[2)], J. Bartke[3)], P.A. Bolokhov[2)], M.A. Braun[2)], P. Christakoglou[4,a)], D.A. Derkach[2)], G.A. Feofilov[2)], M. Gaździcki[5)], S. Gupta[6)], A.S. Ivanov[2)], V. Koch[7)], R.S. Kolevatov[2)], V.P. Kondriatev[2)], A. Leonidov[2)], B. Mohanty[8)], B. Nandi[9)], P.A. Naumenko[2)], St. Mrówczyński[10,11)], T.K. Nayak[12,b)], A. Petridis[4)], S. Pratt[13)], L. Ramello[14)], S. Raniwala[15)], M. Vassiliou[4)], V.V. Vechernin[2)], Y.P. Viyogi[8)], G. Wilk[11)], and C. Zampolli[16)]

[1)] Physics Department, Panjab University, Chandigarh, India.
[2)] V. Fock Institute for Physics of St. Petersburg State University, St. Petersburg, Russia.
[3)] Henryk Niewodniczanski Institute of Nuclear Physics, Cracow, Poland.
[4)] Physics Department, University of Athens, Athens, Greece.
[5)] Institut für Kernphysik, Johann Wolfgang Goethe-Universität, Frankfurt, Germany.
[6)] Tata Institute of Fundamental Research, Mumbai, India.
[7)] Lawrence Berkeley National Laboratory, Berkley, USA.
[8)] Variable Energy Cyclotron Centre, Kolkata, India.
[9)] Indian Institute of Technology, Mumbai, India.
[10)] Institute of Physics, Swietokrzyska Academy, Kielce, Poland.
[11)] Soltan Institute for Nuclear Studies, Warsaw, Poland.
[12)] CERN, Genève, Switzerland.
[13)] Michigan State University, East Lansing, Michigan, USA.
[14)] Facoltà di Scienze dell'Università and INFN, Alessandria, Italy.
[15)] Physics Department, University of Rajasthan, Jaipur, India.
[16)] Museo Storico della Fisica e Centro Studi e Ricerche Enrico Fermi, Roma, and INFN, Italy.
[a)] Now Marie Curie Fellow at Physics Department, CERN, Genève, Switzerland.
[b)] On leave from Variable Energy Cyclotron Centre, Kolkata, India.

Abstract

Fluctuations of thermodynamic quantities are fundamental to the study of QGP phase transition. The ALICE experiment is well suited for precise event-by-event measurements of various quantities and study their fluctuations in order to understand the physics of bulk properties of matter as well as particles with high transverse momenta and jets. Recent lattice calculations have revealed that interesting fluctuation patterns might be observed for situations at small chemical potential which will prevail at LHC energies. The capability of the ALICE detector is explored in terms of measurement of fluctuations in temperature and average transverse momenta, multiplicity and strangeness fluctuations, fluctuations of conserved quantities including net charge fluctuation, balance functions, fluctuation in azimuthal anisotropy, fluctuation in space-time parameters from correlation measurements, disoriented chiral condensates, importance of jets and mini-jet production in fluctuation measurements and long range dynamical correlations.

1 Introduction

It is expected that the hot and dense system created in heavy-ion collisions at ultra-relativistic energies and its evolution in time will show very characteristic behaviour of QGP phase transition, which may vary dramatically from one event to the other [1]. Such interesting behaviour can be studied by the measurement and subsequent analysis of various observables in every single event. Thus event-by-event measurement and the study of various physically observable quantities offer the best possibility for studying the QGP phase transition and the nature of the QGP matter. Because of the production of large number of particles in each event in heavy-ion collisions at SPS, RHIC and LHC energies it is now possible to make precision event-by-event measurements and study fluctuations of various measured quantities for given event classes. The fluctuation measures provide unique ways to study variations in physical quantities from event to event.

Fluctuations of thermodynamic quantities such as temperature or transverse momentum and entropy or particle multiplicity have been proposed to establish the existence of QGP phase transition and also provide direct insight into the properties of the system created in high energy heavy-ion collisions [2, 3, 4, 5, 6, 7]. Large fluctuations in energy density due to droplet formation are expected if the phase transition is of first order. Second order phase transition may lead to divergence in specific heat and would increase the fluctuation in energy density due to long range correlations in the system. It is predicted that near a critical point, i.e., a second order phase transition, fluctuations will be strongly enhanced [3]. Present lattice computations (see the next section for details) reveal that the QCD critical point could be at reasonably small chemical potential [8] but still be too high for the LHC to reach. The situation becomes different with the production of jets and mini-jets at LHC energies. Characterization of jets and their interaction with the medium will be quite interesting to understand the phase transition and physical characteristics of QGP[9, 10]. Formation of disoriented chiral condensates (DCC) [11, 12, 13, 14, 15], which is a consequence of chiral phase transition, would lead to large fluctuations in the ratio of neutral to charged pions.

The rapid development of the event-by-event physics in recent years is directly related to the progress in the field of high-energy nucleus–nucleus collisions. Recent detector technologies and availability of high collision energies along with experiments containing large acceptance detectors allow the detection of a large fraction of thousands of particles produced in each collision at SPS, RHIC and LHC energies. Active study of event-by-event fluctuations in heavy-ion collisions was initiated by experiments at the SPS [16, 17, 18, 19, 20, 21, 22, 23, 24, 25, 26, 27, 28, 29, 30, 31, 32]. These studies include fluctuations in multiplicity of charged particles and photons, kaon to pion ratio, net charge, transverse momentum and formation of DCC domains. These along with more sophisticated analysis results are now available from RHIC experiments [33, 34, 35, 36, 37, 38, 39, 40, 41, 42, 43, 44]. The experimental procedures, statistical tools, and theoretical models are constantly challenged by the requirements of event-by-event study.

The regime of event-by-event physics spans from understanding the bulk properties of matter to high p_t particles including jets. The ALICE experiment has the unique capability to track the majority of the particles produced in heavy-ion collisions, and measure relevant quantities needed for event-by-event physics. In this section the methodology for event-by-event physics and fluctuations and the performance of ALICE detector in terms of these measurements are discussed. The next subsection deals with predictions from lattice calculations, followed by a brief discussion of the physics of correlations and fluctuations. The measurement capabilities of ALICE are discussed after that. The rest of the section contains discussions on temperature and $\langle p_t \rangle$ fluctuations, multiplicity and strangeness fluctuations, fluctuations of conserved quantities, net charge fluctuations, balance functions, fluctuations in azimuthal anisotropy, disoriented chiral condensates, the importance of jets and mini-jet production in fluctuation studies and finally long-range dynamical correlations of various observables measured in separated rapidity intervals.

2 Lattice predictions

Lattice QCD is the theoretical tool of choice for computing the fluctuations of conserved quantities such as charge and energy. Other quantities, such as strangeness, which are conserved by the strong interactions, but not by the weak, are practically conserved within the lifetime of the fireball. Lattice QCD is able to provide a prediction for the fluctuations of such quantities as well. Two regimes of baryon chemical potential, $\mu_{\rm B}$, and temperature, T, are of interest—the intermediate chemical potential regime, $\mu_B \simeq T$, where there is the likelihood of finding a critical point of QCD, and the small chemical potential regime, $\mu_{\rm B} \ll T$, where freeze-out conditions at LHC are likely to operate.

2.1 The QCD critical end point

Following the prediction of a critical end point of QCD using models [3], lattice QCD explorations around the QCD critical point have started. This was obtained on the lattice using several methods, such as reweighting method [45, 46, 47], analytic continuation from imaginary chemical potential [48, 49] and a Taylor series expansion [50, 51, 52]. These computations are performed in lattice QCD with two flavours of light dynamical quarks. Three important parameters in these computations are

- The physical volume of the lattice, V must be sufficiently large in units of the pion's Compton wavelength. In practice, it was found that, in units with $\hbar = c = 1$, one must select $m_\pi V^{1/3} > 5$.
- The quark mass, whose measure is the ratio m_π/m_ρ. In order to get realistic physics, one must have $m_\pi/m_\rho \ll 0.5$, and the actual physical value is $m_\pi/m_\rho = 0.18$.
- The lattice spacing should be extrapolated to zero to get the continuum limit. In practice, one may be able to tolerate a finite lattice spacing as long as the ratio $m_{\rm p}/m_\rho$ is realistic.

None of the computations performed so far could satisfy all the three conditions, in particular all computations work at rather coarse lattice spacings of the order of 0.25 fm. In Ref. [45], the ratio m_π/m_ρ is realistic but $m_\pi V^{1/3} \approx 3$. In [51] $m_\pi V^{1/3} \approx 15$ but $m_\pi/m_\rho \approx 0.7$. A range of volumes $m_\pi V^{1/3} = 3$–10 was explored, and the infinite volume extrapolation performed, in [52] at a quark mass $m_\pi/m_\rho \approx 0.3$, which is also the quark mass value used in [45, 49]. A strong dependence of the position of the critical end point on the volume has been noted as seen in Fig. 1. As a result, the best estimate as of today is $\mu^E/T^E \approx 1$ with $T^E/T_c \approx 0.95$ [52]. This is likely to decrease as the quark mass is decreased to more realistic values.

The chemical potential at LHC energies will be quite small, however, the analysis of particles emitted at forward and backward rapidities (but not the fragmentation region) will be quite interesting as they are emitted at higher chemical potential compared to the particles at central rapidities.

2.2 Thermodynamic fluctuations at small chemical potential

The best established results for fluctuations of conserved quantities come from lattice computations of the quark number susceptibilities [54]. Lattice results are also available for the baryon number susceptibility, χ_B, the susceptibility of the third component of isospin, χ_3, and strangeness, χ_s, which are defined as,

$$\chi_{\rm B} = \left.\frac{\partial^2 P}{\partial \mu_{\rm B}^2}\right|_{\mu_3,\mu_{\rm s},{\rm T},{\rm V}}, \qquad \chi_3 = \left.\frac{\partial^2 P}{\partial \mu_3^2}\right|_{\mu_{\rm B},\mu_{\rm s},{\rm T},{\rm V}}, \qquad \chi_{\rm s} = \left.\frac{\partial^2 P}{\partial \mu_{\rm s}^2}\right|_{\mu_{\rm B},\mu_3,{\rm T},{\rm V}}, \tag{1}$$

where P is the pressure, T the temperature, $\mu_{\rm B}$, μ_3 and $\mu_{\rm s}$ the chemical potentials associated with baryon number, isospin and strangeness, respectively. Results in the continuum limit

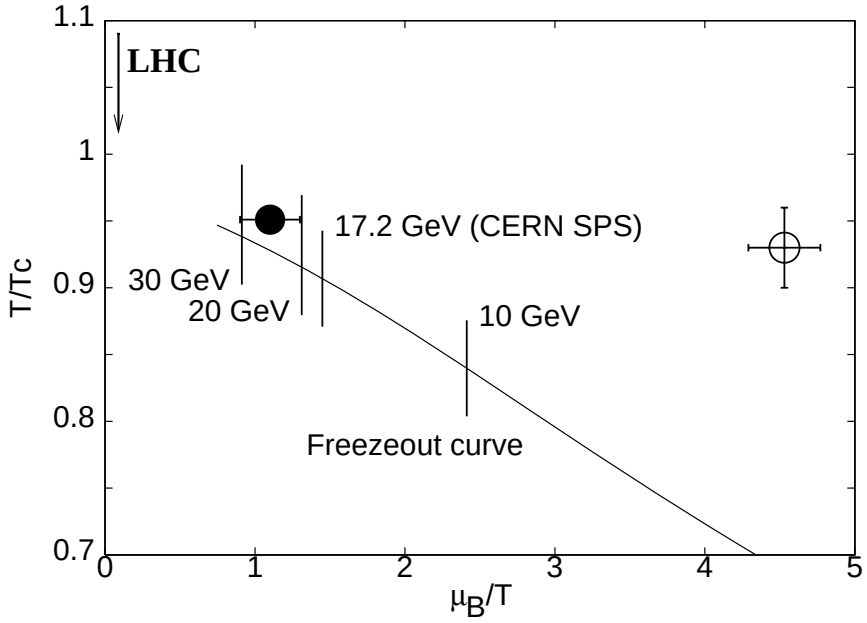

Figure 1: Estimates of the critical end point of QCD overlaid on a freezeout curve [53]. The open and filled circles are estimates for the critical end point from Refs. [45] and [52], respectively, computed for quark mass such that $m_\pi/m_\rho \approx 0.3$. For realistic quark mass, the critical chemical potential corresponding to the critical end point is expected to decrease.

come from quenched QCD computations [55]. Comparison of quenched results with those in dynamical 2 flavour [56, 52] and 2+1 flavour [57] QCD at similar lattice spacing shows that, in the high temperature phase for $T \geq 1.5T_c$, there is at most a 5–10% effect due to unquenching. In the high temperature phase of QCD, above $1.5T_c$, there is good agreement of these lattice results with weak coupling theory [58, 59, 60]. Figure 2 shows the behaviour of baryon chemical potential with temperature for two flavour QCD in the continuum limit.

The susceptibilities, being variances and covariances of quantum numbers, also throw light on the degrees of freedom in the hot phase of QCD [61, 62]. Lattice computations show that this is indeed the case, and the conclusion is independent of quark masses as long as they are substantially lighter than the charm quark [62].

Non-linear quark number susceptibilities (NLS) are higher derivatives of the pressure with respect to chemical potentials [50]. The ratios of the fourth and second order NLS are also sensitive to the presence of valence quarks (as was shown by a computation in quenched QCD [50], and in two flavour QCD both with heavy pions $m_\pi/m_\rho = 0.7$ [63] as well as lighter pions $m_\pi/m_\rho = 0.3$ [64]). These signals indicate that quarks are definitely the flavour carriers for $T \geq 1.25T_c$). However the higher (fourth) order NLS seem to show interesting structure very close to T_c as shown in Fig. 3 [63, 64]. While the origin of this structure is under discussion [64, 65], it provides an excellent oppertunity to be measured in ALICE. Net charge fluctuations as well as fluctuations in terms of the fourth and higher order cumulants can be measured in terms of various collision geometries (event centralities) as well as different cuts in transverse momenta of charged particles.

For fluctuations in energy of a canonical ensemble, or the temperature of a microcanonical ensemble, the appropriate quantity to measure is the specific heat, defined as,

$$c_v = \left.\frac{\partial \epsilon}{\partial T}\right|_{\mu_{\rm B},\mu_{\rm 3},\mu_{\rm s,V}}, \qquad (2)$$

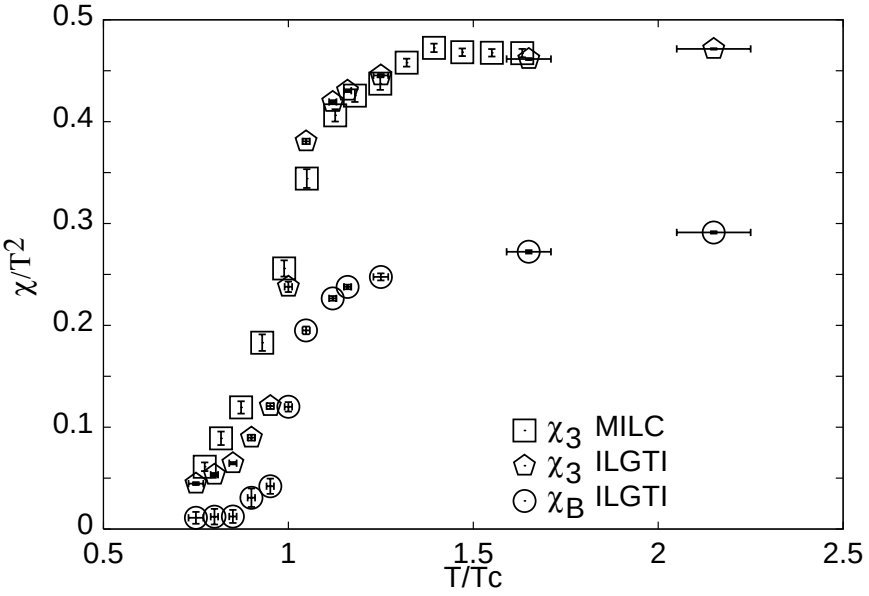

Figure 2: Estimates of χ_3/T^2 and χ_B/T^2 in the continuum limit of two flavour QCD. A scaling factor obtained from the quenched computation of [55] has been applied to the data of Ref. [52] indicated as ILGTI. Values obtained at lattice spacing $1/8T$ with a different way of putting quarks on the lattice [57] are also shown as MILC. The results are in good agreement.

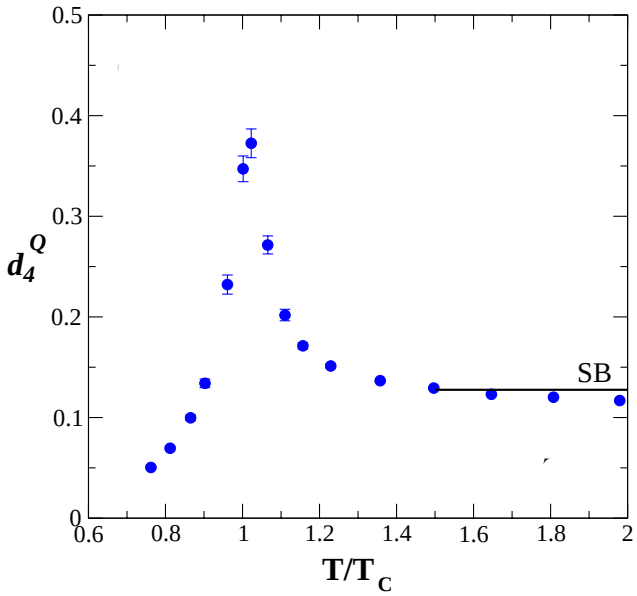

Figure 3: Fourth order cumulant of charge fluctuations showing a peak structure around $T = T_c$, taken from Ref. [63]. Similar structures are also seen for fourth cumulant of quark and isospin number fluctuations. Similar results are also shown in Ref. [64].

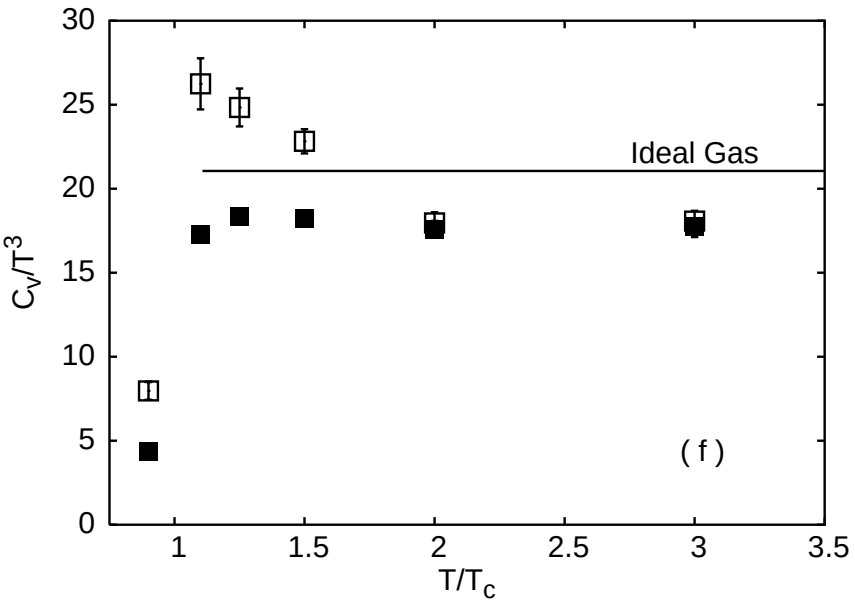

Figure 4: Continuum results for c_v/T^3 (open boxes) and $4\epsilon/T^4$ (filled boxes) from the lattice computation of Ref. [66]. Values corrsponding to the ideal gas situation are also indicated.

where ϵ is the energy density and T the temperature. This has been measured recently on the lattice in quenched QCD [66] and is shown in Fig. 4. It shows strong temperature dependence. For $T > 2T_c$ it is consistent with the predictions of a conformal theory, $c_v/T^3 = 4\epsilon/T^4$. However, it increases as the temperature drops toward T_c. Below T_c the specific heat is lower. If a reliable extraction of the specific heat can be made through event-by-event fluctuations, then the rapid change with T makes this a good candidate thermometer.

3 Correlations and fluctuations

The challenge of event-by-event studies is that, beyond the fluctuations linked to the details of the phase transition, there are a number of other fluctuations which may appear. The observed fluctuations will have contributions from statistical fluctuations and those from dynamical origin. The contribution from dynamical origin comprise of (a) fluctuations which do not change event-to-event, e.g., those from Bose-Einstein (BE) correlations, resonance decays, etc. and (b) the fluctuations which have a new physics origin and may vary from event-to-event. It would be very interesting to probe into fluctuations which have new physics origin. The fluctuations impact different observables in different manner and act on different scales. For example, the energy and momentum conservation correlate all particles in the collision and thus can influence fluctuations at large scales. On the other hand, short-range correlations due to quantum statistics obeyed by fermions and bosons result in suppression (fermions) or enhancement (bosons) of fluctuations at small scales.

The present results at the SPS and RHIC indicate that statistical models of strong interactions reproduce surprisingly well the energy dependence of entropy and strangeness production [67] and the hadronization process [68], resulting in a correct description of hadron yield systematics. However, the interpretation of the data within statistical models is under discussion. The basic assumptions of the statistical models are not according to what is commonly accepted, based on the theory of strong interactions QCD. On the other hand it is difficult to apply QCD for the interpretation of the experimental results since almost all effects connected to the transition to QGP are in the domain of soft processes for which experimentally testable predictions

of QCD are not available. Attempts to build phenomenological, QCD-inspired, models have not been very successful either. Conclusive interpretation of the data within these models seems to be impossible since one cannot estimate the uncertainties due to the approximations introduced.

Thus, the questions concerning interpretation of heavy-ion results unavoidably lead to the more fundamental questions about our understanding of strong interactions and the validity of various frameworks. In particular, further tests on limits of the application of the statistical models are needed. Within this context the study of event-by-event fluctuations plays a special role as it allows for independent tests of competing approaches.

It has been suggested that the processes following QGP hadronization like hadronic rescattering [69] and resonance decays may almost completely wipe out fluctuations originally developed in the QGP phase. Thus the propagation of fluctuation from initial stages of collision to the freeze-out has to be considered before making any conclusions about the fluctuations from QGP and non-QGP stages [70].

There are numerous well-established physical sources of event-by-event fluctuations in high-energy nucleus–nucleus collisions:

- geometrical (impact parameter, number of participants, detector acceptance) [71, 27, 72];
- energy, momentum, charge conservations [73, 74];
- anisotropic flow [75, 76, 77];
- Bose-Einstein correlations [78, 79];
- resonance and string decays [80, 73, 81];
- jets and mini-jets [82, 9, 10];
- quantum statistics [80];
- temperature fluctuations [83];
- Coulomb interactions.

Many exotic (still not observed and/or identified) phenomena may also occur and significantly impact the observed fluctuations. Among them are:

- formation of Disoriented Chiral Condensates (DCC) [11, 12, 13, 14, 15];
- colour collective phenomena [84];
- frozen statistical QGP fluctuations [85, 86];
- formation of colour ropes [87].

Dedicated analysis methods and statistical tools are well established in order to study the majority of the standard processes listed above (geometrical fluctuations, quantum statistics, Coulomb interactions, resonance production, anisotropic flow). Their impact on event-by-event fluctuations can therefore be estimated based on the experimental results and thus they serve as a background above which other effects are sought.

Depending on the nature of QGP phase transition, there will be large density fluctuations leading to droplet formation and hot spots. These will give rise to large rapidity and multiplicity fluctuations of produced particles and have distinct effects on the space time extent of the source [78, 79]. The Bose-Einstein correlation measurement of particle pairs (or the HBT method) give handle on the space-time extent of the system. Up until now it has become impossible to measure the space-time correlations on an event-by-event. As a result of the production of large number of particle pairs in heavy-ion collisions at LHC energy, one can do single event interferometry in ALICE. The correlation measurements in ALICE will be sensitive enough to study fluctuations

in source sizes on an event-by-event basis. Measuring HBT radii on different rapidity window or multiplicity bin will be quite interesting to study in ALICE.

Of special interest at LHC energies is the study of jet and mini-jet production in nucleus–nucleus collisions. Since the jet/mini-jet production cross-section measured in pp($\overline{\rm p}$) interactions strongly increases with energy, one expects that copious jet/mini-jet production may be a dominant feature of heavy-ion collisions at the LHC. Standard methods developed for the jet search in elementary interactions do not work well in the case of heavy-ion collisions on account of the very high background of soft hadrons. Direct jet identification is possible only at very high $\rm p_t$ range. On the other hand, the hadrons originating from a jet are correlated in momentum space, and therefore jet production should lead to an increase of fluctuations. Consequently, the study of event-by-event fluctuations may yield important information on jet/mini-jet production not accessible by direct methods because of high background. Copious jet/mini-jet production and consequently large fluctuations may, however, shadow fluctuations caused by other processes of interest. It is therefore clear that the relation between jet/mini-jet production and search for event-by-event fluctuations needs careful study.

Formation of DCC is a direct consequence of the chiral symmetry restoration at high temperatures and densities. This gives rise to anomalous fluctuations in the ratio of neutral to charged pions. At the SPS, both WA98 and NA49 experiments searched for the formation of DCC. The WA98 collaboration made an extensive study for the formation of DCC in global as well as localized domains in phase space. Based on DCC simulation models upper limits on the production of DCC have been estimated [28, 30, 31, 18]. Several methods to search for DCC have been proposed in the literature. The sensitivity of these methods will be discussed later in the section.

A copious production of partons, mainly gluons, due to hard and semi-hard processes, is expected in heavy-ion collisions at the LHC. During the early stages of collision the system is on average locally colourless, but random fluctuations can break the neutrality. Since the system is initially far from equilibrium, specific colour fluctuations can exponentially grow in time and then noticeably influence the evolution of the system. The very existence of such fluctuations would be a clear manifestation of the quark–gluon plasma where the colour forces act well beyond the confinement scale. The colour plasma instabilities can indeed occur due to the strongly elongated parton momentum distribution [84]. These instabilities, in particular the filamentation instability, generate collective transverse flow in heavy-ion collisions. The occurrence of the filamentation breaks the azimuthal symmetry of the system. The azimuthal orientation of the wave vector will change from one collision to another, while the instability growth will lead to the energy transport along this vector. Consequently, one expects significant variation of the transverse energy as a function of the azimuthal angle. This expectation is qualitatively different from that based on the parton cascade simulations [88], where the fluctuations are strongly damped due to the large number of uncorrelated partons. On account of the collective character of the filamentation instability, the azimuthal symmetry will be presumably broken by a flow of a large number of particles with relatively small transverse momentum. One expects the generation of the collective transverse motion as a result of the anisotropic pressure gradient [89, 90]. The flow is of hydrodynamic nature, and, in contrast to the colour instability driven transport, it is strongly correlated with the orientation of the collision plane. The collective flow can be studied by means of various methods. The fluctuation measure Φ [71] may be used for this purpose which has been proven to be very sensitive to the collective effects [82, 76].

Fluctuations in physical quantities that arise out of hydrodynamic predictions can discern whether the fluid is perfect or not perfect. A dissipation in a non-perfect fluid is related to the fluctuations of these physical quantities [77]. In this context, it has been proposed to study elliptic flow and higher harmonics on an event-by-event basis [76, 77]. Fluctuation in elliptic flow is argued to be sensitive to the following physical effects: (a) filamentation instability initiated due to the strong momentum anisotropy of the partonic system, and the generation and subsequent explosions of the topological clusters and (b) multiplicity fluctuations. Fluctuation

of elliptic flow can be explored in detail in the ALICE experiment.

Additional valuable information on the collision dynamics, specifically on the string fusion and percolation phenomenon, may be obtained in the event-by-event studies of the correlations between various observables measured in separated rapidity intervals (long range correlations). These can be studied in different rapidity intervals for multiplicity correlations, $\langle p_t \rangle$ correlations and multiplicity-$\langle p_t \rangle$ correlations. Model-independent detailed experimental information on long-range correlations between such observables as charge, net charge, strangeness, multiplicity and transverse momentum of specific type particles could be a new powerful tool to discriminate theoretical reaction mechanisms.

The ALICE experiment is well equipped to address all these issues. Event-by-event fluctuations of the measured quantities can be studied in ALICE using specific analysis methods sensitive to phase transition, deconfimement and chiral symmetry restoration. Various aspects of these will be discussed in the rest of the section.

4 Event-by-event measurements in ALICE

ALICE is a multi-purpose experiment with highly sensitive detectors surrounding the interaction point. The experiment is designed for event-by-event measurement of several of the observables. The most important information about a collision or an event is the collision geometry. This is provided by the ZDC and multiplicity detectors. The central detectors ($-0.9 < \eta < 0.9$) with their good particle identification capabilities provide momentum measurement for each particle species in every event. The forward detectors extend the coverage of charged particles and photons. Charged particle multiplicity in the central region is given by a combination of ITS, TPC and TOF. A combination of these three detectors provide momenta information and particle identification of hadrons. The FMD extends the charged particle multiplicity measurements to $\eta = 5.09$. In the central rapidity region PHOS with a limited coverage provides photon multiplicity and photon momenta whereas PMD is designed for multiplicity of photons in the high particle density region of forward rapidity ($2.3 < \eta < 3.5$). A combination of information from these detectors provides excellent opportunity to study event-by-event physics and fluctuation at LHC energies.

5 Centrality selection for fluctuation studies

The characteristics of the phase transition are supposed to be different with differing collision energy and also for different centrality. It is important to have proper control over centrality for the majority of the analysis. Centrality is normally characterized by the impact parameter (b) of the collision or the number of participating nucleons ($N_{\rm part}$). As it is not possible to measure either b or $N_{\rm part}$ directly, estimations of these quantities are based on calorimetric and multiplicity measurements. In ALICE it is possible to determine the centrality quite precisely in every event by using the forward energy from ZDC and multiplicity of produced particles from multiplicity detectors such as ITS, FMD etc. From these one extracts the impact parameter or the number of participants in a model dependent way. This is needed in order connect any measured quantity with theoretical calculations and to compare them with measurements from other experiments.

The importance of proper centrality selection for fluctuation studies is discussed here. An example of multiplicity fluctuation is chosen for the present discussion. In a simple participant model [1, 91, 27], the number of produced particles (N) in a collision depends on the centrality collision expressed in terms N_{part} and the number of collisions suffered by each particle. Mathematically this can be expressed as:

$$N = \sum_{i=1}^{N_{\rm part}} n_i, \tag{3}$$

where n_i is the number of particles produced in the detector acceptance by the i^{th} participant. On an average, the mean value of n_i is the ratio of the average multiplicity in the detector coverage to the average number of participants, i.e., $\langle n \rangle = \langle N \rangle / \langle N_{\rm part} \rangle$. Thus the fluctuation in particle multiplicity is directly related to the fluctuations in $(N_{\rm part})$. In order to infer any dynamical fluctuation arising from various physics processes one has to take care that the fluctuations in $N_{\rm part}$ is minimal.

This has been addressed by the WA98 experiment [27] where the centrality selections were made by using the midrapidity calorimeter and zero-degree calorimeter. Using VENUS event generator[92] and the WA98 simulation framework, $N_{\rm part}$ values are calculated for various centrality bins as derived from the experimental quantities. The fluctuations in $N_{\rm part}$ are obtained from their distributions for any given centrality bin in the following way. For a given variable (X) whose distribution is a Gaussian, the relative fluctuation $(\omega_{\rm X})$ may be expressed as:

$$\omega_X = \frac{\sigma_X^2}{\langle X \rangle}, \tag{4}$$

where σ_X^2 is the variance of the distribution and $\langle X \rangle$ denotes the mean value. The fluctuations in the $N_{\rm part}$ values are extracted using the above formula where X is taken as $N_{\rm part}$.

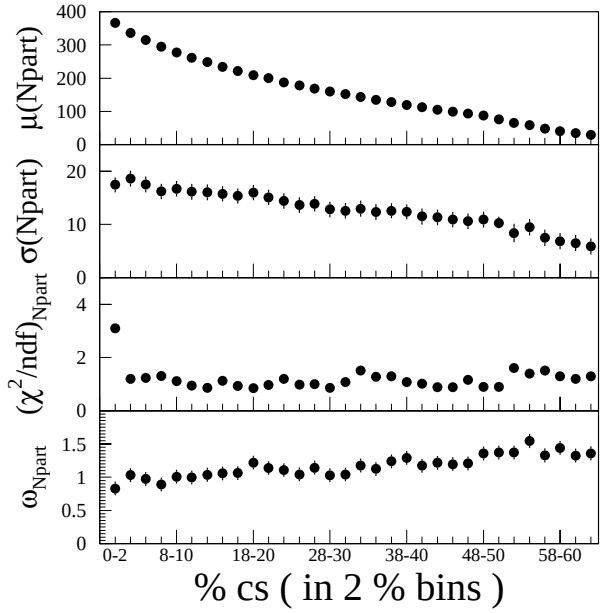

Figure 5: Variation of μ, σ, and χ^2/ndf for the distribution of the number of participants as a function of centrality in case of Pb–Pb collisions at SPS energies are shown in top three panels. The fluctuation in the number of participants, shown in the bottom panel, remain minimal and close to unity for narrow bins in centrality as depicted in the X-axis.

Figure 5 shows the mean, sigma, χ^2/ndf fit value of the Gaussian distribution and extracted fluctuation for the number of participants for narrow centrality bins such as 0–2%, 2–4%, 4–6%, ...50–52% for WA98 experimental setup [27]. The fluctuations in $N_{\rm part}$ remain around unity for most of the centrality bins. On the other hand, for broad centrality bins these fluctuations are much larger and bias the fluctuation study. This suggests narrow cross section slices in the centrality bins are necessary to study any kind of fluctuations and minimize the influence of impact parameter fluctuations.

In ALICE attempts will be made to study fluctuations in narrow bins in centrality with combination of information from ZDC, FMD and central detectors.

6 Temperature fluctuations

The concept of temperature plays a key role in the description of relativistic heavy-ion collisions because the matter produced at early stages of the collision achieves, at least to some extent, local thermodynamic equilibrium. Although the thermodynamic interpretation of temperature is a matter of debate [93], the main point of interest would be to find out whether there is a unique temperature of the system at freezeout or whether the temperature fluctuates from one collision to another [83]. The ALICE experiment is capable of high-precision measurements of the event-by-event temperature fluctuations.

6.1 Methods of study

The temperature can be inferred from the experimental data in several ways. In particular, one analyzes the $\mathrm{p_t}$ distribution which is usually taken in the form

$$\frac{\mathrm{d}N}{\mathrm{d}^2\mathrm{p_t}} \propto \exp\left(-\frac{\mathrm{m_t}}{T}\right) , \tag{5}$$

where $\mathrm{m_t} \equiv \sqrt{\mathrm{m}^2 + \mathrm{p_t}^2}$ with m being the particle mass; T is the *effective* temperature which, as commonly accepted, see for example Ref. [94], combines the genuine temperature $\mathcal{T}$ and transverse flow velocity u according to the approximate relation $T = \mathcal{T}\sqrt{(1+u)/(1-u)}$ [95]. Obviously, the fluctuations of $\mathcal{T}$ and u both contribute to that of T.

The temperature fluctuations influence the shape of the $\mathrm{p_t}$ distribution. As shown in Ref. [96], the T fluctuations in the exponential formula (5) lead in a natural way to the power-like form, known as the Lévy distribution. Indeed, averaging the exponential formula over the fluctuations of $1/T$ which follow the gamma distribution, one gets

$$\frac{\mathrm{d}N}{\mathrm{d}^2\mathrm{p_t}} \propto \left[1 - (1-q)\frac{\mathrm{m_t}}{T_0}\right]^{\frac{1}{1-q}} , \tag{6}$$

where $1/T_0 \equiv \langle 1/T \rangle$. The parameter q - the so-called entropic index or nonextensivity parameter in Tsallis statistics [97] - is connected to the size of the fluctuations. Namely,

$$q - 1 = \frac{\langle 1/T^2 \rangle - \langle 1/T \rangle^2}{\langle 1/T \rangle^2} \cong \frac{\langle T^2 \rangle - \langle T \rangle^2}{\langle T \rangle^2} , \tag{7}$$

where the second approximate equality holds for sufficiently small fluctuations. When $q = 1$ there are no temperature fluctuations and the exponential formula is restored.

The Lévy type (6) distribution has been observed in inclusive processes [98]. The source of such a behaviour is unknown. An event-by-event analysis of the data will help in understanding this because of the fact that when T fluctuates from event to event, the $\mathrm{p_t}$ distribution in a single event differs from the $\mathrm{p_t}$ distribution averaged over many events. In particular, if the single-event $\mathrm{p_t}$ distribution is given by the exponential formula (5) the averaged one is that of Lévy (6). As shown in Ref. [99], a very large multiplicity of the central Pb–Pb collisions allows one to observe the difference for $q - 1$ as small as 0.05.

Fluctuations in temperature may be studied more quantitatively by using a method proposed and developed in references [100] and [101]. The temperature variance can be found by measuring the event's transverse mass defined as

$$\mu_T = \frac{1}{N}\sum_{i=1}^{N} m_T^i , \tag{8}$$

where N denotes the event's multiplicity and m_T^i is the transverse mass of i-th particle. If the single particle $\mathrm{p_t}$ distribution is of the form given in Eqn. 5, then the event's temperature can also be expressed in terms of μ_T. By measuring μ_T on an event-by-event basis one can get the fluctuation in temperature as the variance, defined as, $\langle T^2 \rangle - \langle T \rangle^2$. However, the

statistical fluctuations due to the finite event multiplicity have to be subtracted from the result. The variance of T because of statistical fluctuations has been estimated in terms of a simple simulation [101] to see how well the subtraction procedure works. It appears that for event multiplicity N as small as 10 the value of $q > 1.05$ can be unambiguously observed provided the single-particle $\mathrm{p_t}$ distribution is indeed described by Eqn. (5).

The temperature fluctuations can also be observed by analyzing the event-by-event $\mathrm{p_t}$ fluctuations by means of the Φ measure [71]. The Φ measure is defined by introducing a single-particle variable $z \stackrel{\mathrm{def}}{=} x - \overline{x}$ with the over-line denoting average over a single particle inclusive distribution. The event variable Z, which is a multi-particle analogue of z, is defined as $Z \stackrel{\mathrm{def}}{=} \sum_{i=1}^{N}(x_i - \overline{x})$, where the summation runs over particles from a given event. Finally, the Φ measure is defined as

$$\Phi \stackrel{\mathrm{def}}{=} \sqrt{\frac{\langle Z^2 \rangle}{\langle N \rangle}} - \sqrt{\overline{z^2}} \; . \tag{9}$$

Following this procedure, $\Phi_{\mathrm{p_t}}$ for fluctuating T was computed in [101]. If $P_{(T)}(\mathrm{p_t})$ denotes the single-particle transverse momentum distribution in events with temperature T which is assumed to be independent of the event's multiplicity N, then, the inclusive transverse momentum distribution turns out to be

$$P_{\mathrm{incl}}(\mathrm{p_t}) = \int_0^\infty \mathrm{dT}\; \mathcal{P}(\mathrm{T})\; \mathrm{P}_{(\mathrm{T})}(\mathrm{p_t}) \; , \tag{10}$$

where $\mathcal{P}(T)$ describes the temperature fluctuations. The N particle transverse momentum distribution in the events of multiplicity N is assumed to be the N product of $P_{(T)}(\mathrm{p_t})$ weighted by the multiplicity and temperature distributions. Then, one finds

$$\langle Z^2 \rangle = \sum_N \mathcal{P}_N \int_0^\infty \mathrm{d}T\; \mathcal{P}(T) \int_0^\infty \mathrm{d}p_T^1\; P_{(T)}(p_T^1) \ldots \int_0^\infty \mathrm{d}p_T^N\; P_{(T)}(\mathrm{p_t}^{\mathrm{N}}) \times \left(\mathrm{p_t}^{1} + \ldots + \mathrm{p_t}^{\mathrm{N}} - \mathrm{N}\overline{\mathrm{p_t}}\right)^2 ,$$

where $\mathcal{P}_N$ is the multiplicity distribution. In the limit $m = 0$, the $\mathrm{p_t}$ distribution (5) acquires a simple exponential form and one easily computes $\overline{z^2}$ and $\langle Z^2 \rangle$. Assuming additionally that the N and T fluctuations are small, one gets a very simple result:

$$\Phi(\mathrm{p_t}) = \sqrt{2}\; \langle \mathrm{N} \rangle\; \frac{\langle \mathrm{T}^2 \rangle - \langle \mathrm{T} \rangle^2}{\langle \mathrm{T} \rangle} = \sqrt{2}\; \langle \mathrm{N} \rangle\; \langle \mathrm{T} \rangle\; (\mathrm{q} - 1) \; . \tag{11}$$

Thus, Φ has a linear dependence on the variance of the temperature. The results for the Φ measure is presented in the following subsection.

These three methods of studying temperature fluctuations can be explored for an unambiguous answer about the event-by-event temperature fluctuations and their origin.

6.2 Temperature fluctuation study in ALICE

It is expected that large number particles will be produced in central Pb–Pb collisions at LHC energies. This will permit to have $\mathrm{p_t}$ distributions of identified particles in every event. Presently this is studied in full AliRoot simulation framework starting with HIJING events [102] for impact parameter between 0–5fm. The combined particle identification algorithm is used to get tracks and particle-id for pions, kaons and protons. Using these results multiplicity and $\mathrm{p_t}$ distribution of reconstructed tracks and identified particles are studied. Figure 6 shows the normalized $\mathrm{p_t}$ distribution of identified pions for (a) 3250 events and (b) one typical event. The solid lines are exponential fits to the data. The inverse slope parameters, which give estimates of the temperature, have been extracted from both the spectra. The slope parameters with the error bar (only from fitting) have been indicated in the figure.

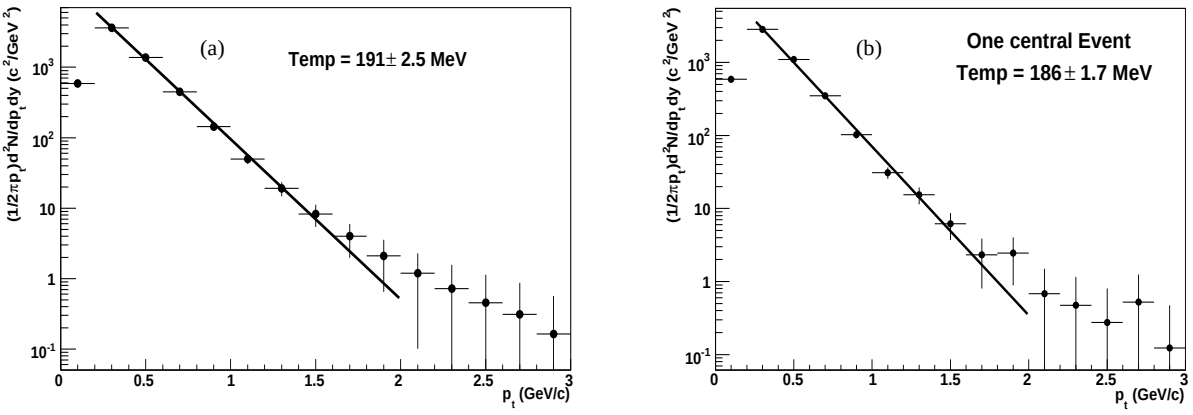

Figure 6: Normalized p_t distribution of pions for (a) 3250 events and (b) a single event for central Pb–Pb collisions at $\sqrt{s}_{NN}$=5.5 TeV. The solid lines are exponential fits to the data points (fits are made within the p_t range of 0.2 GeV/c to 2.0 GeV/c).

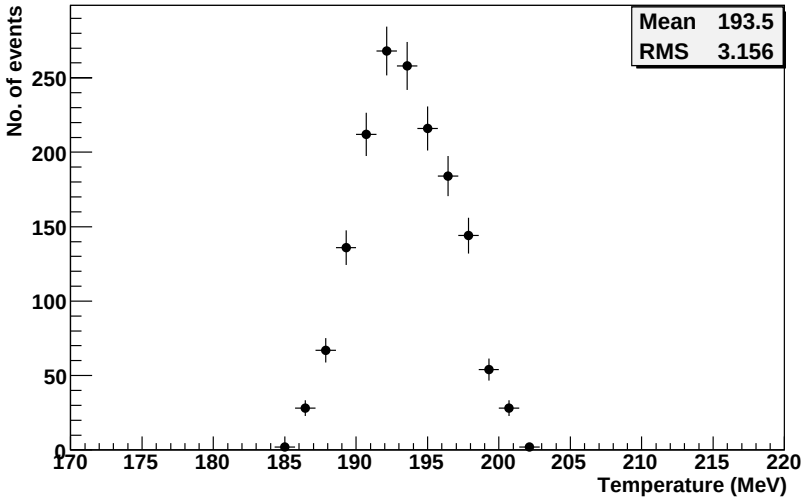

Figure 7: Temperature parameters from the slopes of p_t distribution of pions obtained for single events obtained for central Pb–Pb collisions at $\sqrt{s}_{NN}$=5.5 TeV. The mean value turns out to be 193.5 MeV with an r.m.s. of 3.2 MeV (fits are made within the p_t range of 0.2 GeV/c to 2.0 GeV/c).

Temperatures obtained from single events as in 6(b) for a large number of generated events are plotted in Fig. 7. These distributions can be studied to get information about temperature fluctuations. The nature and amount of fluctuation in the data have to be studied by comparing the data distributions to generated mixed events and information from event generators. The temperature fluctuation extracted from the slopes of fitted p_t distributions provides complimentary information to those obtained from other methods.

7 $\langle p_t \rangle$ fluctuations

The mean transverse momentum of emitted particles in an event is related to the temperature of the colliding system. So the event-by-event fluctuations of average p_t will be sensitive to the temperature fluctuations predicted for QCD phase transitions. The dependence of the $\langle p_t \rangle$ and its fluctuation is predicted to exhibit thermal equilibrium[103].

The fluctuations in $\langle p_t \rangle$ have been measured by NA49, CERES, STAR and PHENIX experiments. NA49 experiment was the first to report Gaussian behavior of the event-by-event mean p_t for central events in Pb–Pb collisions at $\sqrt{s_{NN}}$=17.2 GeV as shown in the left panel of Fig. 8 [18, 17]. Analysis of the mean and sigma of the distribution indicated that the measured fluctuations are consistent with the expectation derived within statistical models of particle production when the effects due to quantum statistics, Coulomb interaction, and resonance decays are taken into account[80, 91].

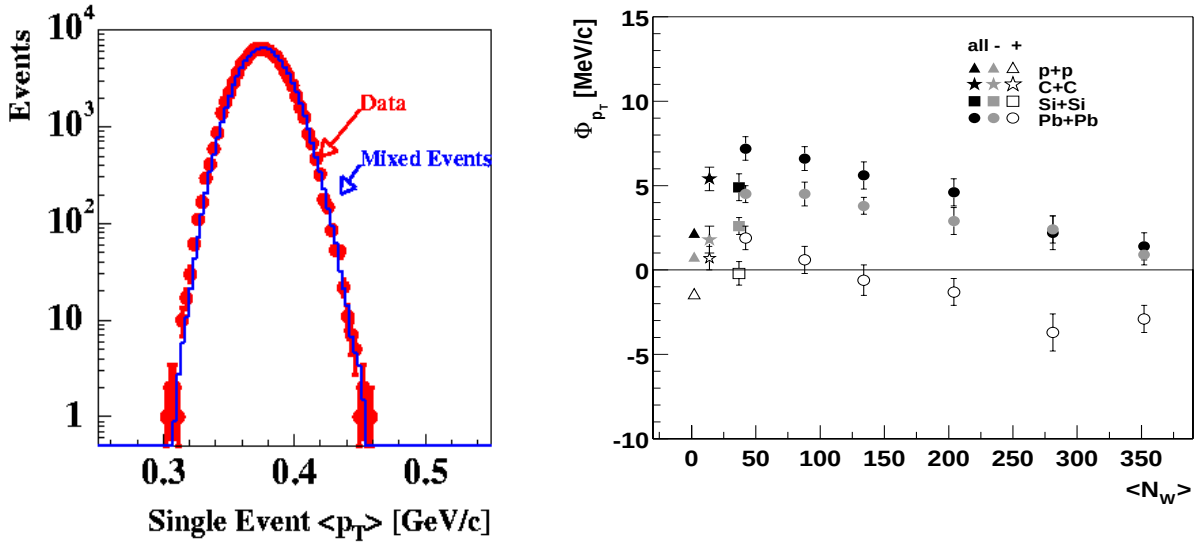

Figure 8: Left panel: the event-by-event fluctuations of the mean transverse momentum for central Pb–Pb collisions at $\sqrt{s_{NN}}$=17.2 GeV as measured by NA49. The solid line indicates the results from mixed events. Right panel: dependence of Φ_{p_t} on the number of wounded nucleons for nucleus–nucleus collisions and inelastic pp interactions at $\sqrt{s_{NN}}$=17.2 GeV. The results indicate significant non-statistical fluctuations for light nuclei as well as peripheral Pb–Pb collisions [17].

Systematic, quantitative study of event-by-event fluctuations is made using the Φ measure of fluctuations [71] or closely related measures [104]. The Φ measure allows us to remove the influence of 'unwanted' volume fluctuations (due to variations in the impact parameter of the collision resulting in turn in variations in the number of nucleons participating in the collision).

It may be noted that the value of Φ_{p_t} for uncorrelated particle production is equal to zero. The values of Φ_{p_t} (the measure of transverse momentum fluctuations) obtained for all inelastic pp interactions and nucleus–nucleus (from C+C to central Pb–Pb) collisions at $\sqrt{s}_{NN}$=17.2 GeV are shown in the right panel of Fig. 8 as a function of the mean number of wounded nucleons [17] at forward rapidities (4.0–5.5). The results indicate a significant non-statistical fluctuations of transverse momentum for light nuclei and peripheral Pb–Pb collisions. Similar results have been reported by PHENIX at RHIC [33, 34]. For central Pb–Pb (Au–Au) collisions significant non-statistical p_t fluctuations are reported at midrapidity by STAR [37, 38] and CERES [32] experiments.

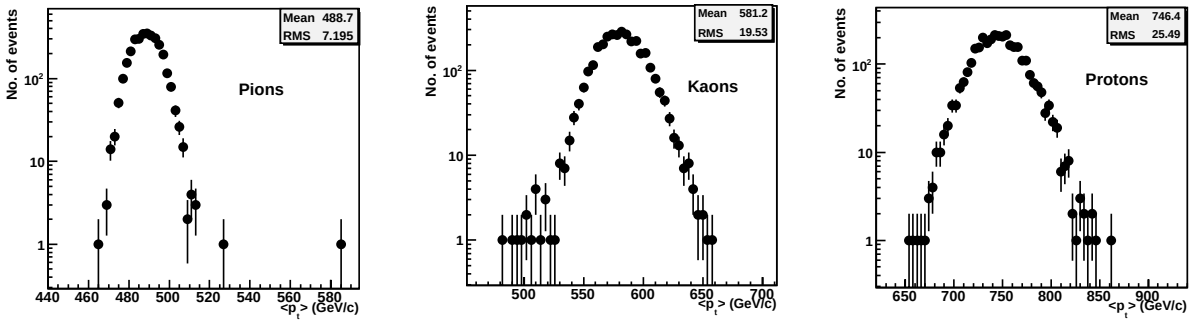

Figure 9: Distributions of the mean transverse momenta for identified pions, kaons and protons in central Pb–Pb collisions at $\sqrt{s}_{NN}$=5.5 TeV.

In ALICE, it will be possible to study fluctuations in mean transverse momenta for identified particles for different colliding systems and system centralities. Using the AliRoot simulated events discussed earlier, mean p_t distributions for identified pions, kaons and protons are obtained for a sample of 3250 events with b¡5fm for Pb–Pb collisions at $\sqrt{s}_{NN}$=5.5 TeV. The distributions are shown in Fig. 9. The mean values of $\langle p_t \rangle$ come out to be 488.7 MeV, 581.2 MeV and 746.5 MeV with r.m.s. values of 7.2 MeV, 19.5 MeV and 25.5 MeV for pions, kaons and protons, respectively. These distributions will be studied in detail along with the mixed events for different fluctuation measures. The values of $\langle p_t \rangle$ and their fluctuations are sensitive to QGP phase transition [2, 3, 4, 5, 6, 7]. It would be interesting to have these values from ALICE and see how it compares to the existing experimental data [105, 106] and theoretical predications.

8 Multiplicity fluctuations

Multiplicity of produced particles is an important quantity to characterize the evolving system in a heavy-ion collision. Fluctuation of particle multiplicity from event to event may thus provide a distinct signal of the phase transition from hadronic gas to QGP phase. Several methods have been proposed to study event-by-event multiplicity fluctuations. A few of these methods are discussed here.

Since the multiplicity distributions for narrow bins in centrality are Gaussians, the WA98[27] and NA49[21] experiments at the SPS have used the normalized variance to quantify multiplicity fluctuations. In a simple participant model the multiplicity of produced particles may be expressed as given in Eqn. 3. The fluctuations in multiplicity may be studied by a simple expression as given in Eqn. 4. Figure 10 shows the minimum bias multiplicity distributions for charged particles and photons in Pb–Pb reactions at $\sqrt{s}_{NN}$=17.2 GeV [27]. The multiplicity distributions for the top 1%, 2% and 5% most central events are shown and fitted to Gaussian distributions. Multiplicity fluctuations of charged particles and photons at various centrality

bins going from central collisions at the left to peripheral at the right are shown in Fig. 11. The results are compared to calculations of participant model and Venus calculations. The experimental data has been found to agree reasonably well with results obtained from a simple participant model that takes into account impact parameter fluctuations. Recent results from NA49 as shown in Fig. 12 show deviations from HIJING calculations [25]. The behaviour of the scaled variance is seen to be similar for positively and negatively charged particles.

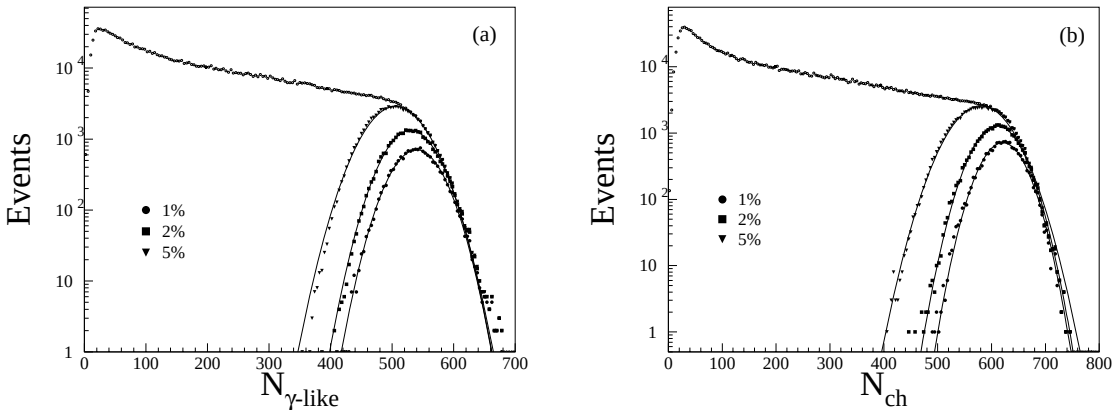

Figure 10: Minimum bias multiplicity distributions of photons and charged particles for Pb–Pb reactions at $\sqrt{s}_{\rm NN}$=17.2 GeV as measured by the WA98 experiment [27]. The distributions for the top 1%, 2% and 5% most central events are also shown and fitted to Gaussian distributions.

Multiplicity fluctuations from the particle multiplicity can be studied for ALICE experimental setup. From the simulated events as described before charged particle multiplicity distribution for central events in ALICE framework is shown in Fig. 13. These distributions will be made for various bins in centrality and compared to results from mixed events as well as participant and other model predictions in order to infer any presence of fluctuations.

9 Fluctuations in particle ratio and strangeness

Early theoretical investigations [107, 108] have suggested that in case of large differences in free enthalpy of the hadronic and the QGP phases, a marked overheating-supercooling fluctuation might set in at temperatures around the critical temperature T_c, which reflects in the broadening of the event-by-event ratio of kaon to pion yields. Recent calculations also suggest that the fluctuation patterns of event-by-event observables may be altered in the vicinity of the QCD phase boundary and especially in the vicinity of tricritical point. It is suggested that strangeness fluctuations, especially fluctuations in K/π ratio, is sensitive to QCD phase transitions.

Both the NA49 experiment at SPS and STAR experiment at RHIC have studied event-wise kaon to pion ratio in detail. Both the experiments are well suited for event-by-event measurement of particle ratios. Recent analysis of event-by-event $[K^+ + K^-]/[\pi^+ + \pi^-]$ and $[\mathrm{p} + \bar{\mathrm{p}}]/[\pi^+ + \pi^-]$ have been performed for Pb–Pb collisions at fixed beam energies of 20, 30, 40, 80 and 158 AGeV by the NA49 collaboration [109, 110, 111, 112]. At all five available beam energies the 3.5% most central Pb–Pb collisions were selected based on projectile spectator energy. The distributions of the particle ratios of kaons to pions and protons to pions at 20, 40 and 158 AGeV are shown in Figs. 14 and 15 [112, 113], respectively. The contribution due to finite number fluctuations in the particle multiplicities and effects of detector resolution are estimated using the mixed event technique. The mixed events are then subjected to the same fitting

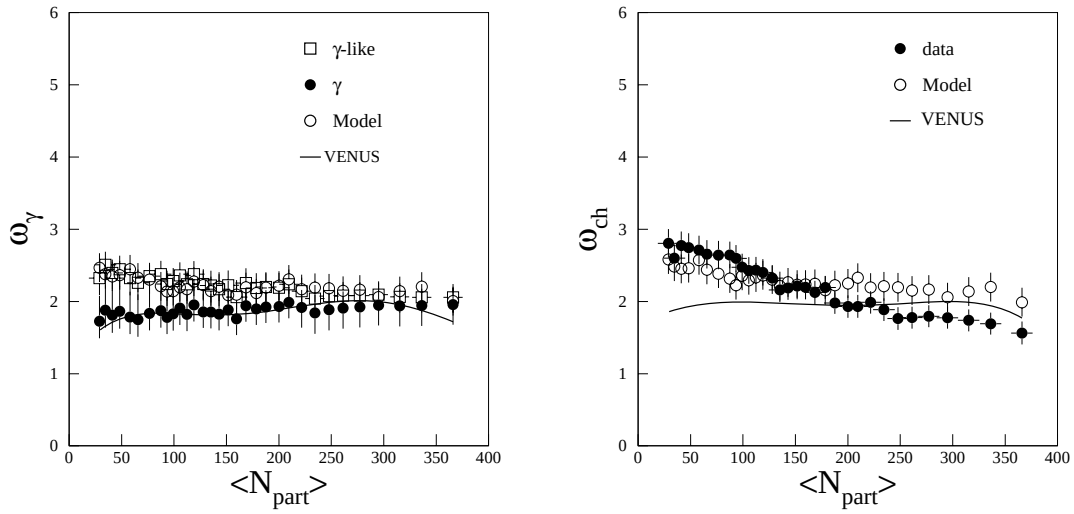

Figure 11: Multiplicity fluctuations of photons and charged particles as a function of number of participants for Pb–Pb collisions at $\sqrt{s}_{\rm NN}$=17.2 GeV from WA98 experiment [27]. Data from the experiment are compared to calculations from participant model and those from VENUS event generator.

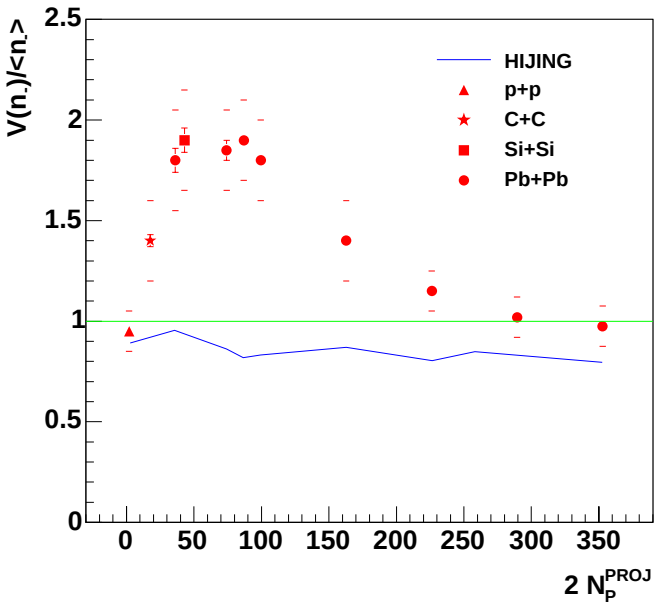

Figure 12: The scaled variance of multiplicity distributions for negatively charged hadrons on the number of projectile participants measured in various reactions at $\sqrt{s}_{\rm NN}$=17.2 GeV by the NA49 experiment [25]. Results obtained within the string-hadronic model HIJING are shown by the solid line.

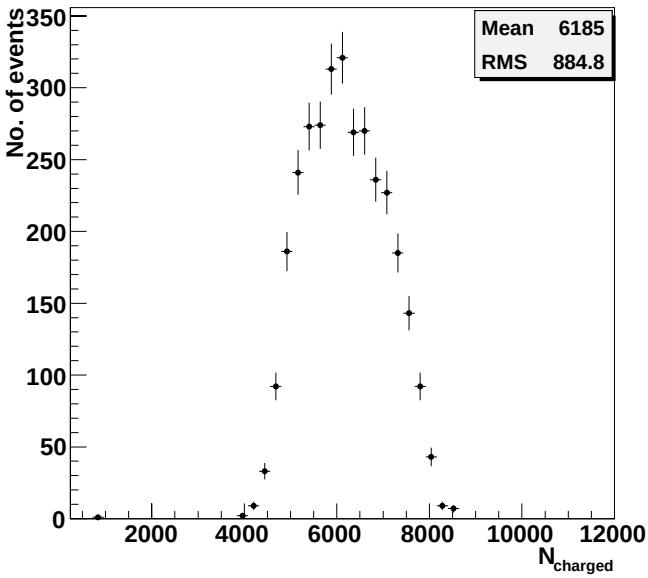

Figure 13: The event-by-event multiplicity distribution of charged particles for simulated Pb–Pb events at $\sqrt{s}_{\rm NN}$=5.5 TeV.

procedure as the real events.

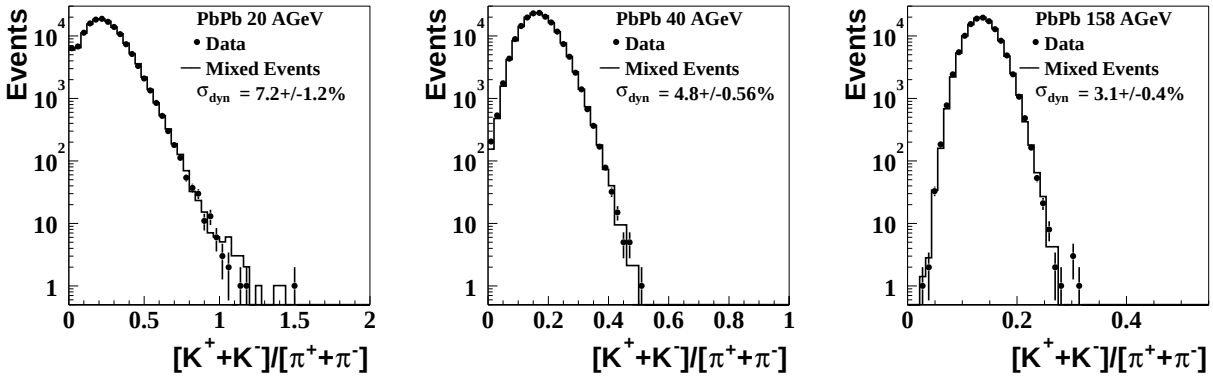

Figure 14: Distributions of the event-by-event $[K^+ + K^-]/[\pi^+ + \pi^-]$ ratios for data (points) and mixed events (histograms) for central (top 3.5%) Pb–Pb collisions at 20, 40, 158 AGeV[109, 110, 111, 112].

For each data set, an estimation of the dynamical fluctuations may be made from the widths of the the distribution of particle ratios in real data compared to those of the corresponding mixed events. This is denoted by:

$$\sigma_{\rm dyn} = sign(\sigma^2_{\rm data} - \sigma^2_{\rm mixed})\sqrt{|\sigma^2_{\rm data} - \sigma^2_{\rm mixed}|}. \quad (12)$$

Figure 16 shows the energy dependence of the event-wise dynamical fluctuations of the $[K^+ + K^-]/[\pi^+ + \pi^-]$ ratio (left panel) and the $[\rm p + \bar{p}]/[\pi^+ + \pi^-]$ ratio (right panel) [112, 113]. Fluctuations of the K/π ratio are positive and decrease with beam energy. The distributions of the $[\rm p + \bar{p}]/\pi$ ratio shows that the width in case of the data is smaller than those of the mixed events. This gives rise to negative dynamical fluctuations which can be understood by considering resonance decays for pions and protons. The magnitude of the negative fluctuation signal in the

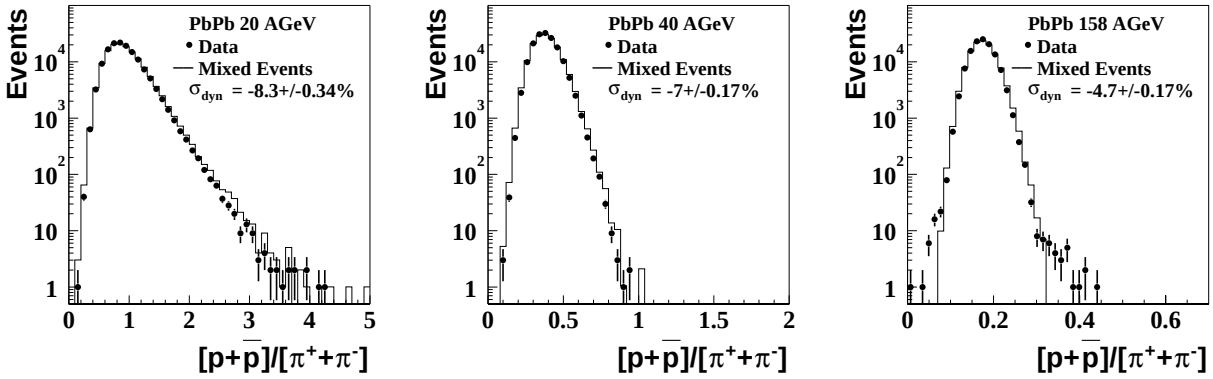

Figure 15: Distributions of the event-by-event $[\mathrm{p}+\bar{\mathrm{p}}]/[\pi^+ + \pi^-]$ ratios for data (points) and mixed events (histograms) for central (top 3.5%) Pb–Pb collisions at 20, 40, 158 AGeV[109, 110, 111, 112].

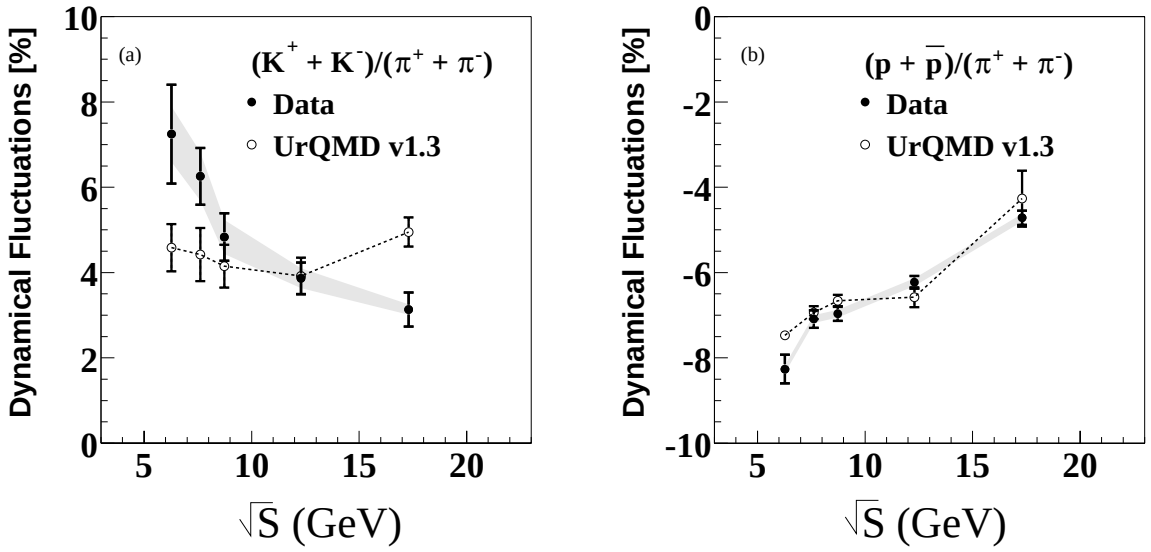

Figure 16: Energy dependence of the event-by-event fluctuation signal of (a) the $[K^+ + K^-]/[\pi^+ + \pi^-]$ ratio, and (b) the ratio of $[\mathrm{p}+\bar{\mathrm{p}}]/[\pi^+ + \pi^-]$. The systematic errors of the measurements are shown as gray bands.

$[p+\bar{p}]/\pi$ channel may be related to the relative contribution of resonance decay products in the final state of the collision.

The data have been compared to a string-hadronic cascade model UrQMD [114]. In this model, by construction, no fluctuations due to a potential phase transition are present, while resonance decays are included as well as effects of correlated particle production due to quantum number and energy–momentum conservation laws. The energy dependence of the event-by-event $[p+\bar{p}]/\pi$ ratio in UrQMD closely matches the energy dependence observed in the data, as shown in Fig. 16. This lends further support to interpreting the negative fluctuation signal resulting from resonance decays. With fluctuations of the event wise K/π ratio, the energy dependence of the signal cannot be reproduced in the cascade model. Since the relative contribution of resonances changes dramatically with incident beam energy, one concludes that in the K/π ratio resonances do not give a significant contribution to the fluctuation signal. The finite fluctuation signal in the UrQMD model can be attributed to correlated particle production due to conservation laws.

The STAR experiment at RHIC has also performed a relevant study on the event wise fluctuations of the K/π ratio for Au–Au collisions at $\sqrt{s_{\rm NN}} = 62.4$ GeVand $\sqrt{s_{\rm NN}} = 200$ GeV [40]. Figure 17(a) shows the distribution of K/π ratio for top 5% central Au–Au collisions at 200 GeV. The distributions from real and mixed events are superimposed to help comparing the widths of the distributions. STAR experiment also measured the K^+/π^+ and K^-/π^- ratios and obtained the corresponding measures of dynamical fluctuations: $\sigma_{\rm dyn} = 3.06 \pm 0.88\%$ and $\sigma_{\rm dyn} = 3.61 \pm 0.67\%$ respectively.

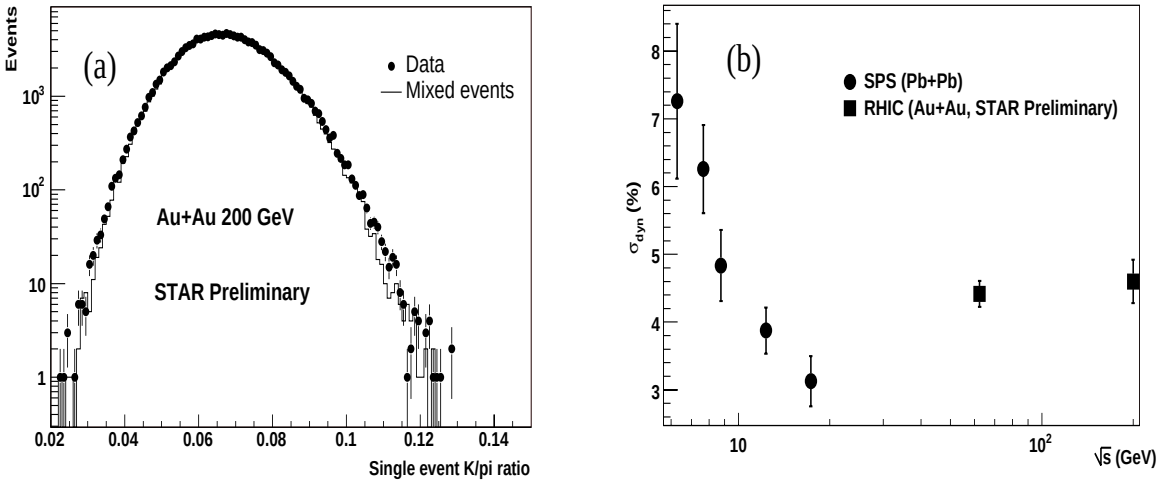

Figure 17: (a) Distribution of K/π ratio from data and mixed events from Au–Au at 200 GeV. The calculated dynamical fluctuation comes out to be $\sigma_{\rm dyn} = 4.6 \pm 0.038\%$. (b) Excitation funciton for $\sigma_{\rm dyn}$ compiled from AGS to RHIC energies.

In Fig. 17(b) the energy dependence (excitation function) of $\sigma_{\rm dyn}$ is plotted [40] from AGS to RHIC energies. One observes that the observed dynamical fluctuations take their maximum value for the lowest SPS energy and then decreases towards the highest SPS energy [112, 113]. The measured dynamical fluctuations increase as one goes to RHIC energies.

Fluctuations in particle ratio and strangeness can be carefully studied in ALICE. Using the simulated events as discussed earlier, ratio of kaons to pions and protons to pions are plotted in Fig. 18 for central rapidity ($-0.9 < \eta < 0.9$). The K/π ratio has a mean of 0.073 and r.m.s. of 0.005 whereas the ratio of p/π has a mean of 0.054 with a r.m.s. value of 0.004. These distributions will be investigated in detail using data from experiment, mixed events and generated events.

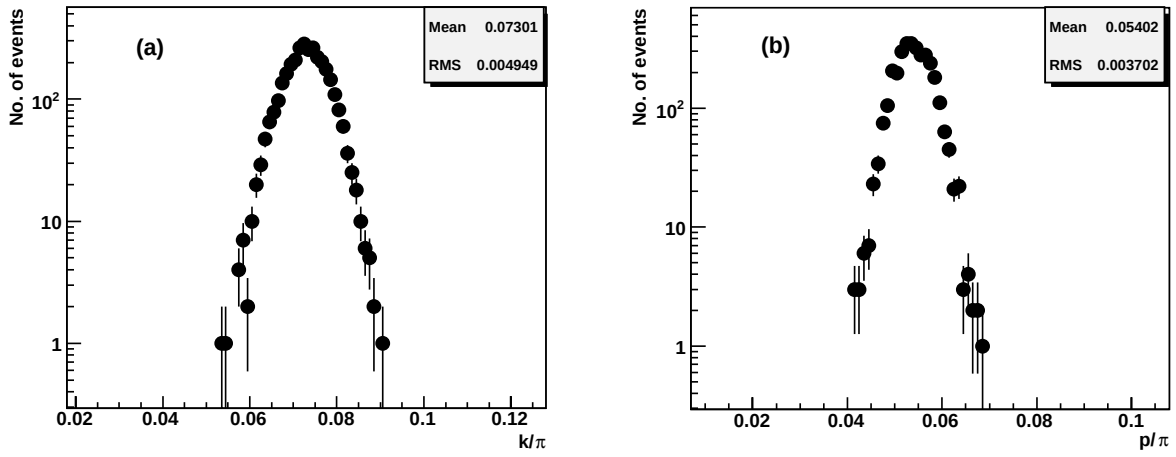

Figure 18: Ratios of event-by-event (a) kaons to pions and (b) protons to pions in simulated central Pb–Pb events at $\sqrt{s}_{\rm NN}$=5.5 TeV within the ALICE acceptance for central detectors ($0.9 < \eta < 0.9$).

10 Fluctuations of conserved quantities

The major advantage [85, 86] of studying fluctuations of conserved quantities is that their relaxation time in a thermal system is much slower than that of non-conserved quantities, since there is no process which can generate conserved quantum numbers from the vacuum or via particle collisions. A detailed discussion of the relaxation time of fluctuation of conserved quantities is provided in Ref. [69]. As a consequence, the fluctuation of conserved charges such as net electric charge or baryon number may provide information from deep inside the system created in these collisions, where possibly a system with different degrees of freedom existed.

In addition, the fluctuations of baryon number and charge are sensitive to the fractional charge to baryon number carried by the quarks in the QGP, and may provide therefore an important signature for the existence of a deconfined phase as discussed in detail below. Of course, global charge conservation leads to vanishing fluctuations once the entire system is considered. Appropriate corrections have to be applied while considering only a fraction of the produced particles.

Fluctuation in electric charge can be simpley expressed by

$$\left\langle (\delta Q)^2 \right\rangle = \left\langle Q^2 \right\rangle - \langle Q \rangle^2 \,, \tag{13}$$

where Q is the net charge measured in the acceptance. For a system of several particle species i with charges q_i and multiplicities n_i, one writes,

$$Q = \sum_i q_i n_i, \langle Q \rangle = \sum_i q_i \langle n_i \rangle \,,$$

$$\text{and} \quad \left\langle (\delta Q)^2 \right\rangle = \sum_i (q_i)^2 \langle n_i \rangle + \sum_{i,k} c^{(2)}_{ik} \langle n_i \rangle \langle n_k \rangle q_i q_k, \tag{14}$$

where $c^{(2)}_{i,k}$ are the normalized two-particle correlation functions given by:

$$c^{(2)}_{ii} = \frac{\langle n_i(n_i-1) \rangle}{\langle n_i \rangle^2} - 1, \tag{15}$$

$$c^{(2)}_{ik} = \frac{\langle n_i n_k \rangle}{\langle n_i \rangle \langle n_k \rangle} - 1 \quad \text{if} \qquad \text{i} \neq \text{k} \,. \tag{16}$$

Correlations introduced by particle interactions, such as resonances affect the fluctuations [115, 116, 117]. The fluctuation measures may also be used to measure particle correlations in these systems. If, on the other hand, the particles are uncorrelated, the second term of Eqn. 14 vanishes.

In a thermal system the charge fluctuations are given by the charge susceptibility:

$$VT\chi_Q = -T\frac{\partial^2 F}{\partial \mu_Q^2}, \tag{17}$$

which for a macroscopic system measures the response to external electric fields.

In the case of a free uncorrelated pion gas the charge fluctuations are then

$$\left\langle (\delta Q)^2 \right\rangle_{\pi-\mathrm{gas}} = \langle N_+ \rangle + \langle N_- \rangle = \langle N_{\mathrm{ch}} \rangle \,, \tag{18}$$

where N_{ch} is the total number of charged particles. For a QGP, on the other hand, assuming uncorrelated quarks and gluons, one obtains

$$\left\langle (\delta Q)^2 \right\rangle_{\mathrm{QGP}} = q_u^2 \langle N_u + N_{\bar{u}} \rangle + q_d^2 \langle N_d + N_{\bar{d}} \rangle = \frac{5}{18} \langle N_q \rangle \,, \tag{19}$$

where N_q is the total number of quarks in the system. The contribution of heavy quarks can be neglected since their yield is suppressed.

Note that in the case of QGP formation, the charge fluctuations depend on the square of the fractional charge of the quarks. In order to expose the dependence on the fractional charge, one should divide the charge fluctuations by the number of particles or the entropy carried by the system. A good measure for the entropy is the number of charged particles in the final state and thus the observable

$$\frac{\langle (\delta Q)^2 \rangle}{\langle N_{\mathrm{ch}} \rangle} \tag{20}$$

should be sensitive to the fractional charges of the QGP. Indeed, using $N_{\mathrm{ch}} \simeq N_q + N_g$ (which follows from the assumption of entropy conservation), where N_g is the number of gluons (for detailed discussion see Ref. [86]) one obtains

$$\frac{\langle (\delta Q)^2 \rangle}{\langle N_{\mathrm{ch}} \rangle}_{\mathrm{QGP}} \simeq 0.2 \tag{21}$$

$$\text{and} \quad \frac{\langle (\delta Q)^2 \rangle}{\langle N_{\mathrm{ch}} \rangle}_{\pi-\mathrm{gas}} = 1 \tag{22}$$

for the pion gas. Correcting for quantum statistics and taking hadronic resonances into account, which introduce correlation terms (see Eqn. 14), for the hadron gas one gets,

$$\frac{\langle (\delta Q)^2 \rangle}{\langle N_{\mathrm{ch}} \rangle}_{\mathrm{hadron-gas}} \simeq 0.75. \tag{23}$$

On the quark–gluon plasma side, one can consult Lattice QCD calculations, available for the charge fluctuations as well as for the entropy as discussed earlier. In this case one finds [86]

$$\frac{\langle (\delta Q)^2 \rangle}{\langle N_{\mathrm{ch}} \rangle}_{\mathrm{QGP}} \simeq 0.25 - 0.4, \tag{24}$$

where the uncertainty is due to the way in which is related to the number of charged particles (see Refs. [86, 85]).

To access this observable in the experiment it is not sufficient to simply measure the charge fluctuations and the number of charged particles separately. As can be seen from Eqn. 14 the magnitude of the charge fluctuations scales with the number of charged particles in the

system, i.e. it scales with the system size. Therefore fluctuations of the system size, or impact parameter fluctuations, which are present even if centrality cuts are applied, will contribute to the charge fluctuations. Of physical interest, however, are the charge fluctuations due to density fluctuations. Thus, the effect of volume fluctuations has to be removed by an appropriate choice of observables.

It has been shown in Ref. [73] that the Φ_q measure is less sensitive to the biasing effects than the originally proposed $\tilde{D}$ measure. Both are sensitive to the hypothetical suppression of charged fluctuations due to QGP creation. Similar information may also be obtained by measuring balance functions described later in this section.

10.1 Net charge fluctuations

Recent suggestions [85, 86] that event-by-event fluctuations of electric charge in high-energy A–A collisions may provide information on the state of matter at the early stage of the collision triggered corresponding experimental studies. The first results [20, 35, 36, 37] indicate that the net electric charge fluctuations are governed by the conservation of electric charge [73, 74, 119] and that additional contributions, if any, are small. Event-by-event fluctuations of the electric charge are expected to be suppressed as a consequence of deconfinement [86, 85]. Estimates of the magnitude of the charge fluctuations indicate that they are much smaller in a quark–gluon plasma than in hadron gas.

Different measures for studying charge fluctuations are applied by the experiments NA49, PHENIX and STAR. One of them is the $\Delta\Phi_q$ which is used by the NA49 experiment and is defined as: $\Delta\Phi_q = \Phi_q - \Phi_{q,GCC}$. Φ_q is the established measure Φ of the event-by-event fluctuations [71, 73] and $\Phi_{q,GCC}$ is the value of Φ_q corresponding to a scenario where particles are correlated only by global charge conservation and is given by [73] $\Phi_{q,GCC} = \sqrt{1-P} - 1$. $P = \langle N_{\rm ch}\rangle / \langle N_{\rm ch}\rangle_{\rm tot}$, with $\langle N_{\rm ch}\rangle$ and $\langle N_{\rm ch}\rangle_{\rm tot}$ being the mean charged multiplicity in the detector acceptance and in the full phase space respectively.

In Fig. 19 the Φ_q and $\Delta\Phi_q$ values are plotted as a function of $\langle N_{\rm ch}\rangle / \langle N_{\rm ch}\rangle_{\rm tot}$ for central Pb–Pb collisions at 20–158 AGeV [22]. The main trend observed in the data is a monotonic decrease with increasing fraction of accepted particles. This is approximately reproduced by introducing global charge conservation as the only source of correlations. One can notice from fig. 19(b) that the measured $\Delta\Phi_q$ values are close to zero as expected for a gas of pions correlated only by global charge conservation [74]. The results of a model which incorporates intermediate resonances [73, 22] show that the decay of the ρ meson may increase the initial QGP charge fluctuations to $\Delta\Phi_q \approx 0$ and thereby completely masking a possible QGP signal at SPS energies.

At RHIC, both PHENIX and STAR experiments have studied net charge fluctuations fr Au–Au interactions at $\sqrt{s_{\rm NN}}$=130 GeV . In the PHENIX experiment, the fluctuations were studied in the variable, $Q = n_+ - n_-$ [35] with a variance:

$$V(Q) = \langle Q^2\rangle - \langle Q\rangle^2 = n_{\rm ch}, \tag{25}$$

The experimental data behave in an almost stochastic matter, and there is a reasonable agreement between data and RQMD calculations, including the effects of global charge conservation and neutral hadronic resonances decays. Furthermore, the data show no centrality dependence [35].

The STAR experiment has discussed the fluctuations as the difference of the number of positive and negative particles in a fixed rapidity range, defined as [104]:

$$\nu_{+-} = \langle (\frac{N_+}{\langle N_+\rangle} - \frac{N_-}{\langle N_-\rangle})^2\rangle. \tag{26}$$

The dynamical fluctuations are defined as $\nu_{+-,\rm dyn} = \nu_{+-} - \nu_{+-,\rm stat}$, where

$$\nu_{+-,\rm stat} = \frac{1}{\langle N_+\rangle} + \frac{1}{\langle N_-\rangle}. \tag{27}$$

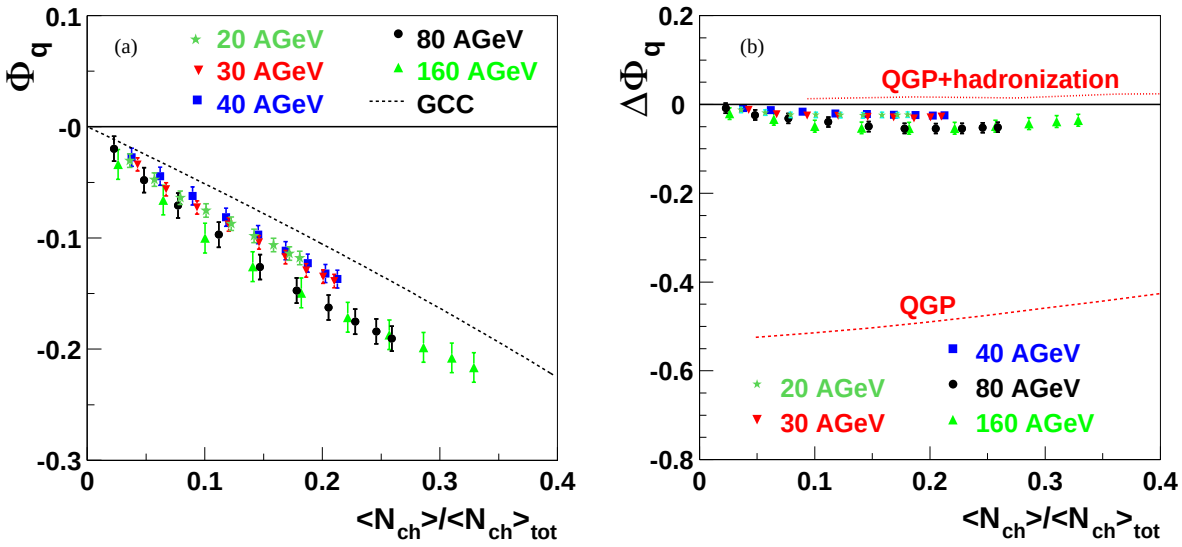

Figure 19: The dependence of (a) Φ_q and (b) $\Delta\Phi_q$ on the fraction of accepted particles for central Pb–Pb collisions at 20–158 AGeV. In (a) the dashed line shows the dependence expected for the case where the only source of particle correlations is the global charge conservation. In (b) the prediction for the ideal QGP is indicated by the dashed curve (QGP), whereas the prediction for the QGP including hadronization and resonance decay is shown by the dotted curve (QGP+hadronization)

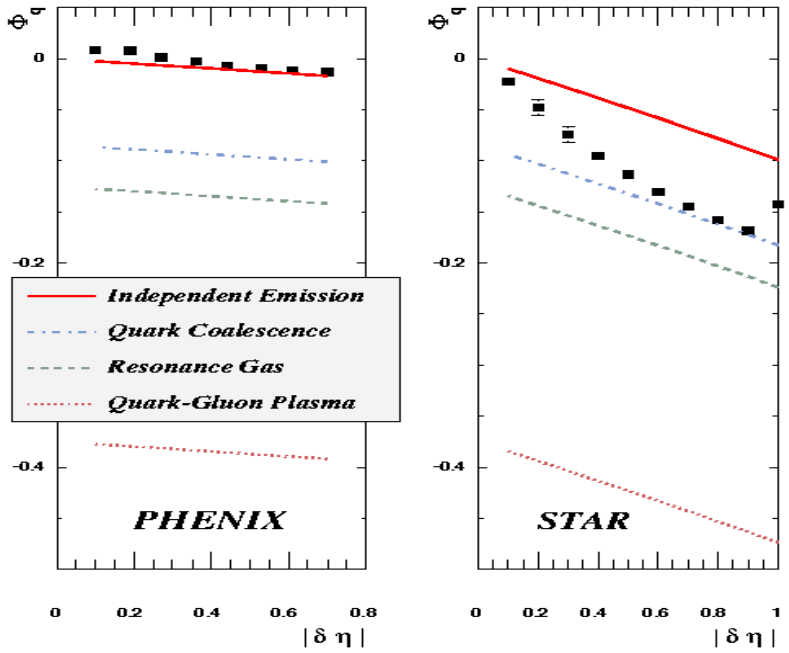

Figure 20: Results for charge fluctuation calculations [120] obtained for PHENIX [35] and STAR [36] experiments for Au–Au collisions at $\sqrt{s_{\rm NN}}$=130 GeV .

The dynamical fluctuations of the 5% most central collisions are obtained as [36]:

$$\nu_{+-,\mathrm{dyn}} = -0.00236 \pm 0.00006(\mathrm{stat}) \pm 0.00012(\mathrm{syst})$$

This was compared to results from PHENIX [35] by modifying the expression of $v(Q)$ in order to take acceptance effect into account [104]:

$$\nu_{+-,\mathrm{stat}} = \frac{4}{N_+ + N_-} \cdot (v(Q) - 1), \tag{28}$$

which gives:

$$\nu_{+-,\mathrm{dyn}} = -0.0018 \pm 0.0004(\mathrm{stat}) \pm 0.0009(\mathrm{syst})$$

in agreement with the value measured by the STAR collaboration for 11% central collisions. A comparison of the STAR measurements with thermal models [86, 121] indicates fluctuations at a level that might be expected if the Au–Au system behaved like a resonance gas. Although the size of the fluctuations is larger than expected for a quark–gluon gas, limitations of the model used [36] prevent a conclusion on the existence or not of a quark–gluon plasma phase based on the above results.

Figure 20 gives a compilation of net charge fluctuation results from PHENIX and STAR experiment [120] for Au–Au collisions at $\sqrt{s_{\mathrm{NN}}}$=130 GeV in terms of Φ_q variable. Superimposed on the plots are curves representing the predictions for independent particle emission, quark coalesence, resonance gas and QGP after correcting for acceptances of the detectors. The results are closer to independent particle emission and the resonance gas scenarios.

11 Balance functions

One important measure of correlations, the Balance function (BF), has been introduced by Bass, Danielewicz and Pratt [122]. It measures the correlation of the oppositely charged particles produced during a heavy ion collision, and its width can be related to the time of hadronization. The BF is derived from the charge correlation function that was used to study the hadronization of jets in pp collisions at the ISR [123] and e^+e^- annihilations at PETRA [124]. The first results on the BF were obtained for Au–Au collisions by the STAR collaboration at RHIC [42].

The motivation for studying the BF comes from the idea that hadrons are produced locally as oppositely charged particle pairs. Particles of such a pair are separated in rapidity due to the initial momentum difference and secondary interactions with other particles. Particles of a pair created earlier are separated further in rapidity because of the expected large initial momentum difference and the long lasting rescattering phase. On the other hand, oppositely charged particle pairs that were created later are correlated within a smaller interval Δy of the relative rapidity. Our aim is to measure the degree of this separation of the balancing charges and to find possible indications for delayed hadronization.

The BF can be studied as a function of several parameters in order to gain insight about different physics mechanisms. The BF can be studied as a function of the relative pseudo-rapidity difference for all charged particles, and can be written as $B(\Delta\eta)$ [42, 23]. In addition, there is the possibility to study the BF for different particle species. For example, one can analyze the correlations between oppositely charged pions, kaons (and thus extend the method to a strange-anti strange correlation study) or even protons (extension to baryon-antibaryon study) [39]. By performing this study, one could gain insight about the possible different mechanisms that are important in the creation process for these species. Furthermore the BF can be studied as a function of the azimuthal angle ϕ as proposed in [125] and thus translate the correlation function into a measure of transverse flow. By doing that one will be able to quantify the transverse flow for different particle species (pions, kaons, protons) by analyzing the $B(\Delta\phi)$ for identified oppositely charged particles. Finally, the BF can be studied as a function of the invariant relative momentum Q_{inv} [126]. This variable is suggested to yield a clearer insight for

interpreting the physics of the balancing charges as well as providing a better illumination of the distorting effects which are subject of this study.

In order to examine the η correlation of charged particles the BF is defined as a difference of the correlation function of oppositely charged particles and the correlation function of like-charge particles normalized to the total number of particles. The general definition of the BF reads [122]:

$$B(P_2|P_1) = \frac{1}{2}\Big[\frac{N(b,P_2|a,P_1) - N(a,P_2|a,P_1)}{N(a,P_1)} + \frac{N(a,P_2|b,P_1) - N(b,P_2|b,P_1)}{N(b,P_1)}\Big], \qquad (29)$$

where a and b could be different kinds of particles, whereas P_1 and P_2 could be intervals in pseudo-rapidity. For example a could refer to all negative particles and b to all positive particles. Alternatively P_2 could be an interval of the relative pseudo-rapidity $\Delta\eta = |\eta_b - \eta_a|$ of the oppositely charged particles, whereas P_1 could be the interval of the pseudo-rapidity of the produced particles that is covered by the detector. In the numerator, $N(b,P_2|a,P_1)$ represents a conditional probability of observing a particle of type b in bin P_2 given the existence of a particle of type a in bin P_1. The terms $N(b,P_2|a,P_1)$, $N(a,P_2|a,P_1)$, $N(a,P_2|b,P_1)$ and $N(b,P_2|b,P_1)$ are calculated using pairs from each event and the resulting values are summed over all events. For example, the term $N(b,P_2|a,P_1)$ is calculated by counting all possible combinations of a positive particle in P_2 and a negative particle in P_1 in an event and summing the number of combinations over all events. The other three terms are calculated analogously. The terms $N(a,P_1)$ and $N(b,P_1)$ are the total number of negative and positive particles, respectively, that are within the studied pseudo-rapidity interval P_1, summed over all events.

In this case, a and b are the negative and positive particles respectively that are within the pseudo-rapidity interval P_1 and have a pseudo-rapidity difference $\Delta\eta$. Thus, with this formulation, the definition of the BF takes the following form:

$$B(\Delta\eta) = \frac{1}{2}\Big[\frac{N_{+-}(\Delta\eta) - N_{--}(\Delta\eta)}{N_-} + \frac{N_{-+}(\Delta\eta) - N_{++}(\Delta\eta)}{N_+}\Big]. \qquad (30)$$

The most interesting property of the BF is its width. Early stage hadronization is expected to result in a broad BF, while late stage hadronization leads to a narrower distribution [122]. The width of the BF can be characterized by the weighted average $\langle\Delta\eta\rangle$:

$$\langle\Delta\eta\rangle = \sum_{i=0}^{k}(B_i \cdot \Delta\eta_i)/\sum_{i=0}^{k} B_i, \qquad (31)$$

where i is the bin number of the BF histogram.

In the following, the corresponding results from both SPS (NA49) and RHIC (STAR) experiments are discussed and reference will be made to the most established theories that provide both qualitative and quantitative interpretation to these results. Finally, extension of the method to LHC energies will be presented.

11.1 System size and centrality dependence

The recent results that are included in this section come from the analysis of pp, C+C, Si+Si and Pb–Pb collisions at $\sqrt{s_{\rm NN}}$=17.2 GeV and $\sqrt{s_{\rm NN}}$=8.8 GeV (NA49-SPS) [23] and the corresponding analysis of Au–Au collisions at $\sqrt{s_{\rm NN}}$=130 GeV (STAR-RHIC) [42]. The conditions and details concerning the analysis procedure are described in [42, 23]. The BF for each centrality class was also calculated for mixed events produced with the shuffling mechanism to estimate the maximum possible value of the width of the BF while retaining the constraint of charge conservation [42, 23].

In order to further investigate the origin of the system size and centrality dependence of the BF, the HIJING event generator [102] was used to generate A+A collisions for the highest SPS and the corresponding RHIC energy. Fig. 21(a) shows the dependence of the width $\langle\Delta\eta\rangle$ of the

BF on the mean number of wounded nucleons $\langle N_W \rangle$ for the highest SPS energy. The results for pp, C+C and Si+Si collisions are also included. The width decreases monotonically with $\langle N_W \rangle$. On the other hand, the width of the BF from both HIJING and shuffled data does not show any clear dependence on centrality [23]. Fig. 21(b) shows the dependence of the width $\langle \Delta\eta \rangle$ of the BF on the mean number of wounded nucleons $\langle N_W \rangle$ for the second SPS energy ($\sqrt{s_{\rm NN}}$=8.8 GeV). The width decreases monotonically with $\langle N_W \rangle$ also for this energy. On the other hand, the width of the BF from shuffled data does not show any clear dependence on centrality.

The results from the nalysis performed for Au–Au collisions at $\sqrt{s_{\rm NN}}$=130 GeV by the STAR collaboration at RHIC [42] are plotted in Fig. 22. The width of the BF decreases from peripheral to central collisions by $17 \pm 3\%$ for the NA49 data, whereas for the higher energy STAR data the corresponding decrease is of the order of $14 \pm 2\%$ [23]. It needs to be mentioned that there should be no direct comparison between the actual values of the widths for the two experiments since first of all the BF is studied in different pseudorapidity intervals and the analysis procedure (event and track quality cuts) is not identical. Thus, the proposed way to compare the two effects is simply by studying the slope.

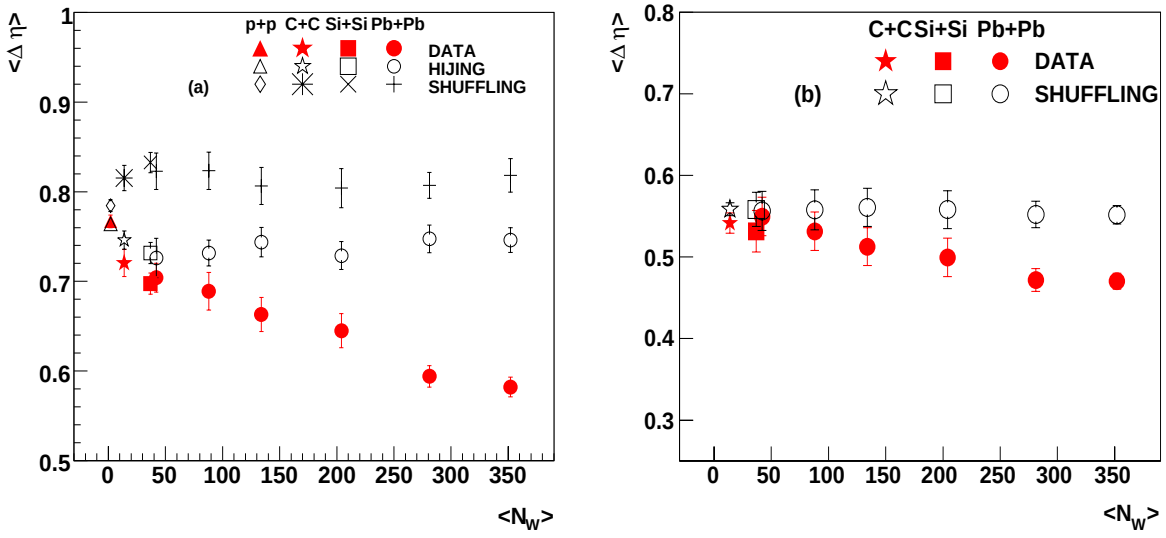

Figure 21: The dependence of the width of Balance function on the number of wounded nucleons for pp, C+C, Si+Si and Pb–Pb collisions at (a) $\sqrt{s_{\rm NN}}$=17.2 GeV, and (b) $\sqrt{s_{\rm NN}}$=8.8 GeV, as measured by the NA49 experiment, shown for different cases.

11.2 Pseudo-rapidity dependence

Furthermore, an attempt to study the centrality dependence of the width for both energies in the NA49 setup was made to study BF in different pseudo-rapidity intervals. This was done in order to test the theory upon which the BF is based [122], and which describes the hadronization process mainly as the creation of oppositely charged particles at the same location in space-time. In order to perform this study, the pseudo-rapidity interval that was analyzed was shifted towards the forward region. In particular, the new intervals are $3.3 \leq \Delta\eta \leq 4.7$ and $4.0 \leq \Delta\eta \leq 5.4$ for $\sqrt{s_{\rm NN}} = 8.8$ and $\sqrt{s_{\rm NN}}$=17.2 GeV respectively while the old ones were $1.8 \leq \Delta\eta \leq 3.2$ and $2.5 \leq \Delta\eta \leq 3.9$.

Figure 23 shows the dependence of the width $\langle \Delta\eta \rangle$ of the BF on the mean number of wounded nucleons $\langle N_W \rangle$ for the $\sqrt{s_{\rm NN}}$=17.2 GeV (left plot) and for the $\sqrt{s_{\rm NN}}$=8.8 GeV (right plot) in

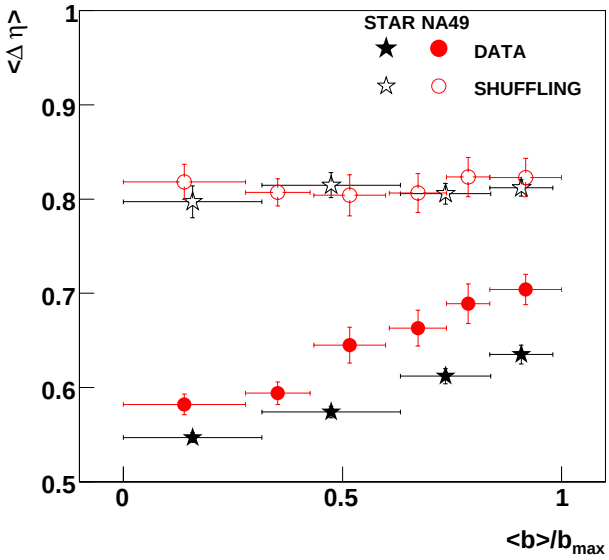

Figure 22: The dependence of the width of BF on the normalized impact parameter $b/b_{\max}$, as measured by NA49 for Pb–Pb collisions at $\sqrt{s_{\rm NN}}$=17.2 GeV and by STAR for Au–Au collisions at $\sqrt{s_{\rm NN}}$=130 GeV.

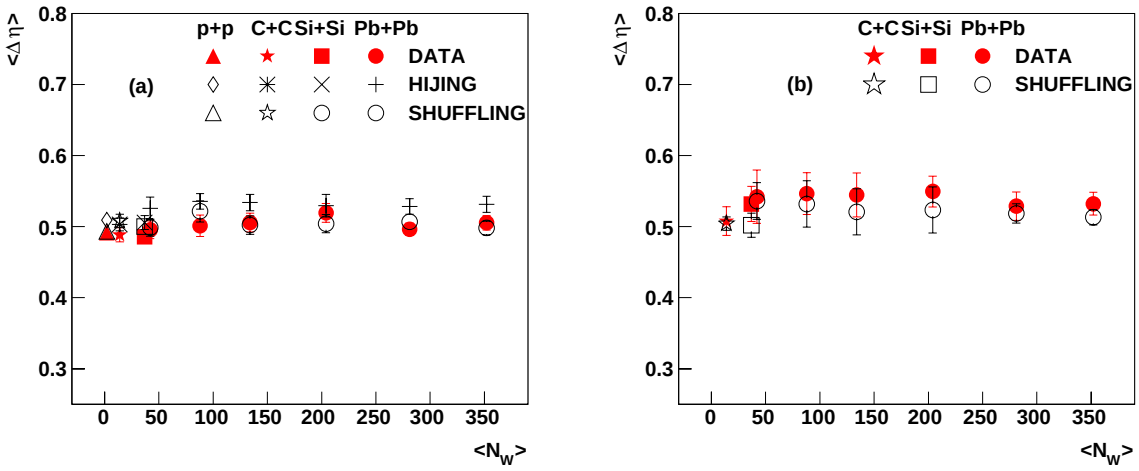

Figure 23: The dependence of the widths of BF on the number of wounded nucleons for pp, C+C, Si+Si and Pb–Pb collisions at $\sqrt{s_{\rm NN}}$=17.2 GeV (left plot) and $\sqrt{s_{\rm NN}}$=8.8 GeV (right plot) in the forward pseudo-rapidity region as measured by the NA49 collaboration [26].

this forward region. The width of the BF for all data samples (real, shuffled and HIJING data) does not show any clear dependence on centrality.

The main conclusion from this study is that the effect is located in the midrapidity region. This can be explained if one takes into account the fact that the width of the BF is a measure of correlations. Thus, this study might allow to claim that there is an excess of correlation in the midrapidity region compared to the forward one.

11.3 Balance function for pions and kaons

An attempt to study the centrality dependence of the BF for identified pions and kaons had been performed by the STAR collaboration [39]. This investigation was motivated by the principles of the BF described in [122], which in particular suggests that the width of the distribution of heavier particles is narrower than the one for lighter particles. Charged kaons and pions produced in Au–Au collisions at $\sqrt{s_{\rm NN}}$=200 GeV and at pp collisions at $\sqrt{s}$=200 GeV were identified and used in order to examine the possible centrality dependence for each particle family. The conclusions extracted from this analysis were that the BF for kaons are narrower than the ones for pions at all centrality classes. This confirms to the original expetations. Furthermore, BF for pions are narrower for central Au–Au collisions than in peripheral Au–Au collisions [39], whereas there is no evidence of such centrality dependence for BF of kaons. The fact that the BF for kaons does not narrow with centrality may indicate a different hadronization process for kaons than for pions.

11.4 Energy dependence

The energy dependence of the BF was studied within the NA49 detector acceptance. The most central Pb–Pb events were analyzed throughout the whole SPS energy range. These data samples passed once again through the shuffling mechanism so that one can estimate the largest value of the width for each energy. The pseudo-rapidity interval analyzed for each energy was limited to the same range. In order to quantify the decrease of the width for different energies, the normalized parameter W is calculated as:

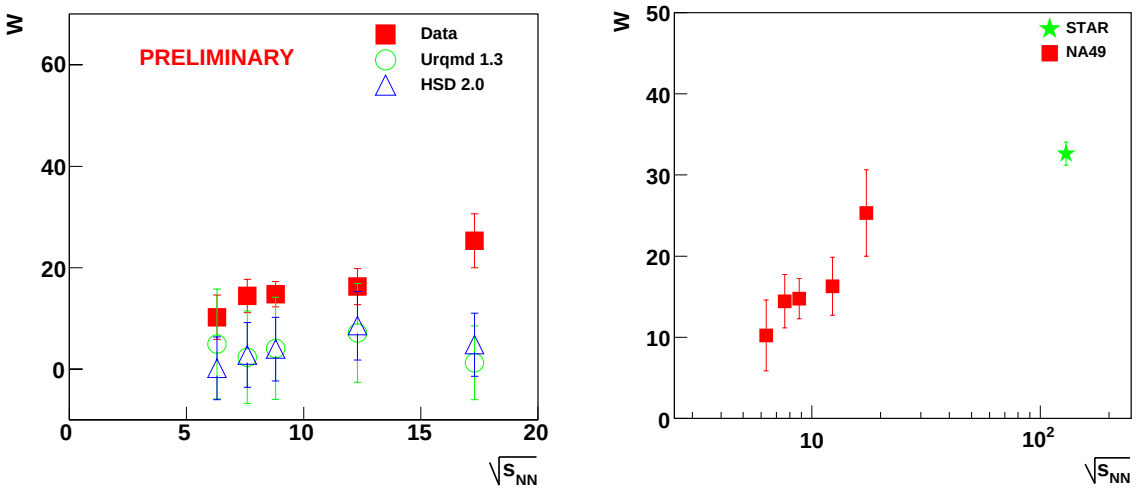

Figure 24: The dependence of the normalized parameter W on the $\sqrt{s_{\rm NN}}$ for central Pb–Pb collisions in the SPS energy range after applying the acceptance filter (left plot). Comparisons with models are also shown. The right panel shows the W parameter from NA49 as well as from STAR experiment for AuAu collisions at $\sqrt{s_{\rm NN}}$=200 GeV.

$$W = \frac{100 \cdot (\langle \Delta\eta \rangle_{\rm shuffled} - \langle \Delta\eta \rangle_{\rm data})}{\langle \Delta\eta \rangle_{\rm shuffled}}. \quad (32)$$

The left panel of Fig. 24 shows the dependence of this parameter on the $\sqrt{s_{\rm NN}}$ [26]. As far as the data is concerned, after the use of acceptance filter, one notices a first indication of an energy dependence. The normalized parameter W takes a small value for the central Pb–Pb collisions at $\sqrt{s_{\rm NN}}$=6.3 GeV. Then takes a somehow constant value for the intermediate SPS energies and finally rises as towards top SPS energy of $\sqrt{s_{\rm NN}}$=17.2 GeV. In addition, two model comparisons are made in order to further investigate this energy dependence. The Ultra-relativistic Quantum Molecular Dynamics model (UrQMD) [114] and the Hadron-String Dynamics (HSD) transport approach [127] are two microscopic models used to simulate (ultra)relativistic heavy ion collisions in the energy range from Bevalac and SIS up to AGS, SPS and RHIC. The points from the corresponding analysis of both UrQMD and HSD generated events throughout the whole SPS energy range can also be seen in Fig. 24. By studying these plots one notices no sign of energy dependence of the W parameter from the models [26].

The NA49 data for the W parameter is plotted along with the data from STAR in the right panel of Fig. 24. This shows the dependence of the W parameter on the $\sqrt{s_{\rm NN}}$ for a large range of energy. The increase of the W parameter from SPS to RHIC energy is significant and the results for ALICE will be interesting to understand the nature of QGP phase transition.

11.5 Interpretation of the results

The measured narrowing of the BF is qualitatively consistent with the delayed hadronization scenario [122, 42] of an initially deconfined phase. Several model calculations have been published which provide a more quantitative description [128, 129, 130, 115]. In particular, within models based on statistical hadronization and hydrodynamic expansion the width of the BF was found to decrease with increasing transverse collective velocity of the matter at freeze-out [128, 129, 130] and thus with the collision centrality. However, a quantitative description of the STAR data was possible only when the condition of global charge conservation (a single fireball model) [129, 130] was substituted by a stronger condition of charge conservation in sub volumes (a multi-fireball model) [128]. The quark coalescence model was applied to the hadronization of the deconfined phase in [115]. When including radial flow, good agreement with the STAR measurements was obtained also in this model calculation.

The influence of the decay of resonances on the width of the BF was estimated using the HIJING event generator. One finds that the BF width increases by about 4% when ρ^0-meson decays are switched off. In the model, the fraction of pions coming from ρ^0 decays (about 19%) is approximately independent of centrality [23]. Therefore, the effect of ρ^0 decay can not explain the strong system size and centrality dependence of the width of the BF that is observed in experimental data.

11.6 Balance function in ALICE

The method of BF has been extended to LHC energies in terms of ALICE experimental setup. Results of analysis performed on reconstructed pp and Pb–Pb simulated data are discussed here.

Proton–proton collisions

The BF was studied for 6×10^4 simulated pp events at $\sqrt{s} = 14$ TeV events that have passed through the whole reconstruction chain of ALICE as a function of the relative pseudo-rapidity interval $\Delta\eta$. This study is done using PYTHIA generator.

The dependence of the width of the BF distribution on $\Delta\eta$, the range of the analyzed pseudo-rapidity window from half a unit up to 0.9 around midrapidity with a step of 0.1, is shown in Fig. 25. This dependence is shown for different runs as well as for the whole data sample. A linear dependence of the width is observed, which is something already seen in both SPS and

RHIC energies. Thus, in order to directly compare the actual values of the width with the corresponding values from RHIC, then one should analyze the maximum phase space interval provided by the detector's acceptance. The errors shown in Fig. 25 correspond to the statistical ones.

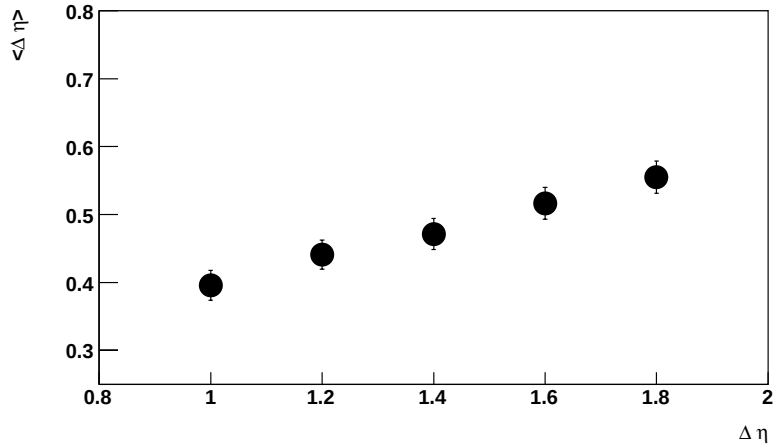

Figure 25: The dependence of the BF width on the pseudo rapidity interval analyzed for simulated pp events at c.m. energy of 14 TeV.

Furthermore, a detailed study was performed in order to estimate the contribution of the systematic errors on the calculated width. In order to do that event and track level quality cuts were varied, and the corresponding width for each distribution was calculated. In fig. 26(a) one sees the dependence of the width of the BF on the range of the cut on z coordinate of the primary vertex. The systematic error that was estimated as the average of the biggest and the smallest value was of the order of the statistical error or even less. The other two plots of fig 26 (b and c) show the dependence of the width on the distance of the track's closest approach to the primary vertex on the r direction (26(b) and on the corresponding distance on the z-coordinate (26c). The stability here is more obvious and the estimated systematic errors are even smaller than the previous one.

In addition, the whole data sample was analyzed with the BF in the whole pseudo-rapidity and transverse momentum space provided by the detectors ($|\eta| < 1.0$) in order to have an indication on any dependence on the multiplicity that might exist. Figure 27(a) shows the width of the BF distribution as a function of the mean multiplicity. One can notice that such a dependence on multiplicity is not apparent.

Moreover, the BF was studied in the whole rapidity space for oppositely charged identified particles such as: $\pi^{\pm}$ pairs, $K^{\pm}$ pairs and p-$\bar{p}$ pairs. Figure 27(b) summarizes the corresponding results. The width $\langle \Delta y \rangle$ gets narrower with increasing mass of the analyzed particle. This effect has already been shown by the STAR collaboration [39], and and was even proposed in [122] as a method to investigate the possible different mechanisms that are important in the production of the different particle species. The ratios of the calculated widths for all particle species are:

$$\frac{\langle \Delta y \rangle_{\pi}}{\langle \Delta y \rangle_{\mathrm{K}}} = 1.362 \pm 0.047, \qquad \frac{\langle \Delta y \rangle_{\pi}}{\langle \Delta y \rangle_{\mathrm{p}}} = 1.589 \pm 0.095, \qquad \text{and} \qquad \frac{\langle \Delta y \rangle_{K}}{\langle \Delta y \rangle_{\mathrm{p}}} = 1.167 \pm 0.070$$

. The corresponding value obtained in [39] from pp collisions at $\sqrt{s} = 200$ GeV is:

$$\frac{\langle \Delta y \rangle_{\pi}}{\langle \Delta y \rangle_{K}} \approx 1.31$$

.

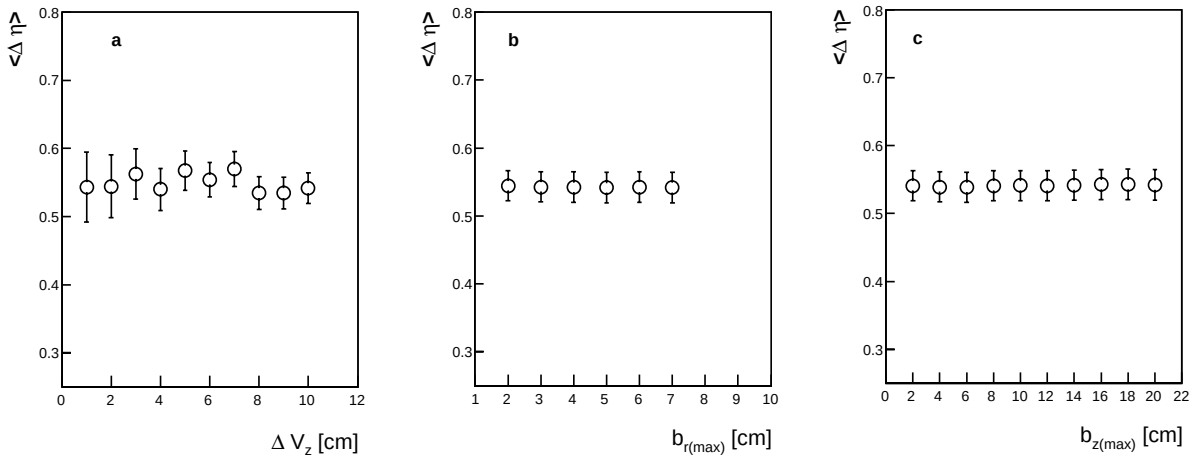

Figure 26: The dependence of the width of the BF on the range of the cuts for different parameters: (a) on the range of the cut on z-coordinate of the primary vertex, (b) on the distance of the track's closest approach to the primary vertex on the r direction, and (c) on the corresponding distance on the z-coordinate.

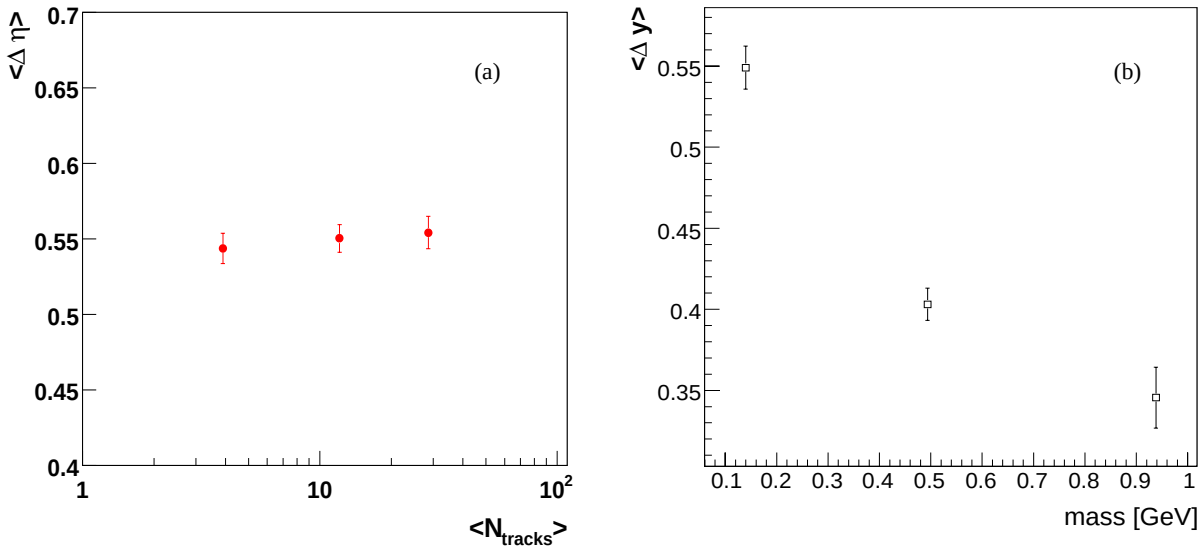

Figure 27: The dependence of the width of the BF for pp collisions at 14 TeV on (a) the mean multiplicity, (b) the mass of the analyzed oppositely charged particle pairs ($\pi^{\pm}$, $K^{\pm}$ and p-$\bar{p}$).

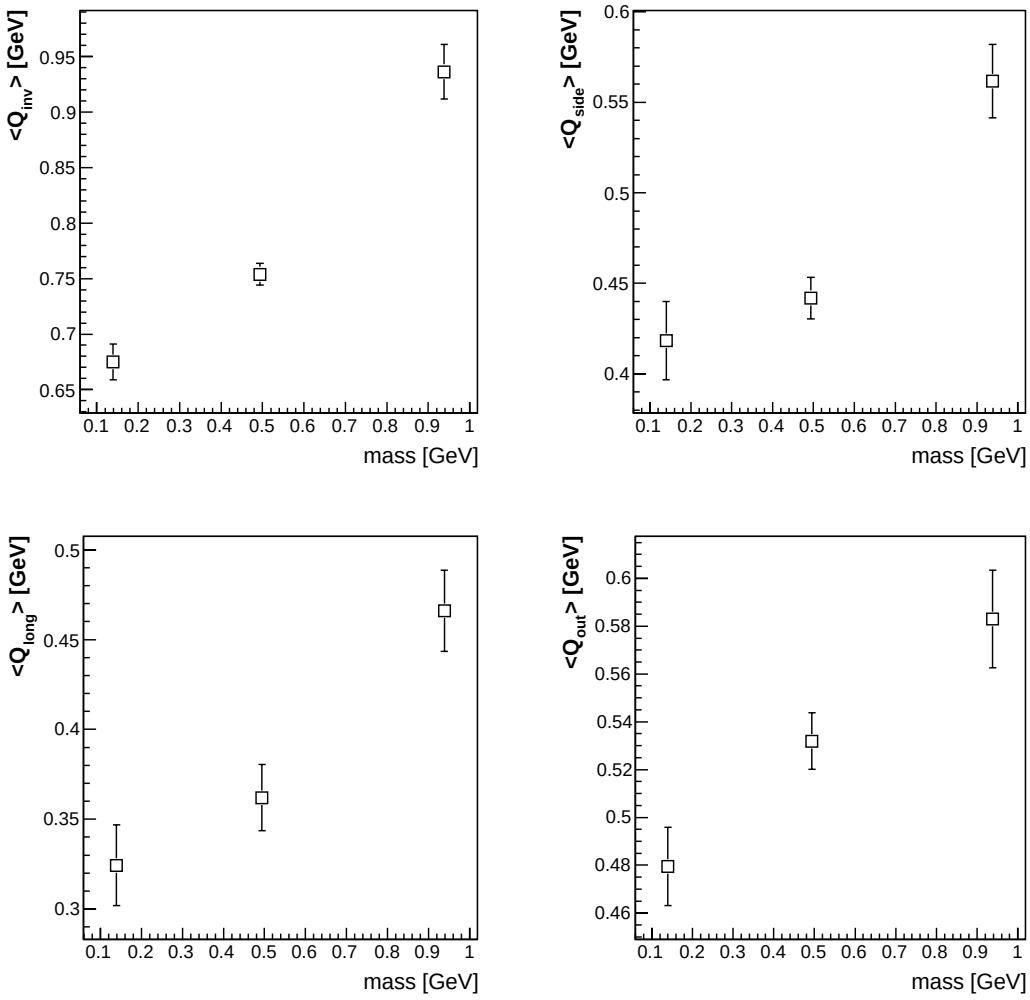

Figure 28: The dependence of the width of the BF measured in all different components of Q ($Q_{\rm inv}$ top left, $Q_{\rm side}$ top right, $Q_{\rm long}$ bottom left and $Q_{\rm out}$ bottom right) on the mass of the analyzed oppositely charged particle pairs ($\pi^{\pm}$, $\rm K^{\pm}$ and p-$\bar{\rm p}$) for pp collisions at 14 TeV.

Finally, the method is extended to study the BF as a function of the two particles relative momentum Q_i as proposed in [126]. As is proposed, studying the BF in these observables yields a clearer insight for interpreting the physics of the balancing charges as well as providing a better illumination of the distorting effects [126]. The BF has been studied for different particle species as a function of $Q_{\rm inv}$ the two particle invariant momentum, of Q_{long} which is the projection of q along the beam axis, of Q_{out} which is the corresponding projection along the outward direction (defined by the pair's transverse momentum) and of Q_{side} which is the projection of q along the sidewards direction (perpendicular to the pair's transverse momentum and to the beam axis). Figure 28 summarizes the main results: the corresponding width ($\langle Q_{\rm inv}\rangle$, $\langle Q_{side}\rangle$, $\langle Q_{long}\rangle$ and $\langle Q_{out}\rangle$) increases with increasing particle mass.

Pb–Pb collisions

The method of BF was also used to analyze centrality selected Pb–Pb reconstructed events. These events correspond to the two extreme centrality classes of ALICE:

- The most central Pb–Pb collisions that correspond to an impact parameter range $0 < b < 5$ fm.

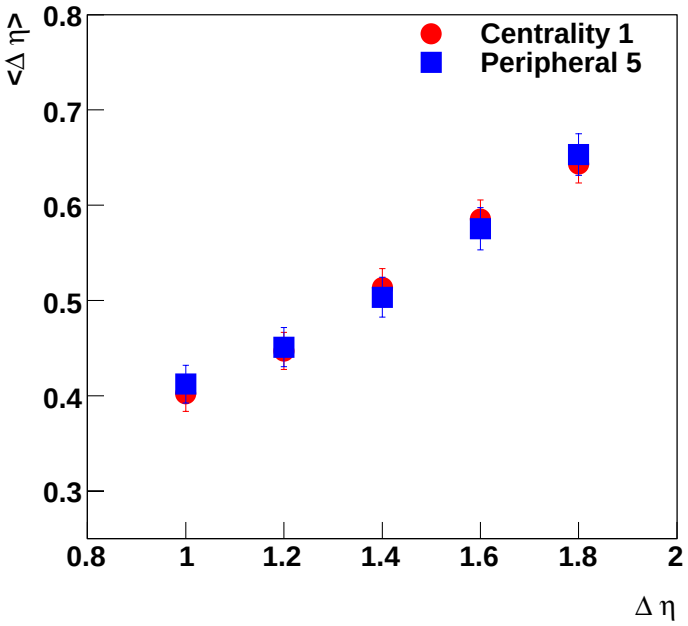

Figure 29: The dependence of the width on the pseudo rapidity interval analyzed for the most central and the most peripheral Pb–Pb collisions at $\sqrt{s_{\rm NN}}$=5.5 TeV.

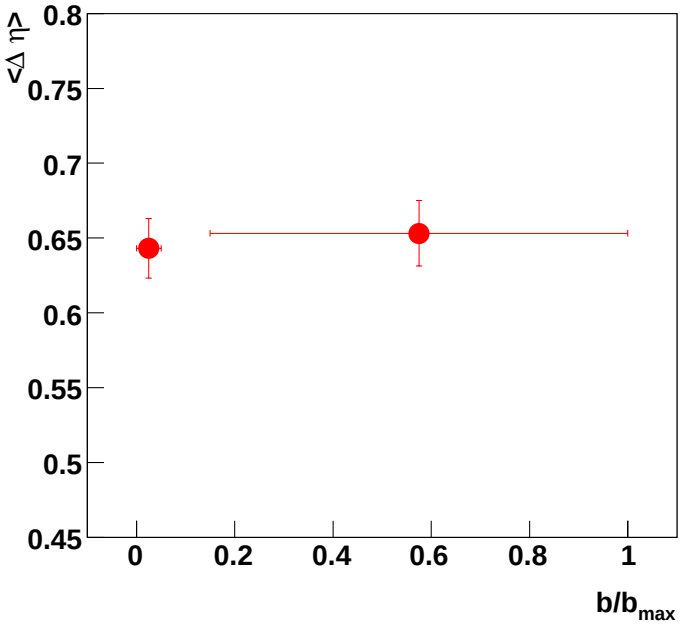

Figure 30: The dependence of the width on the normalized impact parameter ratio $b/b_{\rm max}$ for Pb–Pb collisions at $\sqrt{s_{\rm NN}}$=5.5 TeV.

- The most peripheral Pb–Pb collisions with an impact parameter range $b > 15$ fm.

These events were also passed through the shuffling mechanism in order to extract an estimation for the biggest possible width for each centrality class. Analysis of additional Pb–Pb events is possible in order to extract a final results. Preliminary results are presented here.

The dependence of the width of the distribution on the range of the analyzed pseudo-rapidity window starting from half a unit up to 0.9 around midrapidity with a step of 0.1 is shown in Fig. 29. One notices once again the linearity in the behavior of the width. Figure 30 shows the width of the BF distributions as a function of the normalized impact parameter ratio $b/b_{\max}$ for the most central and the most peripheral Pb–Pb collisions. This picture is consistent for a non QGP hadronization phase because of the lack of the centrality dependence.

12 Fluctuations in azimuthal anisotropy

Fluctuation in elliptic flow and higher harmonics give proper insight to the explosive system produced in heavy ion collisions at the LHC energy [75, 76, 77]. These have been studied in the context of results from the STAR experiment at RHIC [131, 132]. Event-by-event fluctuation in v_2 of photons measured by the PMD in the forward rapidity in ALICE had been investigated earlier [133, 134]. In the central rapidity region of ALICE it may be possible to measure flow on an event-by-event basis using the large coverage of TPC. This has been simulated by taking charged particle rapidity density at $\eta = 0$ to be between 100 to 5000. For each multiplicity class, the data has been generated for a constant flow for each event as well as varying flow within a given range. Flow was introduced by modifying the azimuthal angle of each particle by an amount $\Delta\Phi$ such that

$$\Delta\Phi = -\Sigma_i \frac{2v_n}{n} \sin n(\phi_i - \Psi_r), \tag{33}$$

where Ψ_r is chosen randomly, once for each event, i runs over all particles and n=2 in case of elliptic flow.

The generated data were analysed by dividing the event into two subevents of equal multiplicity, separated by a small rapidity interval, and v_a' is obtained as $< cos2(\phi_a - \psi_b) >$, where the ϕ_a are the azimuthal angles of particles in subevent a and ψ_b is the event plane obtained using particles in subevent b, and the average is over all particles. v_b' is also similarly obtained. Then v_2 can be expressed as,

$$v_2 = \sqrt{\frac{v_a' \cdot v_b'}{\cos 2(\psi_a - \psi_b)}} \tag{34}$$

and is termed v_2^{out}", while the injected flow is termed v_2^{in}. Figure 31 shows the v_2^{out} distribution reconstructed on an event-by-event basis for a given multiplicity class, with two choices for v_2^{in}, namely constant $v_2^{in} = 0.05$ and fluctuating v_2^{in}. For some very low flow values, the geometric mean is replaced by the arithmetic mean. This way v_2 is obtained for each event and is termed as v_2^{out}.

By taking the quadratic difference of the total r.m.s. (as for dotted line) and the r.m.s. intrinsic to the method (as for solid line), one can ascertain the presence of event-by-event fluctuations in v_2 from data. This quadratic difference has been plotted as a function of multiplicity and is shown in Fig. 32. As the multiplicity increases, the quadratic difference reaches the input value of 0.017. This validates the estimates of v_2 for each event.

13 Disoriented chiral condensates

The QCD phase transition is predicted to be accompanied by chiral symmetry restoration at high temperatures and densities. One of the most interesting consequences of chiral transition

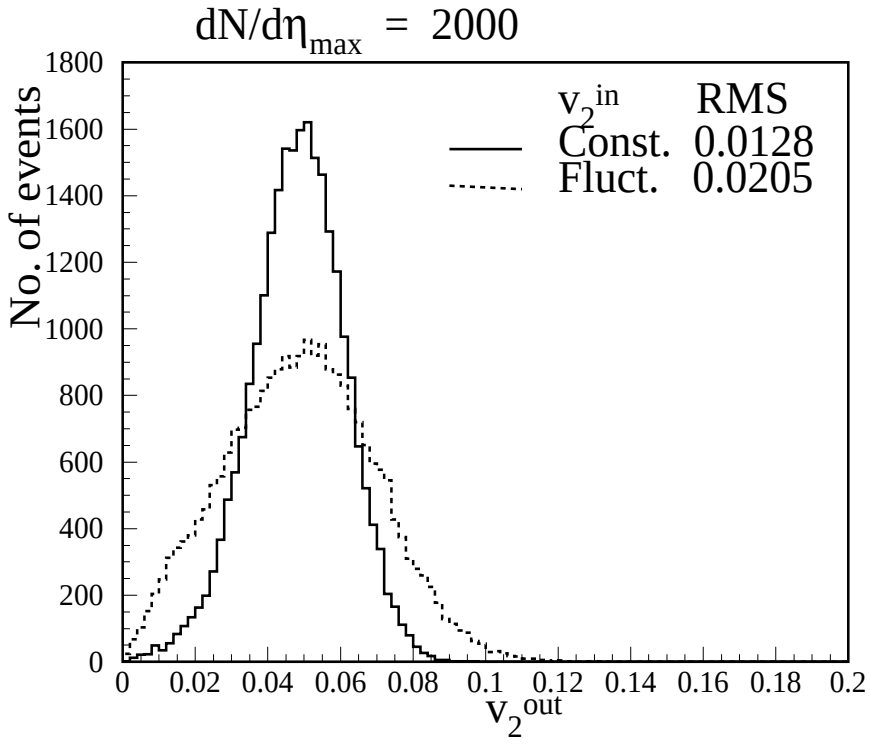

Figure 31: Solid lines correspond to $v_2^{in} = 0.05$ for *each* event and dotted lines correspond to v_2^{in} chosen randomly from a Gaussian distribution peaked at 0.05 with a width of 0.017.

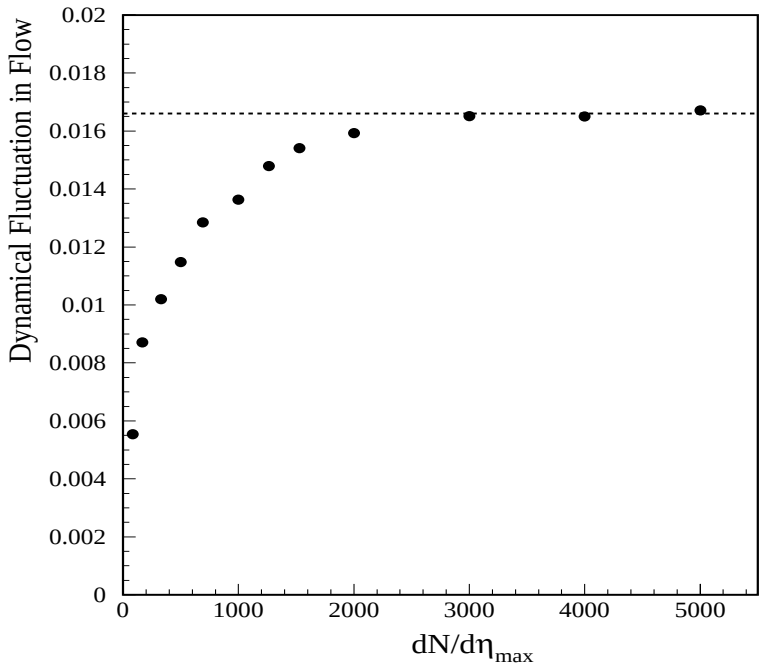

Figure 32: The r.m.s. of the distribution corresponding to constant v_2^{in} is subtracted quadratically from the r.m.s. of the distribution corresponding to fluctuating v_2^{in} and shown for different multiplicities. The dotted line shows the r.m.s. of the fluctuation introduced.

is the formation of a chiral condensate in an extended domain, such that the direction of the condensate is misaligned from that of the true vacuum. This phenomenon is termed as the disoriented chiral condensates (DCC) [11, 12, 13, 14]. The formation of DCC results in an excess of low momentum pions in a single direction in isospin space giving rise to large imbalances in the production of charged to neutral pions. This is studied in terms of the distribution of neutral pion fraction, f, given by,

$$f = \frac{N_{\pi^0}}{N_\pi}, \tag{35}$$

where N_{π^0} and N_π are the number of neutral pions and total pions, respectively. The pions in a normal event would follow a binomial form with a mean of 1/3, whereas within a domain of DCC the probability of pion fraction would follow a binomial distribution pattern such as,

$$P(f) = \frac{1}{2\sqrt{f}}.$$

DCC is a metastable state which results from the cooling down of the high-temperature chiral symmetric phase of quark–gluon plasma. Such a state appears in both linear and non-linear σ-models which are simplified versions of the full chiral effective theory. The condensate may have a large isospin vector oriented in any direction in isospace, and thus it may be a source of secondary pions with any isospin configuration. A DCC state may occupy the full available phase space or only a part of it, and thus it may constitute a source of all secondary pions or only of small fraction of them. Some theoretical models [135, 136, 137, 138] predict 'DCC domains' of sizes 3–4 fm in radius, emitting 50–200 pions. Such a source may be situated in the any kinematic region of the expanding source, and the pion emission pattern might be statistical or coherent. If the pion emission from DCC is indeed coherent, the pions will be collimated in a limited region of phase space and will have small relative transverse momenta. In this case one would expect to find 'jet-like' structures with high isospin imbalance. In view of these it seems plausible to search for DCC in various phase space regions. A recent review of theoretical and experimental aspects of DCC maybe found in Ref. [15].

The formation of DCC was hypothesized in the context of explaining observed abnormal events from cosmic ray experiments [139, 140] which had either excess of charged particles compared to neutrals (called centauro events) or excess of neutrals with respect to charged particles (anti-centauro events). A dedicated experiment, MiniMax, was set up at the Tevatron at Fermilab to study p+$\bar{\text{p}}$ collisions at $\sqrt{s}$ = 1.8 TeV [141]. MiniMax was composed of 24 MWPCs with a removable lead gamma converter, and a segmented electro-magnetic calorimeter behind it. The detector had a very small angular acceptance: a cone with axis at $\eta = 4.1$, with half-angle 0.65. No evidence for DCC was found at a few per cent level.

A thorough DCC search in Pb–Pb collisions at $\sqrt{s}_{\rm NN}$=17.2 GeVwas performed by the WA98 Collaboration at CERN [28, 29, 30, 31]. This was based on a systematic study of photon and charged particle multiplicity correlation using the data from a preshower photon multiplicity detector (PMD) and a silicon pad multiplicity detector (SPMD) for charged particles. No DCC signal was observed and the upper limit for DCC production at 90% CL was established as a function of the fraction of DCC pions among all pions produced. A DCC search was carried out by the NA49 experiment [142] for semi-central Pb–Pb collisions at $\sqrt{s}_{\rm NN}$=17.2 GeV. The ratio of electro-magnetic to hadronic transverse energy, $E_T^{\rm EM}/E_T^{\rm HAD}$, was calculated for each event using the radially and azimuthally segmented cylindrical calorimeter. The distribution of this ratio was found compatible with that predicted by the VENUS model [92], with the mean value close to 0.3, and tails not showing the presence of any anomalous events. The results of DCC search in Au–Au collisions at c.m. energy up to $\sqrt{s_{\rm NN}}$=200 GeVis expected from experiments at RHIC.

Many powerful techniques have now been developed for DCC search. A review of these along with the sensitiveness of ALICE detector is discussed in the following.

13.1 Signatures of DCC formation

A large number of signatures have been proposed as a consequence of the DCC formation in heavy-ion collisions. A short list of important signatures is given below:

- fluctuation in neutral pion fraction, f:
  the event-by-event fluctuation in the neutral pion fraction is the most basic signature of DCC formation. This study is equivalent to studying the fluctuation in the number of charged particles and photons. This study can be carried out in the full phase space or in smaller $\eta - \phi$ domains where DCC formation might give rise to distinct patterns of the emission of pions [143, 144].

- kaon correlations:
  formation of DCC give rise to enhanced correlations of K^+K^- and $K^0_sK^\pm$ [145].

- baryon abundances:
  formation of many small DCC domains may give rise to enhanced production of baryons, particularly, Ω and $\bar{\Omega}$ [146].

- HBT correlations:
  DCC formation will affect the two-particle HBT correlations of identified pions [145].

- direct photons:
  Search for non-equilibrium photons in the direct photon measurements has been proposed a potential test of the formation of DCC [147].

Most of these methods have been proposed for use in the ALICE experiment for the search of DCC. The nalyses so far are based on the fluctuations in neutral to charged particle measurements. Various analysis methods, which are sensitive to details of DCC formation, have been developed. The experimental observation of DCC depends on various factors, such as the probability of DCC occurrence, the number of possible DCC domains in an event, size of the domains, number of pions emitted from the domains, and the interaction of pions with the rest of the system. The sensitiveness of ALICE detectors to each of the DCC cases has been studied by simulation.

13.2 DCC measurements in ALICE

The ALICE detector makes it possible to search for DCC by comparing the emission of charged and neutral pions in two distinct regions of phase space as discussed below:

- Central rapidity region: Combination of PHOS and TPC within a common coverage of $-0.12 < \eta < 0.12$, $\Delta\phi = 100^\circ$ may be used. In this region, photon measurements are made by PHOS whereas charged pions will be measured by TPC. The expected number of photons in this region is about 500 for central Pb–Pb events with similar number for charged particles.

- Intermediate rapidity region: Combination of PMD and FMD within common coverage of $2.3 < \eta < 3.5$, $\Delta\phi = 360^\circ$ will be used. PMD is a preshower detector with good space resolution and the photon detection efficiency is about 70%. The FMD measures charged particles multiplicity. The expected number of photons in the PMD acceptance is about 4000 for central Pb–Pb events with about similar number for charged particles. Due to this large multiplicity, a search for DCC in more restricted regions of phase space can be performed with good accuracy. A description of DCC measurements in this region may be found in [133, 134].

The two sets of detector combinations can also be used to isolate events with large fluctuations in the relative number of charged particles to photons. A comparison of normal to these exotic events may be made in studying other predicted signals of DCC using the rest of the ALICE detectors.

13.3 Simulation of DCC events

The effect of non-statistical DCC-like fluctuations has been studied within the framework of a simple model in which the output of the parametrized HIJING event generator has been modified in a similar manner to those of refs. [148, 149, 150]. Within a domain size given in terms of its extent in η and ϕ, the identity of the charged pions to neutral pions is changed following the neutral pion distribution given in Eqn. 35. The neutral pions are allowed to decay. The parameters of the model are the following:

- domain size in terms of $\Delta\eta$ and $\Delta\phi$,
- production of additional pions,
- percentage of events of DCC-type.

The simulated events are used to study the sensitiveness of DCC detection in the experimental setup.

13.4 $N_\gamma - N_{\rm ch}$ correlation

In a given set of normal events N_γ and $N_{\rm ch}$ are correlated. The presence of events with DCC would show up as deviations from the general correlation. This correlation can be studied in the full detector coverage for global fluctuation study or within a subset of the coverage for localized fluctuations. Inference on the presence of non-statistical fluctuation may be made from the distance of the data points in the correlation plots to a common correlation axis.

Correlations of $N_\gamma - N_{\rm ch}$, measured by the WA98 experiments [28, 30, 31] for SPS energies, are shown in Fig. 33. The left panel shows $N_\gamma - N_{\rm ch}$ distributions in the full available phase space of the detectors and the right panel shows a superimposition of the $N_\gamma - N_{\rm ch}$ distributions where the available phase space is divided to smaller segments of 2,4,8 and 16 bins. The solid lines in both cases show correlation axes (Z).

The distribution of the closest distance of the data points to the correlation axes represent the relative fluctuations of charged particles to photons. The resulting distribution is quantified in terms of the scaled variable $S_z = D_z/\sigma(D_z)$ where D_z is the distance of a point in the $N_\gamma - N_{\rm ch}$ plane to the correlation axis, and $\sigma(D_z)$ is the dispersion of the D_z distribution for 'normal' events.

The S_z distributions for the global case and for two bins in localized cases are shown in Fig. 34. The r.m.s. deviations of the experimental data distributions are then compared to those of the mixed events and simulated events. Since the r.m.s. deviations of the experimental data and the derived mixed events are not so different, upper limits on the predictions of DCC are set by comparing these results to DCC simulated events with various input parameters. The upper limit on global DCC is shown in the left panel of Fig. 35 and for smaller domains of DCC is shown in the right panel of Fig. 35.

In the ALICE experiment the correlation of number of photons in PHOS and number of charged particles in TPC in the common coverage of the central region and the correlation of number of photons in PMD and number of charged particles in FMD can be studied. Further the correlation studies in smaller domains in $\eta - \phi$ in the forward rapidity region can be made to look for possible signatures of DCC formation.

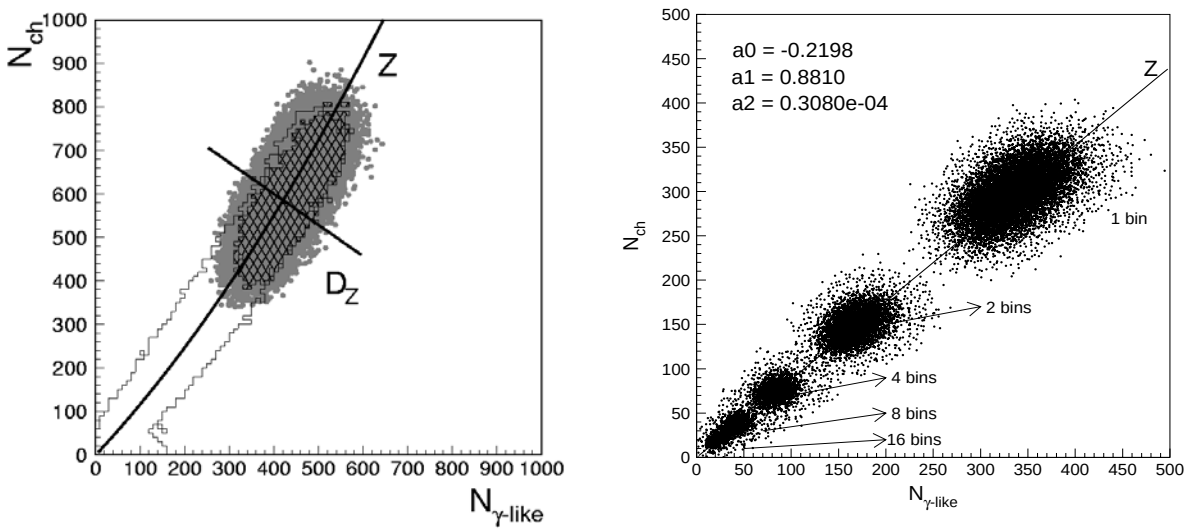

Figure 33: Left panel shows Scatter plots showing the $N_\gamma - N_{\rm ch}$ correlations for the global study (full available phase space of charged particle and photon detectors in the WA98 experiment) and the right panel shows similar distributions for local study for 1,2,4,8 and 16 bins in azimuthal angle for a common coverage of the detectors. The correlation axes are shown by the solid curves.

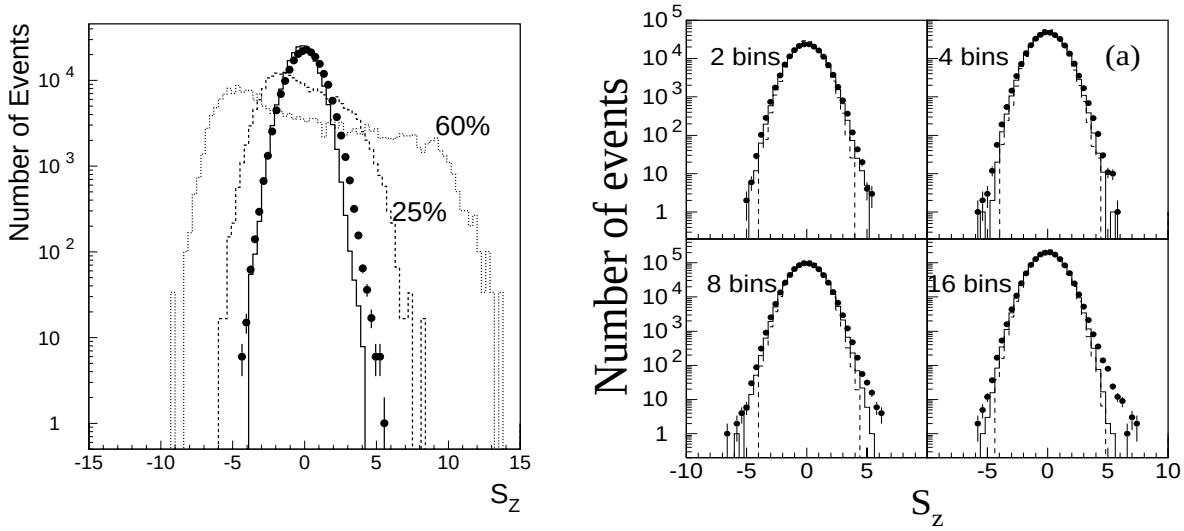

Figure 34: S_Z distributions for the global and local cases. In the left panel the solid points are experimental data and the solid histogram corresponds to the mixed events. DCC simulated events, where 25% and 60% pions are of DCC origin, are superimposed in the figure. In the right panel the experimental data (solid points), mixed event (solid histogram) and GEANT simulated events (dashed histogram) are shown for different bin sizes.

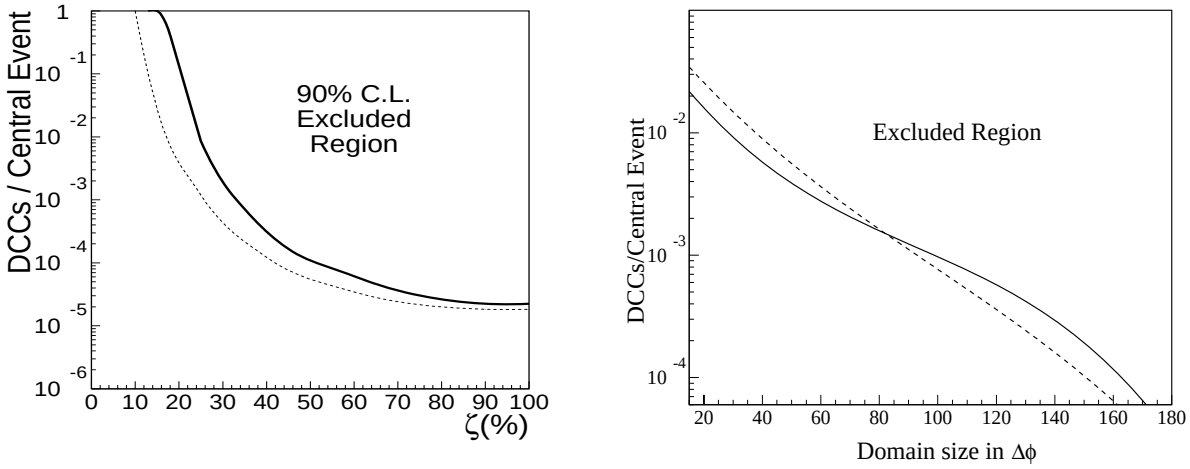

Figure 35: 90% C.L. upper limits on DCC production per central event for the global and local studies from the WA98 experimental data [28, 30, 31]. The X-axis in the left figure gives a fraction of pions which are assumed to be of DCC origin whereas the X-axis on the right figure gives the DCC domain size in azimuthal angle.

13.5 Discrete wavelet technique

Discrete Wavelet Technique (DWT) has been proved to be quite successful in many fields of research to analyze and identify fluctuations at various distance scales [151]. This technique has been suitably adopted to search for bin-to-bin fluctuations in charged particle and photons. The analysis has been carried out by making 2^j bins in the azimuthal angle where j is the resolution scale. The output of the DWT analysis consists of a set of Father Function Coefficients (FFCs) at each scale, j. The distribution of FFC's for normal events is Gaussian whereas the presence of DCC-like fluctuations makes the distribution wider and non-Gaussian. Inference about the presence of DCC can be made by studying the width of FFC distributions. Figure 36 shows FFC distributions for normal and DCC-like events where the increase in the width for DCC events can be seen. The correlation method described previously gives anomalous fluctuation within a given window in $\eta - \phi$ whereas the DWT method has the added advantage that it is quite powerful for studying bin-to-bin fluctuation and can give the exact dimension of the bin in $\eta - \phi$ which has larger fluctuation compared to other bins. The effect of DCC using the DWT method may be quantified using a strength parameter (ζ), defined as [149],

$$\zeta = \frac{\sqrt{(s_{\rm X}^2 - s_{\rm N}^2)}}{s_{\rm N}}, \tag{36}$$

where $s_{\rm N}$ is the r.m.s. deviations of the FFC distribution for normal events and S_X is the r.m.s. deviation for DCC events.

Using the DWT technique, WA98 collaboration has made extensive study for the search of DCC [30, 31]. DWT technique can be easily applied to the data from ALICE for the study of formation of DCC. The forward rapidity region will be particularly suitable for the DWT study where the available phase space can be divided into large number of bins. The sensitivity of the DWT method will be much better compared to that at SPS because of the large multiplicity.

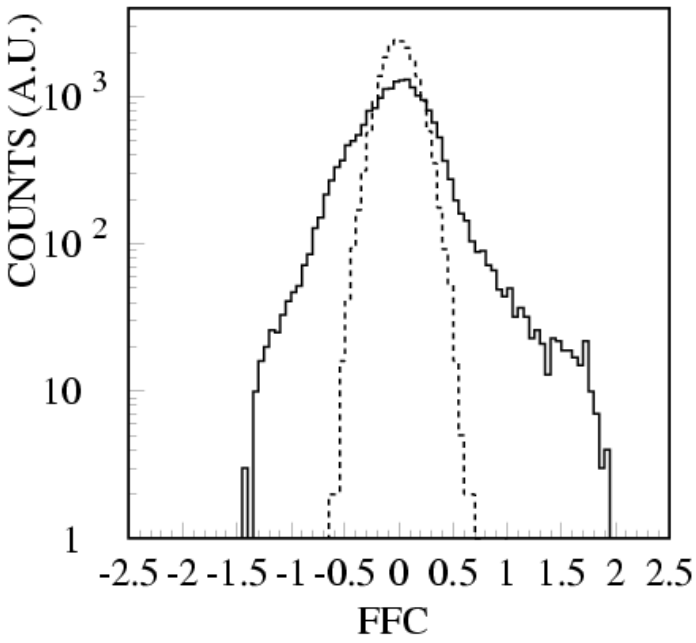

Figure 36: FFC distribution for simulated generic events (dotted line) and pure DCC-like events (solid line).

13.6 Power spectrum analysis

The power spectrum technique [153, 154, 155] can be applied to study event-by-event fluctuation over limited ϕ regions. In this approach, one computes the fraction $f = N_\gamma/N_{\rm ch}$ for a certain window, e.g. a window in azimuthal angle ϕ, and this window is then displaced by a small amount, f is recalculated, etc. The power spectrum is the square of the Fourier transform of the $(f(\phi) - f_o(\phi))$ distribution where $f_o(\phi)$ is the distribution for 'normal' events. It shows a characteristic pattern, with narrow peaks indicating local fluctuations in the original distribution [133]. The capability of the method was investigated by generating a set of 5000 events with a multiplicity of 4000 particles in the common coverage of both FMD and PMD. The power spectrum generated from these events are compared to events with the presence of DCC domains within a domain size of $\delta\eta = 0.1$ and $\delta\phi = 40^\circ$. With a proper selection criteria it was possible to select DCC events with 60% efficiency. This method will be very useful to select exotic events corresponding possibly to DCC formation.

13.7 'Robust' variables

The analysis method used by the Minimax experiment at Fermilab is named as 'robust' observables [156]. This analysis uses the ratios of factorial moments

$$R_{i,1} = \frac{F_{i,1}}{F_{i+1,0}}, \tag{37}$$

$$\text{where} \quad F_i = \frac{< N(N-1)...(N-i+1) >}{< N >^i} \tag{38}$$

$$\text{and} \quad F_{i,j} = \frac{< N_{\rm ch}(N_{\rm ch}-1)...(N_{\rm ch}-i+1)N_\gamma(N_\gamma-1)...(N_\gamma-j+1) >}{< N_{\rm ch} >^i < N_\gamma >^j} \tag{39}$$

The variables R have been named 'robust variables' because the detection efficiencies, often difficult to estimate (especially for photons) cancel out and thus do not influence the results.

The analysis can be done inclusively or event-by-event for high multiplicity events in ALICE. For 'normal' events (statistical uncorrelated emission) $R_{i,1} = 1$, while for DCC $R_{i,1} = 1/(i+1)$ - a remarkable difference for all $i \geq 1$. Results of a DCC simulation using this technique is shown in Fig. 37.

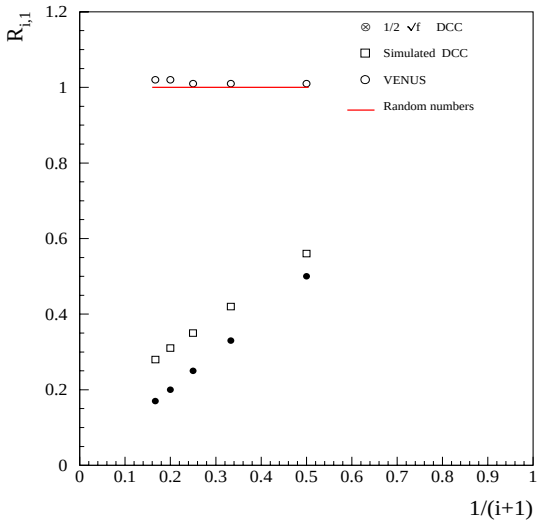

Figure 37: Results of DCC analysis using 'robust' observables. Normal events using VENUS event generator do not show any correlation whereas pure DCC events follow $R_{i,1} = 1/(i+1)$ behaviour. The simulated events with detector effects follow a behaviour similar to that of pure DCC events.

13.8 Event-shape analysis

This method combines the wavelet technique and flow analysis [148]. It is based on the realization that localized DCC formation is expected to lead to an event shape anisotropy which is out of phase for charged particles and photons. The flow direction is found separately for charged particles and photons and compared. For a DCC component a difference between the two directions might be expected. The results of the second-order Fourier analysis is shown in Fig. 38 for the difference in flow angle of photons and charged particles. The presence of DCC leads to an anti-correlation of flow angles in the two detectors peaking at 90°. This will be a very powerful method to study DCC formation in the high multiplicity ALICE environment.

13.9 Sliding window method

The Sliding Window Method (SWM) is developed to search for patches, on an event- by-event basis, having unusual fluctuations in the neutral pion fraction (f) which may arise due to the formation of DCC. In this method one chooses a window in azimuthal plane of size $\Delta\phi$, in the common coverage of charged particle and photon detectors and calculates the neutral pion fraction f. The entire azimuthal range of common coverage is scanned by continuously sliding the window i.e., shifting each time by a small amount, say $\delta\phi$, to search for a patch having the neutral fraction, f, several standard deviations away from the mean value of the generic f distribution. This method utilises the full advantage of azimuthal resolution of the detectors.

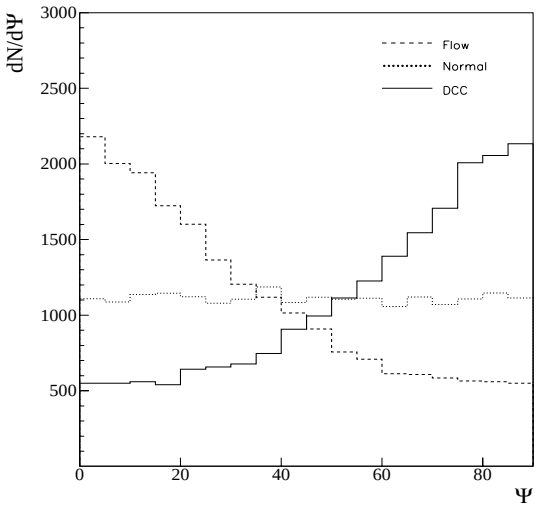

Figure 38: Difference in flow angle distribution for charged particles and photons is plotted for three cases: (a) normal events, (b) events with flow, and, (c) events with DCC. Characteristic differences between three types of events are seen.

The SWM can be used to search for the anti-Centauro and Centauro events by looking for the maximum and minimum f values in an event by continuously sliding the patch depnding upon the detectors' resolutions. It is found that $f_{\rm max}$ and $f_{\rm min}$ distributions for generic events for a given window size are Gaussians whereas for simulated DCC-like events these distributions extend well beyond those of the generic events. This method allows the direct observation of patches having large f values.

The SWM has been applied to the analysis of data in the WA98 experiment which had a photon multiplicity detector and a charged particle multiplicity detector overlapping fully in azimuth over 0.5 unit of pseudorapidity [157]. The azimuthal scanned was performed by sliding the window by $\delta\phi = 2^\circ$. The percentage of events having exotic patches in the top 10% central events, with f value beyond 4.5 σ of the generic f distribution, is found to be 0.39$\pm$0.016, as compared to 0.081$\pm$0.007 in the mixed events and 0.013$\pm$0.008 in the Geant simulated VENUS events. One such event found by this method in the WA98 data is displayed in Fig 39 which shows the photon hits($\bullet$) and charged particle hits ($\Box$) within the common coverage of both the detectors. The patch with the highest $f = 0.77$ is also marked which contains 84 photon hits as compared to only 12 charged partilce hits. This shows the power of the method to search for exotic patches in a given $\eta - \phi$ phase space and can be easily applied to data from ALICE.

14 Fluctuations in intermediate and high p_t sector and jets

Presence of jets and mini-jets affect the event-by-event fluctuation. These have to be understood in detail: (a) to make any inference about the E-by-E fluctuations, and (b) to understand the effect of jets passing through the medium. This may allow one to test various models of jet production in the region not accessible for the standard method for jet production. In this subsetion results are presented based on simulations concerning jet production on event-by-event fluctuations of p_t and E_T.

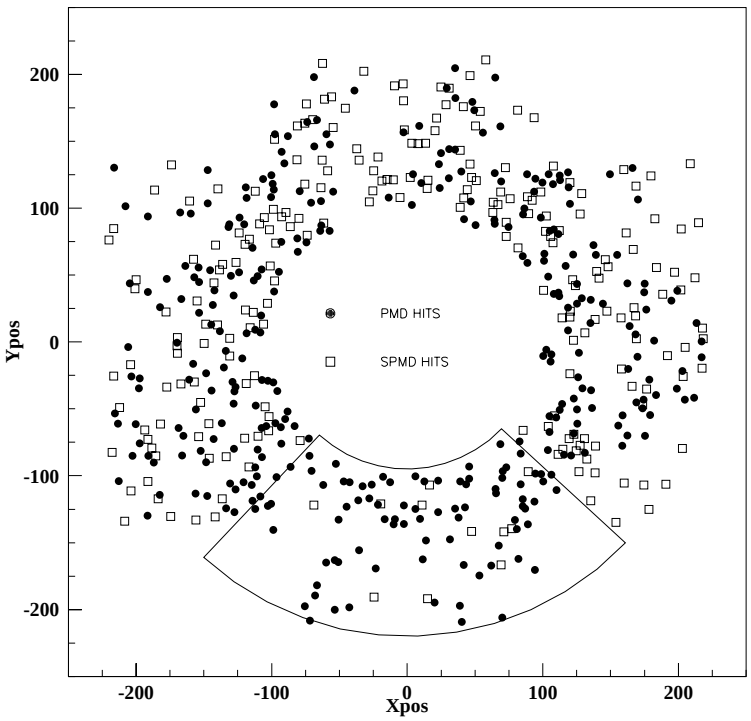

Figure 39: Plot showing photon hits(PMD) and charged particle hits(SPMD) in an azimuthal plane in the WA98 experimental setup [157]. The marked 90° patch corresponds to $f_{\max}$=0.77.

14.1 Fluctuations in p_t

In order to study exclusively the effect of jet production, a simple model of central Pb–Pb collisions at the LHC was developed. Two independent sources of particle production were assumed: the 'soft' component models production of particles at low transverse momenta, whereas the 'hard' component simulates particles originating from jets. The 'soft' component was simulated assuming independent production of charged hadrons. The azimuthal angle distributions were assumed to be uniform. The transverse momentum spectrum was generated according to a 'thermal' distribution:

$$\frac{1}{p_t}\frac{dn}{dp_t} = C \times \exp\left(-\frac{m_t}{T}\right), \tag{40}$$

where T = 190 MeV is an inverse slope parameter, and C is an arbitrary normalization parameter. The rapidity density distribution of the 'soft' component was taken to be Gaussian with a mean of 6000 and σ = 1000. For each event, in addition to 'soft' component, a 'hard' component modeling jet production was generated. The p_t spectrum of jets produced in central Pb–Pb collisions at $\sqrt{s}_{NN}$=5.5 TeV was calculated by scaling the corresponding p_t spectrum obtained for pp interactions at 5.5 TeV using PYTHIA (version 6.1) with the standard (2 jet-events, LO calculations and no initial and no final state radiation) parameters. The scaling factor for the spectrum normalized to mean multiplicity was calculated following the pQCD-based rule $\langle jet\rangle \sim \langle N_W\rangle^{4/3}$, where $\langle N_W\rangle$ is the mean number of wounded nucleons.

The resulting jet p_t-spectrum is presented in Fig. 14.1. The multiplicity distribution of jets was assumed to be Poissonian. The jet fragmentation properties were introduced by a parametrization of the appropriate distributions generated again within PYTHIA.

Events generated according to the model within the ALIROOT framework were passed through the ALICE TPC fast simulation chain, which allowed for a proper introduction of

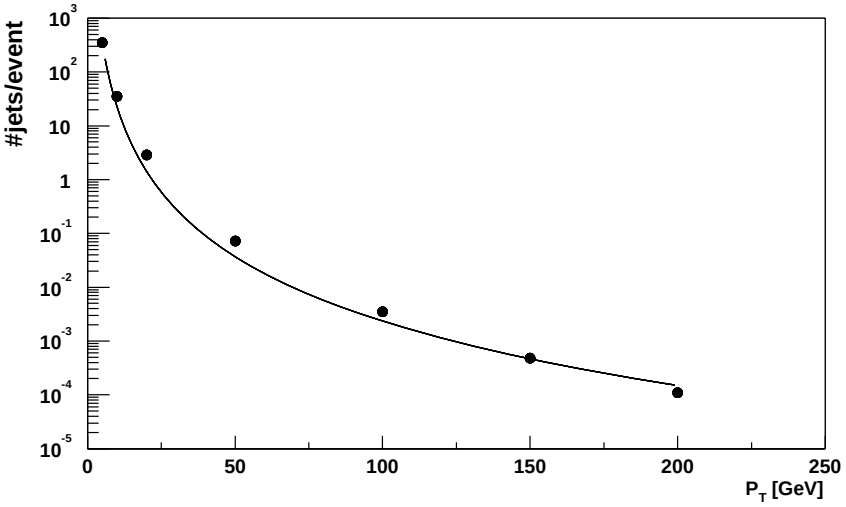

Figure 40: Transverse momentum spectrum of jets in central Pb–Pb collisions at $\sqrt{s}_{\rm NN}$=5.5 TeV assumed in the simulation. The solid line is drawn to guide the eye.

the detector acceptances. For the final analysis of fluctuations, only tracks measurable (long enough for reconstruction) in the ALICE TPC were selected and the $\Phi_{\rm p_t}$ fluctuation measure was calculated for them.

The observed transverse momentum fluctuations depend on the acceptance selected for the study. In order to investigate this effect a rectangular acceptance window is introdued which is defined in azimuthal angle ϕ and pseudo-rapidity η, in addition to the geometrical TPC acceptance. The size of the window

$$L_{\eta,\phi} = \sqrt{\Delta\eta^2 + \Delta\phi^2} \tag{41}$$

was varied by scaling $\Delta\eta$ and $\Delta\phi$ by the same factor. In this procedure, the assumption is that $\Delta\eta/\Delta\phi = 2/(2\cdot\pi) \approx 0.32$.

The dependence of $\Phi_{\rm p_t}$ on $L_{\eta,\phi}$ is shown in Fig. 41(a) for two cases: 'soft' component only and 'soft' + 'hard' components, as defined above. In the case of the 'soft' component, independently of the size of the acceptance window, the value of $\Phi_{\rm p_t}$ was equal to zero. This result was expected because of the assumption of uncorrelated particle production in the 'soft' component model. However, in the 'soft'+ 'hard' case large non-zero values of $\Phi_{\rm p_t}$ were obtained. The strong event-by-event fluctuations result from the correlated particle production in the 'hard' component. The $\Phi_{\rm p_t}$ increases with the size of the acceptance window $L_{\eta,\phi}$. In order to understand this dependence it is useful to consider two asymptotic regions. For very small acceptance ($L_{\eta,\phi} \to 0$) at most one particle from a jet is accepted and thus the correlation of particles within a jet is not seen, $\Phi_{\rm p_t} \to 0$. For very large acceptances all particles from a jet are accepted and a positive value of $\Phi_{\rm p_t}$ is measured. With increasing acceptance one increases proportionally the number of accepted jet- and 'soft'- hadrons. In this limiting case the value of $\Phi_{\rm p_t}$ should be independent of the acceptance because of the 'intensive' property of the Φ measure. The expected saturation of $\Phi_{\rm p_t}$ for large acceptance is, however, not observed in Fig. 41(a). This is because the ALICE TPC acceptance in pseudo-rapidity is too small. Finally, in order to illustrate the sensitivity of the $\rm p_t$ fluctuations on the ratio between 'hard' and 'soft' components, the expected jet multiplicity is increased by a factor of 3; the results are shown as open symbols in Fig. 41(a).

Since the fraction of particles originating from the 'hard' component increases with increasing $\rm p_t$, one expects an increase of $\Phi_{\rm p_t}$ when a low $\rm p_t$ cut is applied to select particles for the analysis. In fact this is observed in Fig. 41(b) where the results without $\rm p_t$ cut (squares) and after a low

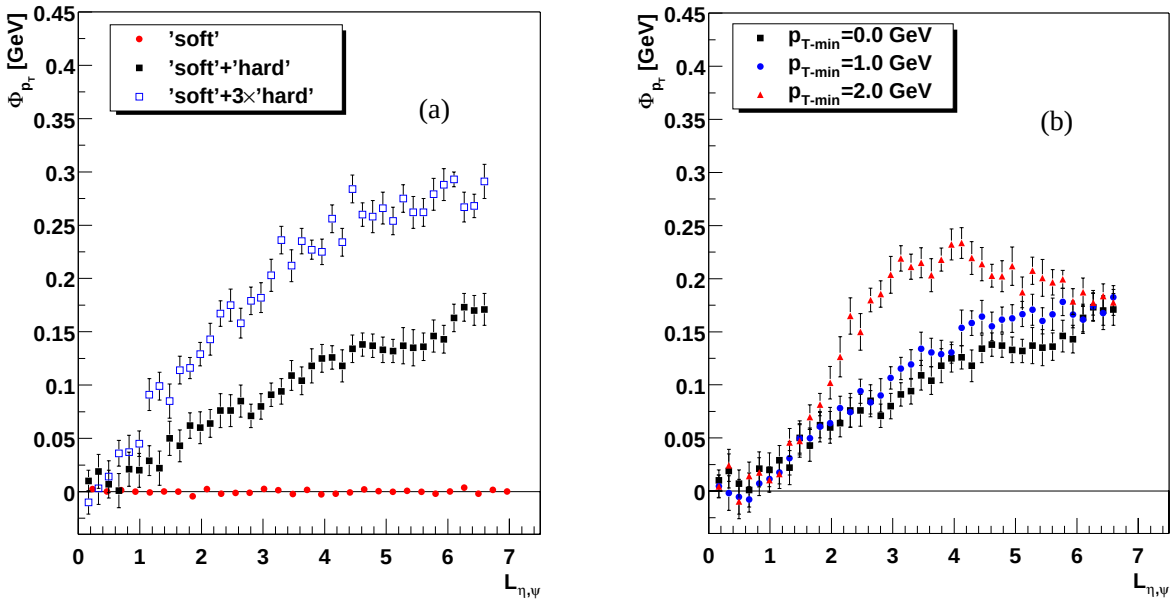

Figure 41: (a) The dependence of Φ_{p_t} on the acceptance for 'soft' component (dots), 'hard' + 'soft' components (squares) and the contribution of hard component increased by a factor of 3 (open squares). (b) The dependence of Φ_{p_t} on the acceptance for 'hard' + 'soft' component model without (squares) and with low p_t cut at 1.0 GeV/c (dots) or 2.0 GeV/c (triangles).

p_t cut at 1.0 GeV/c (dots) and 2.0 GeV/c (triangles) are plotted. The results for a 2 GeV/c cut suggest an early onset of saturation of Φ_{p_t} with $L_{\eta,\phi}$ which may be due to the narrowing of the jet extension in $L_{\eta,\phi}$ after increasing the low p_t cut.

In the previous study only the geometrical acceptance of ALICE TPC was taken into account. Here the influence of detection inefficiency is discussed. First one considers the effect of random track losses due to tracking and fitting problems. In Fig. 42(a) the standard results obtained assuming a perfect detection and the result that includes random losses of 10% are compared. The difference is small in comparison to the expected effect due to the presence of jets. Then losses of tracks that are close in the detector space (effect of the two-track resolution) is simulated. One assumption made here is that tracks that have a neighbour track with $\Delta p_t = |p_{t1} - p_{t2}| <$ cut MeV/c are lost. The results obtained including the effect of two-track resolution are shown in Fig. 42(b). The bias is small in comparison to the expected effect due to presence of jets.

The expected jet production in central Pb–Pb collisions at $\sqrt{s}_{NN}$=5.5 TeV should lead to large event-by-event fluctuations of transverse momentum. This may allow one to test various models of jet production in the jet p_t region not accessible for the standard methods of jet detection. On the other hand, fluctuations due to jet production should be taken into account when considering the detection of fluctuations due to other processes.

The influence of random detection inefficiencies as well as two-track resolution was estimated to be small for p_t fluctuations as expected for unquenched jet production.

14.2 Azimuthal fluctuations in E_T

In this subsection results from an event-by-event azimuthal asymmetry in the transverse energy flow induced by the mini-jet dynamics [158] is discussed. The underlying idea is that the presence of new physics brought in by semihard degrees of freedom should manifest itself through reasonably well-defined changes in the inelasticity pattern that can be measured experimentally, depending on the relative weight of mini-jet and soft hadronic contributions to the inelastic cross-section. Let us stress, that in order to reproduce an experimentally observed transverse

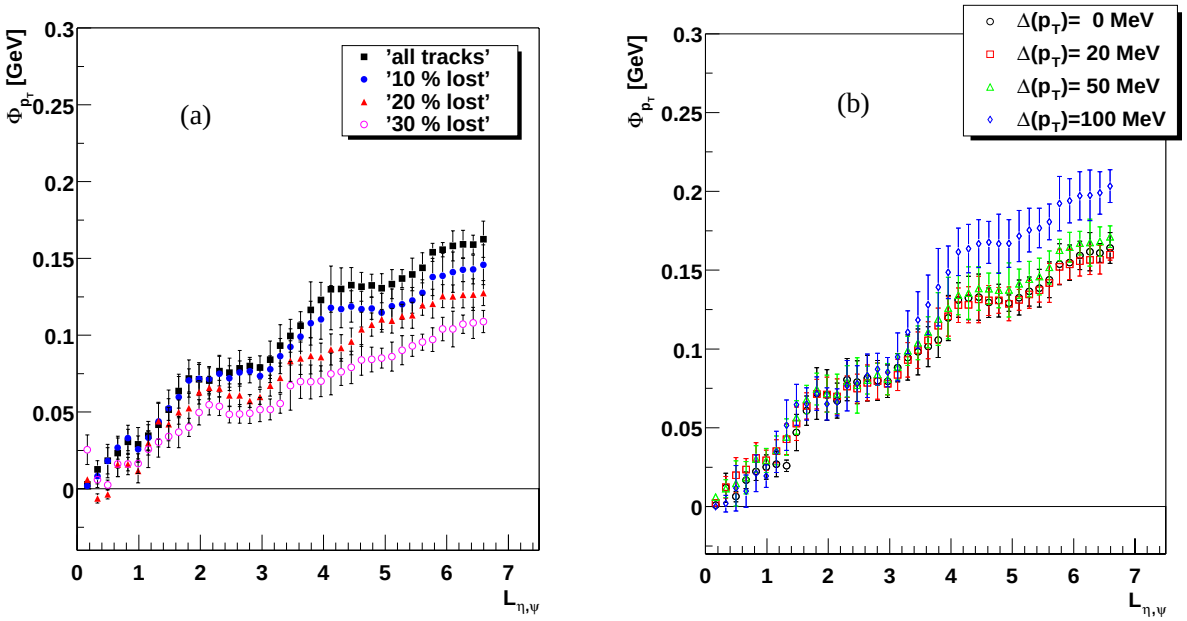

Figure 42: (a) The dependence of Φ_{p_t} on the acceptance for 'hard' + 'soft' component model including possible effect of random track losses due to reconstruction inefficiency. (b) The dependence of Φ_{p_t} on the acceptance for 'hard' + 'soft' component model including possible effect of limited two track resolution modeled by lower cut on transverse momentum difference of two tracks.

energy spectrum, the description of mini-jet dynamics should go beyond the lowest-order elastic scattering and include, in particular, initial and final state radiation (see for example Ref. [159]) as included into the HIJING Monte Carlo event generator [102]. HIJING allows one to study the effects due to the presence of semi-hard degrees of freedom at the early stages of high-energy collision in a simple setting, where the only nontrivial effects distinguishing the nuclear collision from an incoherent superposition of nucleon-nucleon ones are jet quenching, i.e. energy losses experienced by partons traversing the surrounding debris created in nuclear collision, and accounting for nuclear effects in the parton structure functions. Effects of rescattering and possible evolution of the initially produced parton system towards equilibrium are not included in this consideration.

To quantify the event-by-event asymmetry of transverse energy flow, one can study, as proposed in Ref. [160], the difference between the transverse energy deposited in some rapidity window $y_{\min} < y_i < y_{\max}$, and in two oppositely azimuthally oriented sectors with an angular opening $\delta\varphi$ each. The idea of using this quantity as a measure of the presence of semi-hard dynamics comes from the expectation that perturbative transverse energy production mechanisms have a built-in tendency of creating an event-by-event azimuthal asymmetry *in a fixed rapidity window*. For example, the partonic transverse energy flow occurring through binary parton collisions becomes, with increasing collision energy, more and more azimuthally unbalanced, because one of the two scattered partons just misses the rapidity window in question [160]. In the limit of high energies even the binary parton scattering at central rapidities as such becomes azimuthally unbalanced because of the growing contribution of primordial transverse momentum to particle production [161]. In contrast, one expects the soft transverse energy production mechanisms, e.g. string decays, to be more azimuthally balanced *locally in rapidity* on an event-by-event basis because of the small momentum transfer involved.

By denoting the transverse energy going into the 'upper' and 'lower' cones in a given event by $E_T^{\uparrow}(\delta\varphi)$ and $E_T^{\downarrow}(\delta\varphi)$, respectively, the asymmetry in transverse energy production in a given

event is thus described by $\delta E_T(\delta\varphi)$:

$$\delta E_T(\delta\varphi) \;=\; E_T{}^{\uparrow}(\delta\varphi) - E_T{}^{\downarrow}(\delta\varphi). \tag{42}$$

An ensemble of collisions is characterized by an event-by-event probability distribution

$$P(\delta E_T|\delta\varphi) \;=\; \frac{\mathrm{d}\, w(\delta E_T(\delta\varphi))}{\mathrm{d}\,\delta E_T(\delta\varphi)}. \tag{43}$$

This distribution was calculated in Ref. [158] in the HIJING model for central Au–Au collisions at RHIC energy $\sqrt{s}_{NN}$=200 GeV and central Pb–Pb collisions at LHC energy $\sqrt{s}_{NN}$=5.5 TeV for $\delta\varphi = \pi$ and central rapidity interval $-0.5 < y < 0.5$. The distributions $P(\delta E_T|\pi)$ were calculated *both* at partonic level and at the level of final hadrons with semi-hard interactions and quenching on and off. This allowed one to separate the contribution of mini-jets as described by HIJING from the background of soft processes. The resulting distributions for the LHC are shown in Fig. 43 with quenching turned on and the chosen value of the mini-jet's infrared cutoff $p_0 = 2$ GeV.

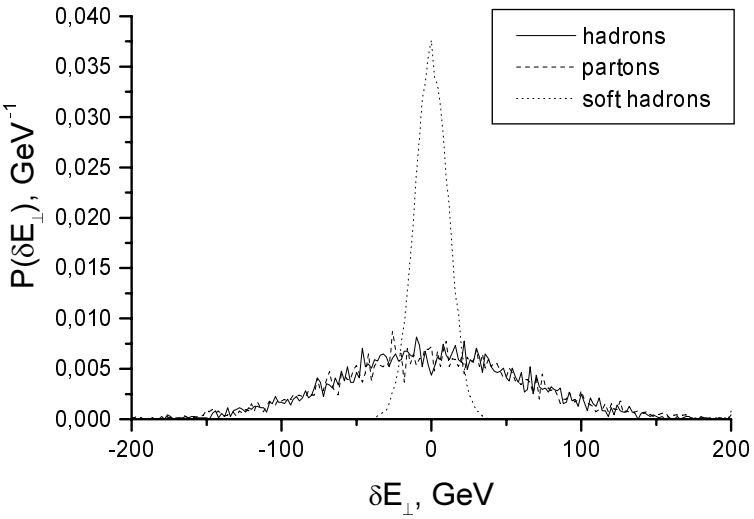

Figure 43: Probability distribution for azimuthal transverse energy imbalance in the unit rapidity window for Pb–Pb collisions at LHC energy $\sqrt{s}_{NN}$=5.5 TeV and $p_0 = 2$ GeV with quenching on.

The numerical values of the standard deviation $\sqrt{\langle \delta E_T{}^2 \rangle}$ characterizing the widths of the corresponding probability distributions are shown in the table 1, where for completeness standard deviations for the cases of quenching turned off and with a larger value for the infrared cutoff $p_0 = 4$ GeV are also reported.

The magnitude of the azimuthal asymmetry is essentially determined by the relative yield of the semihard (mini-jet) contribution. Switching off mini-jets, and thus restricting oneself to purely soft mechanisms, leads to a substantial narrowing of the asymmetry distribution; by the factor of 2.3 at RHIC and by the factor 4.1 at LHC energy, respectively, (these values correspond to the case of quenching turned on). Quite remarkably, the parton and final (hadronic) distributions of δE_T in both cases practically coincide indicating that the contribution to transverse energy due to hadronization of the primordial parton system is, to a high accuracy, additive and symmetric in azimuthal angle and thus cancels out. The transverse energy flow imbalance Eqn. (42) is a sensitive indicator of the presence of primordial semi-hard parton dynamics that can be studied in calorimetric measurements in central detectors at the LHC.

As mentioned earlier, rescattering of produced partons, which is essential for possible evolution of the primordial partons towards equilibration, was not taken into account in the above consideration. In fact one expects parton rescattering to destroy at least some of the initial asymmetry of the transverse energy flow, making its measurement even more interesting.

Table 1: Values of the standard deviation $\sqrt{\langle \delta \mathrm{E_T}^2 \rangle}$ characterizing the widths of the of the probability distributions for different energies and assumptions.

A–A	$\sqrt{s}$ (GeV)	p_0 (GeV)	Asymmetry	$\sqrt{\langle \delta E^2 \rangle}$ (GeV)
Au–Au	200	2	hadrons (quenching on)	16
			hadrons (quenching off)	17
			partons	18
			soft hadrons	7
Pb–Pb	5500	2	hadrons (quenching on)	61
			hadrons (quenching off)	71
			partons	65
			soft hadrons	15
Pb–Pb	5500	4	hadrons (quenching on)	69
			partons	76
			soft hadrons	16

15 Long-range correlations

Soft and semihard parts of the multiparticle production at high energy are successfully described in terms of colour strings stretched between the projectile and target [162, 163, 164]. The hadronization of these strings produces the observed hadrons. In the case of nuclear collision, the number of strings grows with the growing energy and the number of nucleons of colliding nuclei, and one has to take into account the interaction between strings in the form of their fusion and/or percolation [165, 166].

In the case of colour string fusion, a new string is formed which may have higher colour charge at its ends, corresponding to the sum of the initial colour charges of fusing strings. Thus heavy flavor is produced more efficiently in the process of this new string fragmentation. Fusion process results in the reduction of total multiplicity of charged particles, growth of transverse momentum and increase of strange particle yields [167], that was confirmed later [168] in comparison with RHIC data.

Around percolation threshold [169, 170], strong fluctuations in the number of strings with a given colour should appear. As a result one may expect large fluctuations in values of different observables from one event to another. The characteristic and unique feature of string fusion (percolation) phenomenon is that these fluctuations will manifest themselves as the long-range correlations between observables obtained in an event-by-event analysis in separate rapidity windows .

The possible experimental observation of the string percolation phenomenon as an intermediate process, leading to the QGP formation, is extremely interesting. Therefore, the long-range correlations were proposed as the main tool to study the mentioned phenomenon [81, 171, 172, 173, 174, 175, 176, 177].

The benefit of studies of correlations between the variables in two windows sufficiently separated in rapidity has the possibility of eliminating short-range correlations, arising due to other processes such as resonance decays. Besides, it is also possible to discriminate correlations originating from the string fusion and those from multiple jet formation. This can be done by choosing different sizes of rapidity bins and making proper transverse momentum cuts. The additional variables like net charge and strangeness could be used to discriminate existing theoretical scenarios bringing a deeper insight to string fusion and percolation mechanism [168, 177].

15.1 Observables

The long-range correlation studies are made between observables in two different and significantly separated rapidity intervals Δy_F and Δy_B, which are conventionally referred as forward (F) and backward (B) rapidity windows. Within these two windows correlations between two main dynamical variables, the multiplicity of charged particles (n) and the mean transverse momenta ($\mathrm{p_t}$) in the *given event* (44) are used.

$$p_t \equiv \frac{1}{n}\sum_{i=1}^{n} |\mathbf{p}_{ti}|, \qquad \text{where} \qquad y_i \in \Delta y; \quad i = 1, ..., n. \tag{44}$$

Three main types of long-range correlations can be studied within the two rapdity windows: (a) n-n - the correlation between multiplicities of charged particles, (b) $\mathrm{p_t}$-$\mathrm{p_t}$ - the correlation between values of mean transverse momenta [178] and (c) $\mathrm{p_t}$-n - the correlation between mean momentum transverse momenta in one rapidity interval and the multiplicity of charged particles in another interval.

Usually to describe these correlations numerically the average values $\langle B \rangle_F$ of one dynamical variable B in the backward rapidity window Δy_B, as a function of another dynamical variable F in the forward rapidity window Δy_F are studied. Here $\langle ... \rangle_F$ denotes averaging over the events with a fixed value of the variable F in the forward rapidity window. Another type of averaging denoted by $\langle ... \rangle$ that means *averaging over all events* is also used.

As a result, one arrives at a correlation function: $\langle B \rangle_F = f(F)$. In the majority of cases one can use linear parametrization for this function, known as linear regression. For the n-n correlation in this case one gets:

$$\langle n_B \rangle_{n_F} = a + \beta_{nn} \cdot n_F. \tag{45}$$

Here the coefficient β_{nn} characterizes the strength of the n-n correlation, n_B, n_F are the multiplicities of the charged particles, produced in the *given event* in the backward (Δy_B) and forward (Δy_F) rapidity windows.

In case of $\mathrm{p_t}$-$\mathrm{p_t}$ and $\mathrm{p_t}$-n correlation the corresponding correlation coefficients $\beta_{\mathrm{p_t p_t}}$ and $\beta_{p_t n}$ can be defined in a similar manner. One must realize that these correlation coefficients depend on the absolute mean values of the observables $\langle F \rangle$ and $\langle B \rangle$ in the forward and backward windows and that the correlation coefficient $\beta_{p_t n}$ has the dimension of GeV/c.

It is more natural to define the correlation coefficient as the response of $\langle B \rangle_F$ on the variations of the variable F in the vicinity of its average value $\langle F \rangle$. It is also useful to go to *the relative variables*, i.e. to measure a deviation of F from its average value in units of $\langle F \rangle$, and similarly for B. This can reduce the possible influence of experimental bias such as detection efficiency, background, etc. So it is reasonable to define a correlation coefficient b_{B-F} for correlation between observables B and F in backward and forward rapidity windows in the following way:

$$b_{B-F} \equiv \frac{\langle F \rangle}{\langle B \rangle} \left. \frac{d\langle B \rangle_F}{dF} \right|_{F=\langle F \rangle} \qquad \text{or} \qquad b_{p_t-n} \equiv \frac{\langle n_F \rangle}{\langle p_{\mathrm{t}B} \rangle} \left. \frac{d\langle p_{\mathrm{t}B} \rangle_{n_F}}{dn_F} \right|_{n_F=\langle n_F \rangle}, \tag{46}$$

as an example for $\mathrm{p_t}$-n correlation. Here the $p_{\mathrm{t}B}$, $p_{\mathrm{t}F}$ are the mean transverse momentum of the charged particles, produced in the *given event* (44) correspondingly in the backward (Δy_B) and forward (Δy_F) rapidity windows.

It is clear that these relative dimensionless coefficients are simply connected with absolute correlation coefficients defined above:

$$b_{n-n} = \frac{\langle n_F \rangle}{\langle n_B \rangle} \beta_{nn}, \qquad b_{p_t-p_t} = \frac{\langle p_{\mathrm{t}F} \rangle}{\langle p_{\mathrm{t}B} \rangle} \beta_{p_t p_t}, \qquad b_{p_t-n} = \frac{\langle n_F \rangle}{\langle p_{\mathrm{t}B} \rangle} \beta_{p_t n}. \tag{47}$$

These studies can be made in different azimuthal windows and by introducing additional cuts on the transverse momentum of the particles in these rapidity intervals. It can be useful for

discrimination of the correlations originating due to the string fusion phenomenon from other effects such as jets, space phase boundaries or elliptic flow.

Preliminary results for the Pb–Pb collisions at $\sqrt{s}_{\rm NN}$=17.2 GeV [177] from the NA49 experiment indicate the existence of n-n and p_t-n long-range correlations both for minimum bias data and for different classes of collision centrality. In particular, the new effect of *negative long-range correlation* and the transition to *positive one* is observed under the condition of using narrow window in the event selection on the number of participants.

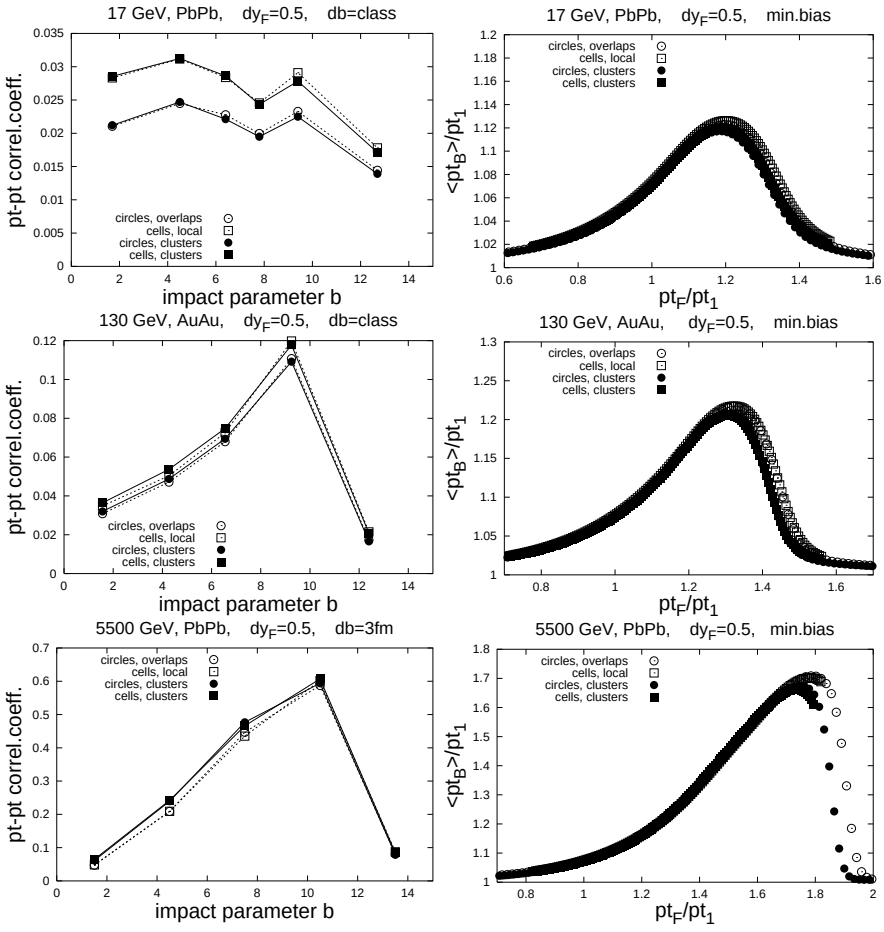

Figure 44: Left panel: String Fusion Model(SFM) MC calculations [176] of the $b_{p_t-p_t}$ long-range correlation coefficient as a function of the impact parameter b for three Pb–Pb collision energies: $\sqrt{s}_{\rm NN}$=17, 130 and 5500 GeV. Right panel: Corresponding p_t-p_t correlation functions $\langle p_{tB}\rangle_{p_{tF}}=f(p_{tF})$, presented in units of $pt_1\equiv\overline{p}$ which is the average transverse momentum of particles produced from a decay of one string.

15.2 Extending from SPS to RHIC to LHC energies

A microscopic explanation of the phenomena of long-range correlation observed at SPS energies and predictions for RHIC and LHC were obtained in the framework of a String Fusion Model (SFM) [171, 172, 178, 173, 177, 176, 179]. The SFM is based on a specific assumption of the interaction of overlapping strings (quark–gluon string fusion) and it takes into account the changes of the mean values of the observables in the case of overlap.

SFM Monte-Carlo calculations of the correlations are done both at fixed values of the impact parameter [173, 179] and taking its fluctuation into account [176]. The calculations with a narrowly selected number of nucleons-participants of the collision were also performed [177].

Predictions for observation of long-range correlation at RHIC and ALICE at the LHC are done based on the results of comparison of theoretical SFM description of the experimental NA49 data on long-range correlations.

The results of SFM calculations [176] of the $b_{p_t-p_t}$ correlation coefficient as a function of the impact parameter b for three Pb–Pb collision energies $\sqrt{s_{\rm NN}}$=17; 130 and 5500 GeV are presented in Fig. 44. In these calculations the forward rapidity interval was chosen to be 0.5 units and within the central ALICE acceptance. Black and open circles and squares in Fig. 44 represent different approaches (see [176] for the details). Results show the considerable growth of the $\rm p_t$-$\rm p_t$ correlation coefficient in transfer from the SPS to the LHC energies. The results of SFM MC calculations for the $\rm p_t$-$\rm p_t$ correlation function $\langle p_{{\rm t}B}\rangle_{p_{{\rm t}F}} = f(p_{{\rm t}F})$ are presented in this figure [176]. A drastic change of the shape of this correlation function with energy is observed.

15.3 Long-range correlation studies at ALICE

ALICE installation provides charged particle multiplicity information in a wide rapidity range up to $\eta = 5.09$. Precise $\rm p_t$ measurements and detailed particle composition data are provided event-by-event in the central rapidity window up to $\eta = 0.9$. Therefore, studies of long-range correlations in ALICE will be done using the information obtained from the ITS, TPC and the TOF detectors in combination with event-by-event multiplicity from the SPD and the FMD.

It is important to start the long-range correlation investigations in ALICE from the pp collisions, which will form the base for pA and A–A collisions. In particular, scanning the impact parameter space for the Pb–Pb collisions using the ZDC data gives the possibility to change the density of the overlapping strings by moving from the most peripheral to the central collisions [81]. Therefore the onset of the critical fluctuations relevant to the string fusion and/or percolation phenomenon could be obtained in ALICE from the observation of behaviour of the long-range correlation coefficients vs. event centrality. These will provide the important information on the early stages of the QGP formation.

16 Summary

To summarize, the capability of ALICE experiment in terms of making detailed event-by-event measurement has been discussed in order to address the issue of the nature of QGP phase transition. Recent findings from the lattice calculations at small chemical potentials have been discussed. These calculations have revealed that interesting fluctuation patterns will prevail for heavy-ion collisions at LHC energies. The issue of correlations and fluctuations and the complexity in interpreting the results because of several competing processes has been addressed. The importance of controlling centrality in fluctuation studies is discussed. In ALICE, fluctuations in temperature can be estimated from the event-by-event measurement of the slope of $\rm p_t$ distribution of identified hadrons in addition to those from the fluctuations in $\langle \rm p_t \rangle$. Fluctuation measurements in particle multiplicity, strangeness, net charge and the ratio of particles can be performed with high accuracy. The method of studying fluctuations through balance functions has been explored in ALICE environment. Possibility of event-by-event measurements of source sizes and azimuthal asymmetry parameters are discussed. The capability of ALICE in terms of measurement of the formation of disoriented chiral condensate has been discussed. An attempt has been made to understand the event-by-event fluctuations in the presence of jets and minijets. This is important in order to make any inference about the nature of event-by-event fluctuations as well as to understand the effect of jets passing through the high density medium created in heavy-ion collisions. It has been shown that information about the collision dynamics, especially on the string fusion and percolation phenomenon can be obtained from the study of long-range correlations. Extraction of long-range correlation coefficients for different colliding systems and centralities will help to understand critical fluctuations relevant to the string fusion and percolation phenomena.

References

[1] H. Heiselberg, Phys. Rep. **351** (2001) 161.
[2] L. Van Hove, Phys. Lett. **B118** (1982) 138.
[3] M. A. Stephanov, K. Rajagopal and E. Shuryak, Phys. Rev. Lett. **81** (1998) 4816.
[4] A. Barducci *et al.*, Phys. Lett. **B231** (1989) 463.
[5] J. Berges and K. Rajagopal, Nucl. Phys. **B538** (1999) 215.
[6] M. A. Halasz *et al.*, Phys. Rev. **D58** (1998) 096007.
[7] M. A. Stephanov, K. Rajagopal and E. V. Shuryak, Phys. Rev. **D60** (1999) 114028.
[8] O. Philipsen, *Preprint* hep-lat/0510077.
[9] Qing-jun Liu, Thomas A. Trainor, Phys. Lett. **B567** (2003) 184.
[10] M.J. Tannenbaum *et al.*, PHENIX collaboration, J. Phys. **G30** (2004) S1367.
[11] A.A. Anselm and M.G. Ryskin, Phys. Lett. **B266** (1991) 482.
[12] J.-P. Blaizot and A. Krzywcki, Phys. Rev. **D46** (1992) 246.
[13] J.D. Bjorken, K.L. Kowalski and C.C. Taylor, SLAC-PUB-6109, April 1993.
[14] K. .Rajagopal, F. Wilczek, Nucl. Phys. **B399** (1993) 399.
[15] Bedanga Mohanty, Julien Serreau, Phys. Rep. **414** (2005) 263.
[16] R. Stock, Proceedings of the NATO Advanced Study Workshop on Hot Hadronic Matter: Theory and Experiment, Divonne-les-Bains, France, 27 June–1 July 1994.
[17] T. Anticic *et al.*, (NA49 Collaboration), Phys. Rev. **C70** (2004) 034902.
[18] H. Appelshauser *et al.* (NA49 Collaboration), Phys. Lett. **B459** (1999) 679.
[19] S. V. Afanasiev *et al.*, (NA49 Collaboration), Phys. Rev. Lett. **86** (2001) 1965.
[20] C. Alt *et al.* (NA49 Collaboration), *Preprint* hep-ex/0311009.
[21] M. Rybczynski *et al.* (NA49 Collaboration), J. Phys. Conf. Ser. **4** (2005) 74.
[22] C. Alt *et al.* (NA49 Collaboration), Phys. Rev. **C70** (2004) 064903.
[23] C. Alt *et al.* (NA49 Collaboration), Phys. Rev. **C71** (2005) 034903; P. Christakoglou *et al.* (NA49 Collaboration), Nucl. Phys. A **749** (2005) 279.
[24] S. V. Afanasiev *et al.* (NA49 Collaboration), Phys. Rev. **C66** (2002) 054902.
[25] M. Gazdzicki *et al.* (NA49 Collaboration), J.Phys.G30 (2004) S701.
[26] P. Christakoglou *et al.* (NA49 Collaboration), *Preprint* nucl-ex/0510045.
[27] M.M. Aggarwal *et al.*, (WA98 Collaboration), Phys. Rev. **C65** (2002) 054912.
[28] M. M. Aggerwal *et al.* (WA98 Collaboration), Phys. Lett. **B420** (1998) 169.
[29] T.K. Nayak *et al.* (WA98 Collaboration), Nucl. Phys. **A638** (1998) 249c.
[30] M. M. Aggerwal *et al.* (WA98 Collaboration), Phys. Rev. **C64** (2001) 011901.
[31] M. M. Aggerwal *et al.* (WA98 Collaboration), Phys. Rev. **C67** (2003) 044901.
[32] D. Adamova *et al.* (CERES Collaboration), Nucl. Phys. **A727** (2003) 97.
[33] K. Adcox *et al.* (PHENIX Collaboration), Phys. Rev. **C66**, (2002) 024901.
[34] S.S. Adler *et al.* (PHENIX Collaboration), Phys. Rev. Lett. **93**, (2004) 092301.
[35] K. Adcox *et al.* (PHENIX Collaboration), Phys. Rev. Lett. **89** (2002) 082301.
[36] J. Adams *et al.* [STAR Collaboration], Phys. Rev. **C68** (2003) 044905.
[37] C. Pruneau *et al.* (STAR Collaboration), *Preprint* nucl-ex/0401016.
[38] Z. Ahammed *et al.* (STAR Collaboration) Pramana **60** (2002) 993.
[39] G. D. Westfall *et al.* (STAR Collaboration), J. Phys. **G30** (2004) S345.
[40] S. Das *et al.* (STAR Collaboration), *Preprint* nucl-ex/0503023.
[41] J. Adams *et al.* [STAR Collaboration], Phys. Rev. **C71** (2005) 064906.
[42] J. Adams *et al.*, (STAR Collaboration) Phys. Rev. Lett. **90** (2003) 172301.
[43] K. Wozniak *et al.* (PHOBOS Collaboration), Jour. of Phys. **G** (2004) S1377.
[44] C. Zhengwei *et al.* (PHOBOS Collaboration), *Preprint* nucl-ex/0509027.
[45] Z. Fodor and S. Katz, Jour. High Energy Phys. **0203** (2002) 014.
[46] Z. Fodor and S. Katz, Jour. High Energy Phys. **0404** (2004) 050.
[47] C.R. Allton *et al.*, Phys. Rev. **D66** (2002) 074507.
[48] M.-P. Lombardo and M. d'Elia, Phys. Rev. **D67** (2003) 014505.

[49] Ph. de Forcrand and O. Philipsen, Nucl. Phys. **B642** (2002) 290.
[50] R.V. Gavai and S. Gupta, Phys. Rev. **D68** (2003) 034506.
[51] C.R. Allton, *et al.*, Phys. Rev. **D68** (2003) 014507.
[52] R.V. Gavai and S. Gupta, Phys. Rev. **D71** (2005) 074013 (*Preprint* hep-lat/0412035).
[53] J. Cleymans, J. Phys. **G28** (2002) 1582 and private communication.
[54] S. Gottlieb *et al.*, Phys. Rev. Lett. **59** (1987) 2247.
[55] R.V. Gavai and S. Gupta, Phys. Rev. **D67** (2003) 034501.
[56] R.V. Gavai, S. Gupta and P. Majumdar, Phys. Rev. **D65** (2002) 054506.
[57] C. Bernard *et al.*, Phys. Rev. **D71** (2005) 034504.
[58] J.-P. Blaizot, E. Iancu and A. Rebhan, Phys. Lett. **B523** (2001) 143.
[59] A. Vuorinen, Phys. Rev. **D68** (2003) 054017.
[60] P. Chakraborty, M. G. Mustafa and M. H. Thoma, Phys. Rev. **D68** (2003) 085012.
[61] V. Koch, A. Majumder and J. Randrup, *Preprint* nucl-th/0505052.
[62] R. V. Gavai and S. Gupta, *Preprint* hep-lat/0510044.
[63] S. Ejiri, F. Karsch and K. Redlich, *Preprint* hep-ph/0509051.
[64] R. V. Gavai and S. Gupta, Phys. Rev. **D72** (2005) 054006.
[65] J. Liao and E. V. Shuryak, *Preprint* hep-ph/0510110.
[66] R.V. Gavai, S. Gupta and S. Mukherjee, Phys. Rev. **D71** (2005) 074013 (*Preprint* hep-lat/0412036 and hep-lat/0506015).
[67] M. Gaździcki and M. I. Gorenstein, Acta Phys. Pol. **B30** (1999) 2705.
[68] F. Becattini, Z. Phys. **C69**, (1996) 485; F. Becattini and U. Heinz, Z. Phys. **C76**, (1997) 269; F. Becattini, M. Gaździcki and J. Sollfrank, Eur. Phys. J. **C5**, (1998) 143.
[69] E. Shuryak and M.A. Stephanov, Phys. Rev. **C63** (2001) 064903.
[70] B. Mohanty, J. Alam, T.K. Nayak, Phys. Rev. **C67** (2003) 024904.
[71] M. Gaździcki and St. Mrówczyński, Z. Phys. **C54** (1992) 127.
[72] D.P. Mahapatra, B. Mohanty, S.C. Phatak, Int. J. Mod. Phys. **A17** (2002) 675.
[73] J. Zaranek, Phys. Rev. C **66** (2002) 024905
[74] S. Mrowczynski, Phys. Rev. C **66** (2002) 024904
[75] L. Csernai, Phys. Rev. **E56** (1997) 6668.
[76] S. Mrowczynski, Acta Phys. Pol. **B31** (2000) 2065 (*Preprint* nucl-th/9907099).
[77] S. Mrowczynski and E. Shuryak, Acta Phys. Pol. **B34** (2003) 4241.
[78] Henning Heiselberg, Axel P. Vischer, Phys. Lett. **B421** (1998) 18.
[79] H. Heiselberg, A.D. Jackson, *Preprint* nucl-th/9809013.
[80] St. Mrówczyński, Phys. Lett. **B439** (1998) 6.
[81] P.A. Bolokhov, M.A. Braun, G.A. Feofilov, V.P. Kondratiev, V.V. Vechernin, Internal Note/PHY, ALICE-INT-2002-20 (2002).
[82] F. Liu *et al.*, Eur. Phys. J. **C8** (1999) 649.
[83] L. Stodolsky, Phys. Rev. Lett. **75**, 1044 (1995); E.V. Shuryak, Phys. Lett. **B423** (1998) 9.
[84] St. Mrówczyński, Phys. Lett. **B314** (1993) 118; *ibid.* **B393** (1997) 26; Phys. Rev. **C49** (1994) 2191; St. Mrówczyński and M. Thoma, Phys. Rev. **D62** (2000) 036011.
[85] M. Asakawa, U. Heinz, B.Muller, Phys. Rev. Lett. **85** (2000) 2072.
[86] S. Jeon and V. Koch, Phys. Rev. Lett. **85** (2000) 2076.
[87] A. Capella, E.G. Ferreiro and A.B. Kaidalov, *Preprint* hep-ph/9903338; A. Capella, Acta Phys. Pol. **B30** (1999) 3541 (*Preprint* hep-ph/9910219).
[88] K. Geiger, Phys. Rep. **258** (1995) 237.
[89] N.S. Amelin *et al.*, Phys. Rev. Lett. **67** (1991) 1523.
[90] J.-Y. Ollitrault, Phys. Rev. **D46** (1992) 229.
[91] G. Baym and H. Heiselberg, Phys. Lett. **B469**, (1999) 7.
[92] K. Werner, Phys. Rep. **232** (1993) 87.
[93] C. Kittel, Phys. Today **5** (1988) 93; B.B. Mandelbrot, Phys. Today **1** (1989) 71; T.C.P. Chui, D.R. Swanson, M.J. Adriaans, J.A. Nissen and J.A. Lipa, Phys. Rev. Lett. **69** (1992) 3005;

H.B. Prosper, Am. J. Phys. **61** (1993) 54; G.D.J. Phillies, Am. J. Phys. **52** (1984) 629.
[94] E. Schnedermann and U. Heinz, Phys. Rev. Lett. **69** (1992) 2908.
[95] P.J. Siemens and J.O. Rasumssen, Phys. Rev. Lett. **42** (1979) 880.
[96] G. Wilk and Z. Włodarczyk, Phys. Rev. Lett. **84** (2000) 2770.
[97] C.Tsallis, J. Stat. Phys. **52** (1988) 479.
[98] W.M. Alberico, A. Lavagno and P. Quarati, Eur. Phys. J. **C12** (2000) 499; O.V. Utyuzh, G. Wilk and Z. Włodarczyk, J. Phys. **G26** (2000) L39; I. Bediaga, E.M.F. Curado and J.M. de Miranda, Physica **A286** (2000) 156; F.S. Navarra, O.V. Utyuzh, G. Wilk and Z. Włodarczyk, Nuovo Cim. **24C** (2001) 725; G. Wilk and Z. Włodarczyk, Physica **A305** (2002) 227.
[99] O.V. Utyuzh, G. Wilk and Z. Włodarczyk, *Preprint* hep-ph/0103273.
[100] *ALICE Technical Proposal*, CERN/LHCC 95-71, LHCC/P3, Geneva, 1995, p.195.
[101] R. Korus, St. Mrówczyński, M. Rybczyński, and Z. Włodarczyk, Phys. Rev. **C64** (2001) 054908.
[102] X.-N. Wang and M. Guylassy, *Phys. Rev.* **D44** (1991), 3501; **D45** (1992), 844; Comput. Phys. Commun. **83** (1994), 307; Phys. Rev. **C71** (1999) 1859.
[103] S. Gavin, Phys. Rev. Lett. **92** (2004) 162301.
[104] C. Pruneau, S. Gavin, S. Voloshin, Phys. Rev. **C66** (2002) 044904.
[105] Bedangadas Mohanty, Jan-e Alam, Sourav Sarkar, Tapan K. Nayak, Basanta K Nandi, Phys. Rev. **C68** (1003) 021901.
[106] Michael Kliemant, Benjamin Lungwitz, Marek Gazdzicki, Phys. Rev. **C69** (2004) 044903.
[107] J. Rafelski, Phys. Rep. **88** (1982) 331.
[108] J.I. Kapusta, A. Mekjian, Phys. Rev. **D33** (1986) 1304.
[109] S.V. Afanasiev *et al.*, Phys. Rev. Lett. **86** (2001) 1965.
[110] C. Roland, Ph.D Thesis University Frankfurt (1999).
[111] M. Gaździcki, Nulc. Phys. **A590** (1995) 197c.
[112] C. Roland, J. Phys. **G30** (2004) S1381.
[113] C. Roland, J. Phys. **G31** (2005) S1075.
[114] M. Bleicher *et al.*, J. Phys. G**25** (1999) 1859.
[115] A. Bialas, Phys. Lett. **B579** (2004) 31.
[116] S. Jeon and V. Koch, Phys. Rev. Lett. **83** (1999) 5435.
[117] S. Jeon and S. Pratt, Phys. Rev. **C65** (2002) 044902
[118] M. Bleicher, S. Jeon, and V. Koch, Phys. Rev. **C62** (2000) 061902.
[119] A. Bialas, Phys. Lett. **B532** (2002) 249,
[120] J.T. Michell, *Preprint* nucl-ex/0404005.
[121] S. Jeon, V. Koch, M. Bleicher, Nucl. Phys. **A698** (2002) 261.
[122] S. A. Bass, P. Danielewicz and S. Pratt, Phys. Rev. Lett. **85** (2000) 2689.
[123] D. Drijard et al, Nucl. Phys. **B155** (1979) 269; D. Drijard et al, Nucl. Phys. **B166** (1980) 233; I.V. Ajinenko *et al.*, Nucl. Phys. **C43** (1989) 37.
[124] R. Brandelik *et al.*, Phys. Lett. **B100** (1981) 357. M. Althoff *et al.*, Z. Phys. **C17** (1983) 5; H. Aihara *et al.*, Phys. Rev. Lett. **53** (1984) 2199; H. Aihara *et al.*, Phys. Rev. Lett. **57** (1986) 3140; P.D. Acton *et al.*, Phys. Lett. **B305** (1993) 415.
[125] P. Bozek, Phys. Lett. **B609** (2005) 247.
[126] S. Pratt and S. Cheng, Phys. Rev. **C68** (2003) 014907.
[127] W. Ehehalt, W. Cassing, Nucl. Phys. **A602** (1996) 449.
[128] S. Cheng *et al.*, Phys. Rev. **C69** (2004) 054906.
[129] P. Bozek, W. Broniowski, W. Florkowski, *Preprint* nucl-th/0310062.
[130] W. Florkowski, P. Bozek, W. Broniowski, *Preprint* nucl-th/0402028.
[131] J. Adams *et al.* (STAR Collaboration), Phys. Rev. **C72** (2005) 014904.
[132] M. Miller and R. Snellings, *Preprint* nucl-ex/0312008.
[133] ALICE Collaboration, ALICE Technical Design Report: Photon Multiplicity Detector (PMD), CERN-LHCC-99-32, CERN-OPEN-2000-184, Sep 1999.

[134] ALICE Collaboration, Addendum to the TDR of the Photon Multiplicity Detector (PMD), CERN-LHCC-2003-038, Sep 2003.
[135] S. Gavin *et al.*, Phys. Rev. Lett. **72** (1994) 2143.
[136] S. Gavin and B. Muller, Phys. Lett. **B329** (1994) 486.
[137] J. I. Kapusta and A.P.Vischer, Z.Phys. **C75** (1997) 507.
[138] S. Digal, R. Ray, S. Sengupta, A.M. Srivastava, Int. J. Mod. Phys. **A15** (2000) 2269.
[139] C.M.G. Lates, Y. Fujimoto and S. Hasegawa, Phys. Rep. **65** (1980) 151
[140] For an extensive review on "centauros" and related phenomena see E.Gładysz-Dziaduś, INP Report No.1879/PH, Cracow, 2001.
[141] T.C. Brooks *et al.*, Phys. Rev. **D55** (1997) 5667
[142] P. Seyboth (NA49 Collaboration) in Proc.XXV Int. Symposium on Multiparticle Dynamics, Stara Lesna, Slovakia, Sept.1995, D. Brancko,L.Sandor and J.Urban eds., World Scientific 1996, p.170
[143] S. Pratt, Phys. Lett. **B301** (1993) 159
[144] S.V. Akkelin, Yu.M. Sinyukov, Nucl. Phys. **A661** (1999) 661.
[145] Sean Gavin, J.I. Kapusta, Phys. Rev. **C65** (2002) 054910. Sean Gavin, *Preprint* nucl-th/0204064
[146] J.I. Kapusta, A.M. Srivastava, Phys. Rev **D52** (1995) 2977; J.I. Kapusta, S.M.H. Wong, Phys. Rev. Lett. **86** (2001) 4251; S.M.H. Wong, J.I. Kapusta, Nucl. Phys. **A715** (2003) 715.
[147] Y-Y Charng, K-W Ng, C-Y Lin, D-S Lee, Phys. Lett. **B548** (2002) 175.
[148] B.K. Nandi, G.C. Mishra, B. Mohanty, D.P. Mahapatra, T.K. Nayak, Phys. Lett. **B449** (1999) 109.
[149] B.K. Nandi, T.K. Nayak, B. Mohanty, D.P. Mahapatra, Y.P. Viyogi, Phys. Lett. **B461** (1999) 142.
[150] B. Mohanty, T.K. Nayak, Y.P. Viyogi, D.P. Mahapatra, Int. Jour. of Mod. Phys. **A19** (2004) 1453.
[151] A. Graps, IEEE Comm. Sci. Eng. **2** (1995) 50.
[152] I. Bearden *et al.* (NA44 Collaboration), *Preprint* nucl-ex/0107007.
[153] F. Takagi, Phys. Rev. Lett. **53** (1984) 427.
[154] A.C. Das and Y.P. Viyogi, Phys. Lett **B380** (1996) 437.
[155] M.M. Aggarwal, V.S. Bhatia, A.C. Das and Y.P. Viyogi, Phys. Lett **B438** (1998) 357.
[156] T.C. Brooks *et al.* (Minimax Collaboration) Phy. Rev. **D55** (1997) 390.
[157] M.M.Aggarwal *et al.* (WA98 Collaboration), Pramana **60** (2003) 987.
[158] A. Leonidov and D. Ostrovsky, Phys. Rev. **C63** (2001), 03791.
[159] A. Leonidov, *Preprint* BNL-NT-00/12.
[160] A. Leonidov and D. Ostrovsky, Eur. J. Phys. **C16** (2000), 683
[161] A. Leonidov and D. Ostrovsky, Phys. Rev. **D62** (2000), 094009
[162] A. Capella and A. Krzywicki, Phys. Rev. **D18** (1978) 4120.
[163] A. Capella, U. P. Sukhatme, C.–I. Tan and J. Tran Thanh Van, Phys. Lett. **B81** (1979) 68; Phys. Rep. **236** (1994) 225.
[164] A.B. Kaidalov, Phys. Lett., **B116** (1982) 459; A.B. Kaidalov K.A. Ter-Martirosyan, Phys. Lett., **B117** (1982) 247.
[165] M.A. Braun and C. Pajares, Phys. Lett. **B287** (1992) 154; Nucl. Phys. **B390** (1993) 542; N.S. Amelin, M.A. Braun and C. Pajares, Phys. Lett. **B306** (1993) 312; Z.Phys. **C63** (1994) 507.
[166] M.A. Braun and C. Pajares, Phys. Lett. **B603** (2004) 21.
[167] N.S. Amelin, N. Armesto, C. Pajares and D. Sousa, String Fusion Model: PSM-1.0 User's Manual, (2000); N. S. Amelin, N. Armesto, C. Pajares and D. Sousa, Eur. J. Phys. **C22** (2001) 149.
[168] M.A. Braun, F. del Moral, C. Pajares, Phys. Rev. **C65** (2002) 024907; N. Armesto, C. Pajares and D. Sousa, Phys. Lett. **B527** (2002) 92.

[169] M.A. Braun, C. Pajares, J. Ranft, Int. J. Mod. Phys. **A14** (1999) 2689;
[170] M.Nardi and H.Satz, Phys. Lett. **B442** (1998) 14; H.Satz, Nucl. Phys. **A661** (2000) 104c.
[171] N.S. Amelin, N. Armesto, M.A. Braun, E.G. Ferreiro, C.Pajares, Phys. Rev. Lett. **73** (1994) 2813.
[172] M.A.Braun and C.Pajares, Eur. Phys. J. **C16** (2000) 349.
[173] M.A. Braun, R.S. Kolevatov, C. Pajares and V.V. Vechernin, Eur. J. Phys. **C32** (2004) 535.
[174] M.A.Braun, C.Pajares and V.V.Vechernin. Phys. Lett. **B493** (2000) 54.
[175] M.A. Braun, C. Pajares and V.V. Vechernin Internal Note/FMD, ALICE-INT-2001-16 (2001).
[176] R.S. Kolevatov and V.V. Vechernin, Reports at the XVIII International Workshop on the Quantum Field Theory and High Energy Physics (2004) and at the XVII International Baldin Seminar on High Energy Physics Problems (2004), *Preprint* hep-ph/0501179 and hep-ph/0502069.
[177] G. Feofilov, *Experimental Studies of Long-Range Forward-Backward p_t and Multiplicity Correlations at ALICE*; Reports at XVI International Baldin Seminar on High Energy Physics Problems, Dubna, Russia, June 10-15, 2002. G. Feofilov in the proceedings of the Workshop on the Quantum Field Theory and High Energy Physics (QFTHEP2004), St. Petersberg, June 17-22, 2004. G. Feofilov *et al.* in the proceedings of ISHEPP XVII, Relativistic Nuclear Physics and Quantum Chromodynamics, Dubna, Russia, September 27-October 2, 2004, page.59.
[178] M.A.Braun and C.Pajares, Phys. Rev. Lett. **85** (2000) 4864.
[179] V.V. Vechernin, R.S. Kolevatov, *Preprint* hep-ph/0304295 and hep-ph/0305136.